Sea Level Change and Sea Surface Temperature Reconstruction in the Southern Equatorial Pacific Ocean Relative to the Society Islands, French Polynesia

Dissertation

Zur Erlangung des Doktorgrades

Dr. rer. nat

Der Mathematisch-Naturwissenschaftlichen Fakultät

der Christian-Albrechts-Universität

zu Kiel

vorgelegt von

Rashid Juma Rashid

Kiel, 2015

Referent: Prof. Dr. Anton Eisenhauer
Koreferent: Prof. Dr. Wolf-Christian Dullo
Tag der Disputation: 17.03.2015
Zum Druck genehmigt: Ja

Der Dekan

Erklärung

Hiermit erkläre ich an Eides statt, dass die vorgelegte Dissertation von mir selbständig und ohne unzulässige fremde Hilfe angefertigt und verfasst wurde, dass ich alle verwendeten Hilfsmittel angegeben habe, und dass alle Stellen, die ich wörtlich oder dem Sinne nach aus anderen Veröffentlichungen entnommen habe, kenntlich gemacht worden sind. Diese Arbeit wurde nach den Regeln guter Wissenschaft erstellt.

Ebenso erkläre ich, dass die Dissertation in der vorgelegten oder einer ähnlichen Fassung weder zu einem früheren Zeitpunkt an der Christian-Albrechts-Universität zu Kiel noch einer anderen in- oder ausländischen Hochschule als Dissertation eingereicht worden ist.

Kiel, den 2015

Rashid Juma Rashid

Table of Contents

List of Figures

Chapter One

Chapter Two

Chapter Three

Chapter Four

List of Tables

Chapter Three

Chapter Four

Zusammenfassung

Um zu verstehen wie sich das Klima in der Zukunft verändern wird, ist es essentiell zu untersuchen, in welchen zeitlichen Skalen das Klima in der Vergangenheit variierte und welche Konsequenzen diese Schwankungen mit sich brachten. Korallenskelette sind das wohl bekannteste Klimaarchiv aus tropischen und subtropischen Regionen. Als sogenannte Klimaproxies werden eine Vielzahl von stabilen Isotopen und Spurenelemente verwendet, die während des Korallenwachstums in das Skelett eingebaut werden. Diese Proxies erlauben es Aussagen zu treffen, wie die Umweltbedingungen des Meerwassers zu der Zeit des Skelettwachtums gewesen sind.

Skelette fossiler, massiver Korallen der Art *Porites* werden vielfach für die Rekonstruktion von erdgeschichtlichen Veränderungen der Meerwassertemperatur und des Meeresspiegels verwendet, mittels einer Kombination von Elementverhältnissen wie Strontium/Kalzium (Sr/Ca), Uran/Kalzium (U/Ca), der Systematik von stabilen Sauerstoffisotopen ($\delta^{18}O$), sowie der Thorium-Uran-Datierung. Normale fossile *Porites* Kolonien und *Porites* Mikroatolle wurden auf verschiedenen Inseln in Französisch Polynesien gesammelt und decken eine erdgeschichtlich Zeitspanne vom Mittel- bis zum Spätholozän ab. Zwei verschiedene Wuchsformen von *Porites* wurden gewählt: Mikroatolle sind Kolonien die and der Oberseite abgeflacht sind. Dieses Wachstum deutet daraufhin, dass sie direkt unterhalb des Meeresspiegels gewachsen sind und können zur Rekonstruktion des einstigen Meeresspiegels herangezogen werden. *Porites*-Kolonien weisen diese Charakteristik nicht auf und man kann dahernur eingeschränkt abshätzen, in welcher Tiefe sie im Riff gewachsen sind. Über lange geologischen Zeiträume können sich Korallenskelette diagenetisch verändern und diese Veränderungen müssen bei der Datierung und Rekonstruktion der Meerwassertemperatur berücksichtig werden. Es wurde vorab untersucht, wie sich diagenetische Veränderungen in den Skeletten manifestierten und wie die Skelette dennoch zur Klimarekontruktion herangezogen werden können.

Meeresspiegelschwankungen wurden mittels der fossilen Korallen bestimmt, die im Bereichdes heutigen Meeresspiegelniveaus gesammelt wurden (~1.5 m unterhalb bis 1.8 m oberhalb des mittleren Meerespiegelniveaus). Das Alter der Korallen und die Position in Relation zum heutigen Meeresspiegel geben Aufschluß darüber, wie sich der Meerespiegel im Lauf der Zeit

verändert haben könnte. Hierzu musste noch berücksichtigt werden, dass die Inseln vulkanischen Ursprungs sind und jede mit einer spezifischen Rate absinkt. Vor etwa 5400 Jahren lag der Meeresspiegel mindestens um 1.5m höher als heute. Erst 3000 Jahre später kam es zu einem Abfall des Meeresspiegels auf das heutige Niveau. Das spätholozäne Abfall des Meeresspiegels in diesen Meeresbereichen in großer Entfernung von den glazialen Eisschilden ("far-field areas") ist wahrscheinlich die Folge des post-glazialen Zurückfederns der früher eisbedeckten Gebiete und des Kollaps der Randwülste der glazialen Eisregionen. Dies führte zum Abwandern von Wassermassen aus den polfernen Regionen ("far-field") in den durch das Absinken der Eis-Randwülste geschaffenen Raum in der nahen Umgebung der Eisschilde ("near-field"). Zusätzlich dürfte die zusätzliche gravitative Wirkung der isostatischen Landhebung der vormaligen Eisgebiete diesen polwärtigen Wassertransport forciert haben ("ocean siphoning effect"). Unser theoretisches Meeresspiegelmodel, dass all diese Effekte berücksichtigt, stimmt mit den empirischen Daten überein, einzig die Dimensionen der Schwankungen sind nicht ganz kongruent und diese müssen noch gezielter untersucht und verifiziert werden.

Eine Vielzahl von Proxies können herangezogen werden, um zeitgeschichtliche Schwankungen der Meerestemperatur zu rekonstruieren. Hier wurden folgende geochemische Proxies analysiert: *Sr/Ca, $\delta^{18}O$ and U/Ca.* Aus den Daten wurde ersichtlich, dass die Meerestemperatur in Französisch Polynesien vom Mittel- bis zum Spätholozän periodischen Schwankungen unterlag. Es konnten verschiedene Intervalle identifiziert werden. Im Interval I und III vor 1800-2800 und 3700-4000 Jahre waren die Meere in dieser Gegend um 1-2°C wärmer als heute. Im Gegensatz dazu waren sie in den Intervallen II und IV vor 2800-3700 und 4000-4900 Jahren um 1-2°C kühler. Diese Schwankungen stimmen mit Veränderungen der Sonnenaktivität überein und nur teilweise mit rekonstruierten Veränderungen des atmosphärischen Kohlendioxidgehalts. Dies führt zu der Schlussfolgerung, dass die Sonnenaktivität einen stärkeren Einfluss auf die Veränderung der Meerestemperatur hatte.

Diagenetische Veränderungen können die Temperaturrekonstruktionen maßgeblich beeinflussen. Anhand von mikroskopischen Untersuchungen konnten diese Veränderungen lokalisiert und charakterisiert werden. Es wurde untersucht wie stark diese die Proxy-Werte beeinflussen. Proben bereiche in denen sich 2.5-3% sekundärer Aragonit in den Skelettporen angelagert haben,

können zu deutlichen Veränderungen der Geochemie der Gesamtprobe führen. Rekonstruiert man die Temperatur aus so einer diagenetisch veränderten Gesamtprobe liegt diese um 0.5-1.6°C niedriger.

Abgesehen von diagenetischen Veränderungen zeigen die Sr/Ca-Verhältnisse eine starke Variabilität, wenn man sie räumlich hochauflösend untersucht. Innerhalb von wenigen µm variieren die Sr/Ca Werte zwischen 5.4 und 9.9 mmol/mol. Solche Variationen sind keineswegs Indikatoren von starken Meerestemperaturschwankungen, sondern vielmehr repräsentieren sie einen physiologischen Einfluss der Koralle auf die Element-Verhältnisse – den sogenannten "Vitaleffekt".

Es wurde gezeigt, dass *Porites* Kolonien und Mikroatolle sowohl zur Rekonstruktion von erdgeschichtlichen Veränderungen der Meerestemperatur als auch des Meeresspiegels geeignet sind. Diagenetische Veränderungen fossiler Korallen müssen jedoch berücksichtigt werden, können aber mittels gezielter Beprobung der Skelette umgangen werden.

Abstract

Establishing Mid to Late Holocene climate history is the key to understand climate on both decadal and millennial time scales, which can help to anticipate future climate change and its oscillations. In tropical and sub-tropical regions, massive corals provide the ideal archive of climate information prior to satellite era because they incorporate a diverse suite of isotopic and trace elemental proxies into their aragonitic skeleton where behaviors of these elements during the incorporation are related to environmental processes of the ambient sea water. Using elemental ratios such as Strontium/Calcium (Sr/Ca), Uranium/Calcium (U/Ca) and isotope systematics such as Oxygen Isotopes ($\delta^{18}O$), Uranium (U) and Thorium (Th) from massive fossil corals (*Porites* and *Porites* micro atoll) from the Society Islands in French Polynesia which are currently exposed above the present mean sea level (apmsl), we have reconstructed Mid to Late Holocene sea level and sea surface temperature (SST) variability in this region. Furthermore, micro-scale intra-skeletal variability of Sr/Ca ratio within coral aragonite skeleton and post depositional early diagenetic alteration with its implications on SST estimates have also been investigated.

Sea level change was constrained using fossil *Porites* and *Porites* micro atolls collected at their original growth position from emerged fossil coral platforms between ~1.5 m below the present mean sea level (bpmsl) to ~1.8 m above the present mean sea level (apmsl). Uranium/Thorium (U/Th) dating and sample elevation relationship was used to constrain the age of these corals and sea level variations in this area. Since these islands were volcanic in origin, the specific subsidence rate of each island was taken into consideration to correct for the sample elevations relative to the modern sea level. The results indicate that ~5.4 ka the sea level was at least 1.5 m above the present mean sea level. With minor fluctuations it has remained above the modern sea level for duration of ~3000 years before dropping to the modern sea level. The Late Holocene sea level fall in these areas which are far from former ice sheets (far-field areas) is probably a result of post-glacial rebound of the areas of former ice mass cover that has led into collapsing of fore bulges surrounding these areas. This caused migration of water from the far-field into the near-field regions (close to former ice sheets) vacated by the collapsing fore bulges. In addition, the extra gravitational force of the emerging landmasses pressed into Earth's mantle during continental glaciation also force water to flow from southern ocean to the north (ocean siphoning

effect). Our theoretical predicted model accounting for all these effects named “Glacial Isostatic Adjustment (GIA)” related sea level variations were also in agreement with our empirical data. However, discrepancies on the amplitudinal variation of the theoretical predicted relative sea level (rsl) are still pending to future re-calibration.

Sea surface temperature (SST) was reconstructed using a multi-proxy approach through geochemical analysis of Sr/Ca, $\delta^{18}O$ and U/Ca of the coral samples. The results revealed periodic temperature variation in four main intervals for Mid to Late Holocene in the Society Islands. Interval I (1.8-2.8 ka) and III (3.7-4 ka) show higher temperatures in the order of 1-2°C above the modern mean temperature of the study area. Colder temperatures in the order of ~1-2°C below the modern mean SST were also observed during interval II (2.8-3.7ka) and IV (4.0-4.9 ka). These intervals are in good agreement with reconstructed solar activity and partly agree with reconstructed carbon dioxide concentration of the Mid to Late Holocene. This led to the conclusion that most likely solar activity is the main driver of SST and hence sea level variation on this region.

Fossil corals may undergo diagenetic alteration that can fundamentally change the skeletal geochemical composition obscuring reliable SST estimates. In this study diagenetic alteration was investigated on skeletal sections using microscopic observation, micro-mill sampling and microprobe analysis that involve the massive and pore-edges of the coral skeletons. The results indicate that 2.5 to 3% of carbonate derives from secondary precipitated aragonite within the skeletal voids (the pore edges) of the coral skeleton. This secondary aragonite differs in Sr/Ca ratio to the primary coral skeleton values and shifted the reconstructed $SST_{Sr/Ca}$ towards colder temperatures of ~0.5 to 1.6°C compared to $SST_{Sr/Ca}$ solely derived from the primary part of aragonite skeleton.

In addition, micro-scale intra-skeletal variability of Sr/Ca was investigated using line analysis of elemental distribution maps obtained from Electron Microprobe (EMP) analysis. The results show that Sr/Ca is not homogeneously distributed within a coral skeleton. At micro-scale level our samples Sr/Ca ratios vary between 5.4 and ~9.9 mmol/mol. This probably reflects the

physiological control of the corals on its trace metal uptake and the rates of $CaCO_3$ precipitation called “vital effect”.

Therefore, it is concluded that that *Porites* and *Porites* micro atolls are suitable to reconstruct past sea level variations and the SST of the past. Diagenetic alternations need to be taken into consideration before SST reconstruction from fossil corals. Here it was shown that micro-scale sampling allows accurate SST reconstruction by careful skeletal sampling.

Acknowledgment

All the praises and thanks are to Allah (S.W), the Lord of mankind, jinn and everything that exist and peace be upon prophet Muhammad (S.A.W) who is the master of the Messengers.

I wish to express my sincere gratitude to my supervisor Prof. Dr. rer. nat. Anton Eisenhauer for giving me this opportunity to carry out my PhD work at GEOMAR - Helmholtz Centre for Ocean research Kiel and for his continuous support that include knowledge, time and experience throughout my study, without his support the success of this work would not be possible. I am also thankful to Prof. Dr. rer. nat. Wolf-Christian Dullo for accepting co-supervision of my PhD study. Thanks go to Prof. Dr. rer. nat. Martin Frank for accepting being a chairperson of my examination committee. Words cannot sufficiently express my gratitude to Prof. Dr. Martin Wahl for introducing me to my supervisor during my PhD application.

Special thanks should also go to my advisor Dr. Volker Liebetrau for his guidance, constructive criticisms, help, support, advice and encouragement during the entire period of my work. I am grateful to Dr. Jan Fietzke, Dr. Florian Böhm and Ana Kolevica for their untiring explanations and sharing their knowledge with me during the whole period of my study. Many thanks to Tyler Goepfert for fruitful discussions that benefit a lot in my PhD work. In addition, I am grateful to members of my group for their support during all time of my study and also to all members of GEOMAR that provided me support on one way or another to successful completion of my work.

My deep appreciation goes to my beloved mother “the symbol of my life” for her continuous support during the whole time of my life, without her I can’t imagine how my life would be at the moment. Special thanks to my family whose support and encouragements enabled me to reach to this stage. To my wife I say “You have been a symbol and source of motivation and support in my whole stay in Germany, thanks a lot”. Baba wangu: “You are the one that always keep me strong when I feel weak”. To Arif “I am always happy when I see you happily growing”. To Jamila “Your courage and kindhearted support will never be forgotten: sister indeed”. Finally, I would like to thank everyone whose contribution in one way or another has made this work a successful one.

The success of this PhD was possible through financial support of Deutscher Akademischer Austausch Dienst (DAAD) in collaboration with the Ministry of Education and Vocational Training of Tanzania (MOEVT) that facilitated my stay in Germany during my PhD period.

Chapter One

1. General introduction

1.1. Archives for past climate

Future climate predictions rely on understanding the climate in the past which proves to be a challenge for times that go beyond instrumental climate recordings (Gagan et al., 2000; Grottoli, 2001). Since there are no means of a direct measure the climate in the past, proxy indicators are relied as indirect indicators of these processes. Prior to instrumental records, reconstruction of the Earth climate history is only possible using physical, chemical and biological proxies that respond to environmental conditions. The application of a particular proxy for the paleo-climate reconstruction relies into the fact that, the characteristic of the incorporation of materials, deposition or the rate of growth of some materials in the archives have been influenced by the climatic conditions during the time of its formation (Bradley, 1999).

Paleo-climate records can be obtained from natural archives such as ice cores, tree rings, fossil pollen, corals, speleothems, lake and ocean sediments (Jones and Mann, 2004). Different proxies offer different time span of climatic history with different degrees of precision and record different aspects of climatic conditions. Together they provide many aspects of the history of the climate in the past. In order to apply these proxies for reconstruction careful calibrations and cross-validation procedures are necessary to establish a reliable relationship between a proxy indicator and the climatic variable or variables assumed to represent. This involves studies of modern climatic records of a proxy material to understand how and to what extent proxy is climate-dependent and this is transferred as a function through which the past climate can be estimated. Based on this knowledge, it is possible to have a good understanding of the extent and patterns of the climate variability that provides a better perspective for interpreting recent climate which could help to project the climate in the future.

1.1.1. Corals as environmental archives

Scleractinian corals are among others considered to be one or the most important archives in paleo-climate history (Corrège, 2006). This is because during calcification, they secrete $CaCO_3$ aragonitic skeleton and incorporate multiple of chemical signatures such as trace elements and isotopes reflecting the environmental conditions of the ambient sea water such as temperature,

salinity, upwelling or cloud cover and pH of water (Grottoli, 2001). This concept is used as basis for reconstructing different aspects of environmental history (Beck et al., 1992; de Villiers et al., 1995; Grottoli and Eakin, 2007; McCulloch et al., 1996; Min et al., 1995; Mitsuguchi et al., 1996; Schrag, 1999; Shen et al., 1996). Compared to other archives, corals offer continuous, undisturbed long chronological records reflecting climatic conditions during each stage of growth. However skeletal boring by organisms, grazing by fish or bleaching events can interrupt the growth or physiology of a particular coral and consequently affecting the reliability of a particular tracer (Corrège, 2006). Among the Scleractinia massive corals are considered to be most reliable climate proxy recorders because they are distributed throughout the tropical and subtropical waters. A massive skeleton form provides a wave-resistant structure that is more resilient to physical erosion. Furthermore, high growth rate (up to 1cm/year) and clear undisturbed annual skeletal banding offers excellent chronological control and sub-seasonal sampling (Felis et al., 2004). Reef building corals are usually found immediately below the sea surface to a depth of less than 50 meters in the ocean. For this reason they yield information on surface waters and on the upper thermocline (Corrège, 2006). Deep water corals live in the cold, dark waters of the oceans (more than 100 meters deep) and usually they record the information of deep oceans such as water temperature and ocean circulation of the deep sea environments (Goldstein et al. 2001; Gass & Roberts 2011).

1.2. Coral types and their nature

Corals comprise a large group of organisms belonging to the Phyllum Cnidaria and Class Anthozoa. They comprise more than 6000 species including sea anemones, sea fans and sea pansies (Barnes, 1987; Barnes and Hughes, 1999). Stony corals belong to the order Scleractinia which is primarily responsible for precipitating $CaCO_3$ skeletons which support and protect their tissues (Allemand et al., 2011). They are divided into two main groups, hermatypic corals and ahermatypic corals. Hermatypic corals live in clear, oligotrophic, shallow tropical waters within the photic zone. They are considered as the word's primary reef-builders. The driving force behind reef growth is the symbiotic association (mutualism) between coral polyps and the unicellular algae (zooxanthellae) which live inside the tissue of polyps. In this relationship zooxanthellae benefit from the nutrients derived from coral excretion, instead they provide food and carbon dioxide to the corals as a results of their photosynthesis as long as they receive

enough light and nutrients. Ahermatypic corals are not reef building corals and usually live in cold deep waters. They do not have mutualism with zooxanthellae instead they mainly depend on preying on zooplanktons that drift past the coral framework with currents (Rogers, 2004). Due to this, they have comparatively lower growth rates because they form insufficient carbonate materials to build the reefs. These corals are found in all regions of the oceans (tropics, temperate and polar) below the photic zone more than 1000m deep.

1.3. Anatomy of a hard coral

Hard corals are formed through precipitation of $CaCO_3$ skeletons by small invertebrate animals called polyps. Polyps are characterized by a limited degree of organ development. They have a ring of tentacles, a simple stomach (gastrovascular cavity) that opens only on one end with no central nervous system (Grottoli, 2001). Each polyp consists of three basic tissue layers: An outer layer (ectoderm), the inner layer (endoderm or gastroderm). Between ectoderm and endoderm there is a supporting structure less jelly-like layer of substance termed mesogloea which is secreted by the cell layers of the body wall (Barnes, 1987).

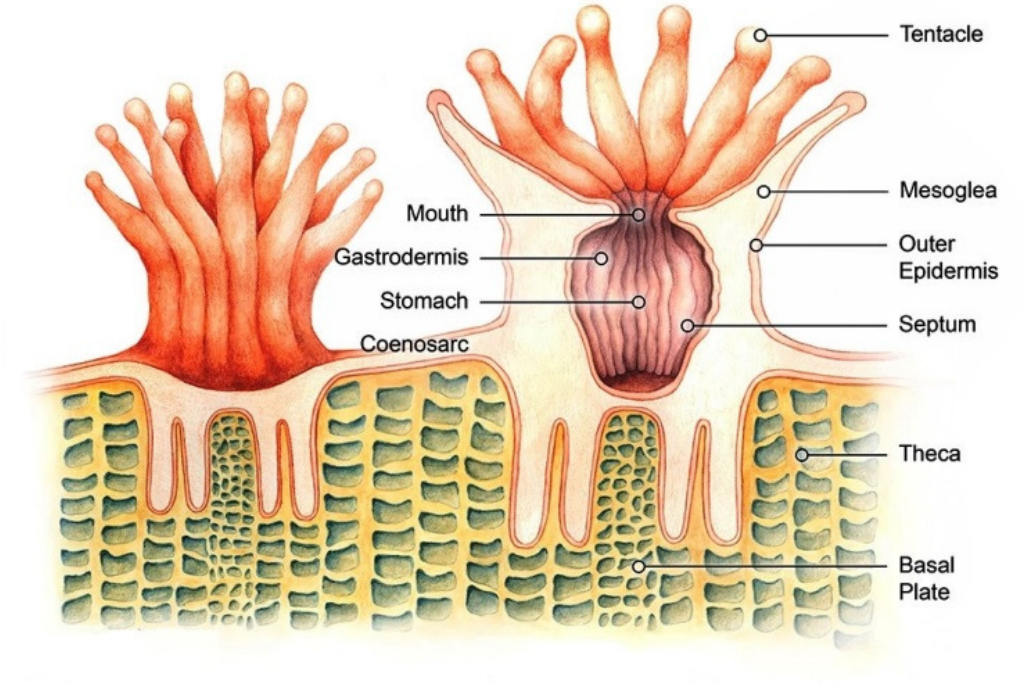

Figure 1: Anatomy of the coral polyp (Source: http://coral.org/coral-reefs-101/coral-reef-ecology/coral-polyps/)

The polyp is usually firmly attached to the base of the cup like structure where it sits. The stomach opens to single central opening which is used both to ingest food and to expel waste. This opening is surrounded by tentacles which serve for the tactile sense and food capture and for defense. The tentacles contain stinging cells, called nematocysts or cnidae that are used to attack the preys such as copepods, fish larvae, planktons (Barnes, 1987). In a colony they are united by a common tissue called the coenosarc. In case of hermatypic corals (reef building corals) that have symbiotic association with unicellular algae (zooxanthellae), these algae live within the cells of the coral's gastrodermis (Pernice et al., 2012).

1.3.1. Reef growth and development

As reefs grow the polyps deposit calcium carbonate as a skeletal structure beneath and around themselves, pushing the coral's head upwards and outwards. As new layers of the coral reef are built, the polyps leave the lower layers, therefore, only the top layer of a coral reef contains living polyps as shown in figure 1. Corals can exist as individual polyps, or colonial with hundreds to thousands of small polyps (Barnes, 1987). Scleractinian corals are colonial organisms composed of hundreds to hundreds of thousands of individual polyps (Barnes, 1987; Lalli and Parsons, 1995). In the colony each polyp is connected by living tissue to form a community. However, some corals, such as *Fungia* plate corals, are solitary and have single polyps that can grow as large as 25 cm in diameter (Kotpal, 2004).

1.3.2. Coral calcification

During calcification corals draws large amount of Ca^{2+} and inorganic carbon from the surrounding sea water to build up its skeleton (Allemand, 2004). At a very small scale (about a nanometer) the individual aragonite crystals ($CaCO_3$) are continually precipitated and arranged at the lower portion of the polyp using the following proposed chemical reaction:

$$Ca^{2+} + HCO_3^- \leftrightarrow CaCO_3 + H^+$$

However, the entire mechanism is more complex and not fully understood and is still under debate (Cohen and McConnaughey, 2003; Gaetani et al., 2011; Allemand et al., 2011). It is suggested that the extracellular precipitation of $CaCO_3$ is facilitated by calicoblastic cells (Weiner and Dove, 2003; Tambutté et al., 2011). However the pathway of ions from the sea

water to the area of calcification is not fully constrained. Some studies suggest that the paracellular pathway (transport of ions between the seawater and the calcifying fluid via diffusion or advection through the intercellular space of the cells) as a dominant pathway for calcification (Tambutté et al., 1996; Tambutté et al., 2011; Allemand et al., 2011). However, the transcellular pathway using Ca^{2+} mediated-ATPase pumps is also known to exist (Tambutté et al., 2011; Clode and Marshall, 2002; Allemand et al., 2011). During calcification process, the trace metals are also incorporated into the coral skeletal structure, this is further discussed in section 1.9. Periodically polyps lift their bases and deposit a new floor to their calyx as the means of growth (Barnes, 1987; Sumich, 1996).

1.4. Coral reefs distribution and habitat

The majority of reef building corals are restricted in warm waters of tropical and subtropical conditions at latitude between 30°N and 30°S. This is because higher calcification and growth rate of reef building corals require specific environmental conditions. Under optimal conditions, formation of large reef platforms is possible in the areas where temperature does not fall below 18°C for extended periods of time. However, in some areas coral species can tolerate temperature as low as 14°C (Veron, 2000) and as high as 40°C for limited period of time (Loya, 2004).

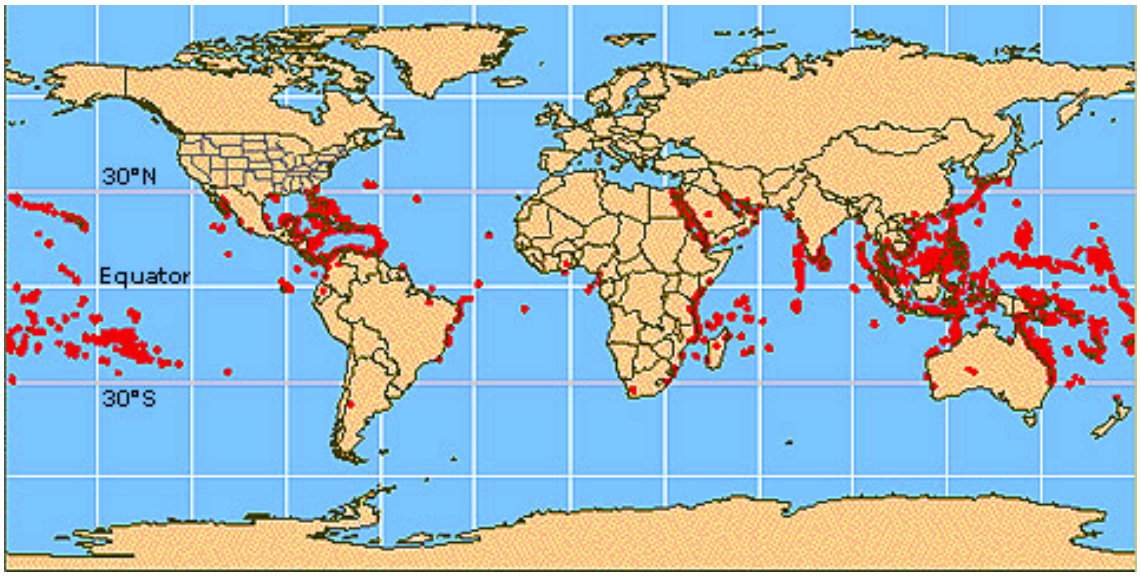

Figure 2: The global distribution of coral reef marked by red points (Source: http://oceanservice.noaa.gov/ education/kits/corals/media/ supp_coral05a.html)

Most of the coral reef can tolerate salinity range between 32-42‰. They require oligotrophic and clear water that permits high light penetration (Lalli and Parsons, 1995) that is why most of these corals are found in the photic zones of warm tropical oceans. The number of species and abundance decrease rapidly in deeper waters due to insufficient light that reduce the coral growth (Barnes, 1987).

1.5. Coral reef as an archive of sea level variation

Massive tropical corals like *Porites* are considered among others a paleo-sea level indicator due to their dense massive structure that is resistant to strong waves, mechanical breakage as well as erosion compared to branching species (Corrège, 2006). They grow between a few millimeters to 3 cm per year, forming annual growth bands which can be used for chronology (Grottoli 2001). In general, they grow from very close to sea level to ~25 m below sea level (Carpenter et al., 2008; Pratchett et al., 2013). Because of a large range of growth the normal massive *Porites* alone do not necessarily provide precise constraints on the position of local sea level. For this reason in Fossil *Porites* micro atolls are considered as a useful marker of the sea level (Woodroffe, C. D, 2005). *Porites* micro atoll put a distinct constraint on the position of a past sea level because they grow only a few centimeters below the sea level, their vertical growth is limited by the longer period of exposure at low tide (Flora and Ely, 2003; Smithers and Woodroffe, 2001; Woodroffe, C. D, 2005). In case of low availability of fossil micro atoll, a combination of normal fossil *Porites* and micro atoll in the reconstruction can help to reduce the depth uncertainty in the sea level reconstruction. Under normal conditions growth direction of the corals in the tropical oceans follows the water level (Davies and Marshal., 1980). When the sea level increases, the dominant direction is vertical. The still-stand position or falling of the sea level imposes restrictions on the vertical growth of a reef resulting into reef exposure (Davies and Marshal., 1980; Eisenhauer et al., 1999). Most of the corals tend to with stand short period of exposure, while longer periods are generally fatal and cause mortality.

Geological evidences from South Pacific and Indian Ocean islands (far-field areas) predicted that the sea level was ~1-3m above the present at ~6.5 ka (Mid Holocene) during the sea level high stand (Woodroffe and Horton, 2005). This was caused by the immense volumes of water from

the melting of ice sheets during the last interglacial resulting into raising sea level in regions which are far from the major glaciation centers (far-field locations). For the Late Holocene these areas experienced the relative sea level (rsl) drop to the present level (Banerjee, 2000; Deschamps et al., 2012; Eisenhauer et al., 1993; Woodroffe and Horton, 2005).

The concept of rising and falling of the sea level in the far-field areas is governed by the theory concerning the former ice sheets dynamics and Glacial Isostatic adjustments (Lambeck et al., 2002; Milne et al., 2009; Mitrovica and Milne, 2002) that induce water migrations through the process. During the Last Glacial Maximum (~20,000yrs ago) the weight of continental ice sheets was exerting the downward pressure causing deformation of the crust that forced sub-lithospheric flow of mantle away from the centers of load that has caused the low geoid in these areas. This in turn caused formation of the fore-bulge (flexural bulge) around the ice load (Fig. 3a). The ice sheets exerted a gravitational pull of the ocean water causing a slight sea level increase in the around these areas (Mitrovica and Milne, 2002). During deglaciation the lack of gravitational pull which was previously exerted by ice mass on the ocean water resulted in a sea level drop nearby the formerly glaciated area and in a sea level rise higher than the eustatic value at the opposite end (Mitrovica and Milne, 2002; Woodward, 1888). Therefore, the ocean averaged sea level change exactly corresponds to the eustatic change (Suess and Waagen, 1888), but the local sea level change may be significantly different, or even opposite in sign depending on gravity and the distance from the former ice masses. Because the load of ice decreases as the ice melt, the formerly glaciated areas undergo isostatic rebound (rise of the land mass) which is caused by sub-lithospheric flow back of the mantle towards the unloaded former glaciated regions inducing the collapsing of the fore-bulges in order reach new isostatic equilibrium (Fig. 3b).

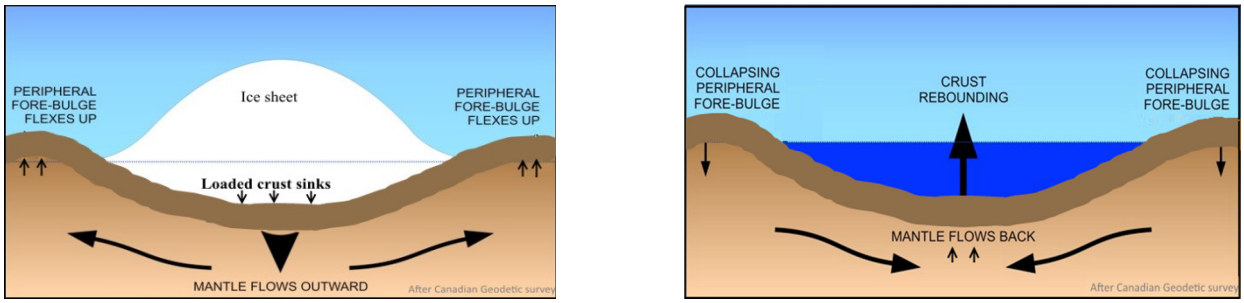

Figure 3a: Illustrates the downward pressure exerted into the Earth lithosphere forcing sub-lithospheric flow of mantle away from the centers of load to form the fore-bulges on the periphery of the ice cover. Figure 3b: Isostatic rebound of the Earth crust as a result of melting of the continental ice sheets causing for-bulges to sink as a result of mantle flowing away from the bulges.(Source: http://xenon.colorado.edu/spotlight/index.php?product=spotlight&station=CHUR).

This resulted into the so called "Ocean siphoning effect" migration of water from the far-field equatorial oceans towards the subsiding peripheral fore bulges (near-field areas) to fill the space vacated by these subsiding bulges (Fig. 4) causing sea level regression in the far-field areas (Mitrovica and Milne, 2002). Note, an increase in gravity of the rebound areas also add an effect (gravitational pull) on the migration of water towards the near-field areas.

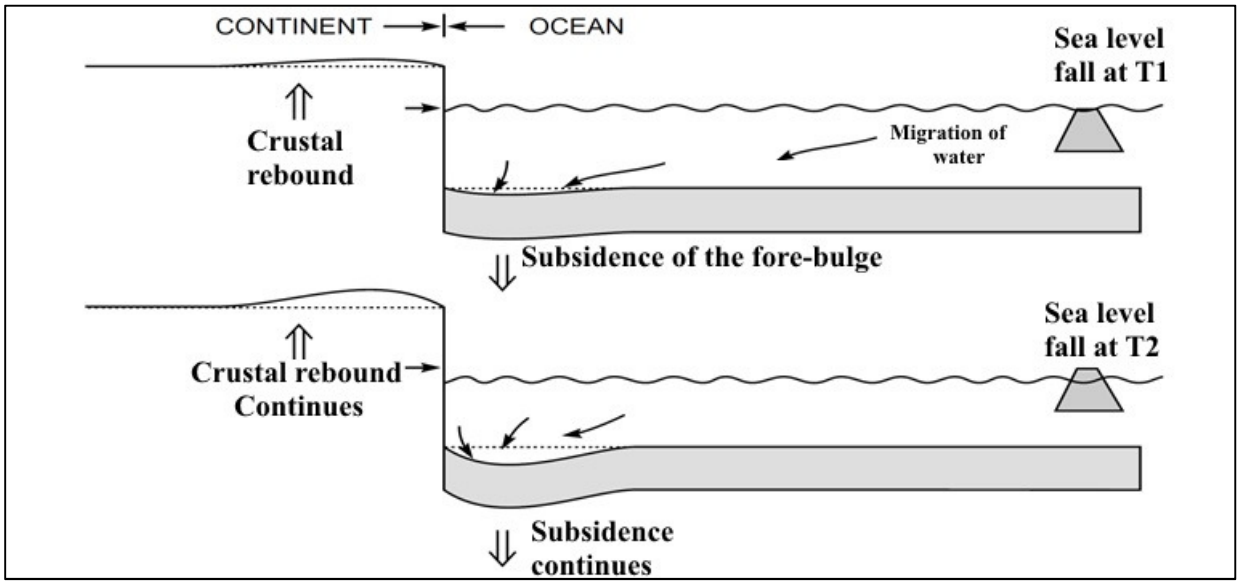

Figure 4: Isostatic rebound (crustal rebound) of the Earth lithosphere to maintain isostatic equilibrium (Source: Mitrovica and Milne, 2002). This causes the collapse of the fore-bulge that induces migration of water to the near field areas to fill the space vacated by collapsing fore-bulges. As a consequence, the sea level fall in the far-field equatorial regions that resulted into exposure of the coral platforms along the coastal areas of the far-field regions. These are the characteristic platforms that are found in the Pacific and Indian Ocean.

As a consequence of sea level regression, the coral reefs developed extended emerged fossil reef platforms (Fig. 5) which are currently 1-3 m above the modern sea level (Eisenhauer et al., 1999; Eisenhauer et al., 1993; Grossman et al., 1998; Montaggioni and Pirazzoli, 1984; Pirazzoli et al., 1988; Rashid et al., 2014; Woodroffe and Horton, 2005). These platforms are characteristic of Chagos Islands, Cocos (Keeling), Maldives, Laccadives in Indian Ocean and most of islands in the Southern Pacific Ocean (Eisenhauer et al., 1999; Montaggioni and Pirazzoli, 1984; Pirazzoli et al., 1988). Barbados is described by Pirazzoli (1996) as being located in an intermediate field site which corresponds to the peripheral bulge around a former ice margin. This tends to subside in late and post-glacial times, to compensate the uplift in nearby formerly glaciated areas.

Figure 5a: Exposed fossil reef platform in Moorea Island that was formed as a consequence of migration of water away from these areas as a result of ocean siphoning effect. Figure 5b: Fossil *Porites* in growth position (*in situ*). Figure 5c: Fossil *Porites* micro atoll in growth position. These images were taken during our field study.

To reconstruct sea level variations for these platforms which are currently exposed above the present sea level the elevation of an exposed fossil coral relative to present mean sea level and its age estimate (either by ^{14}C or U/Th dating) is used. For islands of volcanic origin (e.g. Society Islands), the island's specific subsidence rate needs to be applied in order to constrain the actual height of a sample above the sea level (Rashid et al., 2014).

1.5.1. The principle applied for coral U/Th age dating

Corals can be accurately dated using U-series disequilibrium method which is based on the radioactive decay of radionuclides within the naturally occurring decay chains. Dating of fossil corals is done by measuring concentrations of radioisotopes incorporated within the skeletal matrix at the time of accretion (skeletogenesis) and the concentration of the daughter nuclei that have grown with time since accretion (Bourdon et al., 2003). For U/Th dating of corals we consider ^{238}U as the original parent taken from the sea water and ingrowth of the ^{230}Th as the daughter nuclei (decayed from the parent nuclide) within the coral skeleton. In this case it is assumed that during skeletogenesis ^{230}Th is not incorporated into the skeleton due to its insolubility in the sea water, and the system remains closed after deposition (U and Th are not remobilized). In nature uranium mainly exists in two oxidation states (U^{4+} and U^{6+}). The U^{6+} is soluble and appears to be dominant in the form as uranyl ion and in various uranyl carbonate forms (*Edwards et al., 2003*). The U^{4+} is insoluble and thus far less mobile. In contrast to uranium Th is insoluble in natural waters. Because it is particle reactive, once transported into the sea water it is adsorbed to particles or minerals and settles mostly at the bottom waters in sediments.

During skeletogenesis (formation of skeletal $CaCO_3$) corals incorporate uranium from the seawater in the $CaCO_3$ crystal matrix and almost free of ^{230}Th. Fractionation between the different U isotopes (^{234}U and ^{238}U) does not occur during coral growth therefore distribution of $^{234}U/^{238}U$ ($\delta^{234}U$) in the ocean is homogenous at an average of 149.6±3 ‰ (*Delanghe et al., 2002*).

As time passes ^{234}U in the sample, with a half-life of 245,250±490 years, decays to ^{230}Th (Cheng et al., 2000). The decay of excess ^{234}U and the growth of ^{230}Th can be expressed as a function of age (Kaufman and Broeker, 1965) under the following criteria:

1. The sample should have primary aragonitic skeletal structure.
2. The carbonate should remain a closed system with respect to uranium and its decay products.
3. Uranium ^{238}U concentration should reflect the modern analogues from the same region.
4. The initial $\delta^{234}U$ values should lie within the range of modern corals and sea water between 141‰-157‰.

5. The ^{232}Th concentration should be <2 ppb
6. Abundance of calcite from X-ray diffraction must be below detection limits (<1% calcite)

Unfortunately the assumption that initial incorporation of uranium from the sea water is free from ^{230}Th during skeletogenesis is not fulfilled (Edwards et al., 2003) therefore, correction of initial non radiogenic ^{230}Th (detrital) is necessary. Since it is not possible to distinguish between the radiogenic and detrital ^{230}Th, therefore, ^{232}Th is used as an indicator of detrital contamination because it has the same chemical properties as ^{230}Th. Note that, the formula applied for age calculations and the detrital corrections are shown in the methodology (section 2.3. 2). Only U-series ages that fulfil all these requirements are considered to be reliable and can be used for paleo-climate reconstructions.

1.5.2. Corals as archives for sea surface temperature (SST) reconstruction

Massive scleractinian corals offer a reliable tool for estimating environmental and climatic parameters to the time period beyond instrumental records. This is because they incorporate chemical signatures (elements) from the ambient sea water during calcification process (Felis and Pätzold, 2004). The behaviors of many of these elements (isotopes to trace metals) are believed to be more or less controlled by external environmental conditions of ambient sea water, thus providing us with an ability to use them as a reliable tracer (Corrège, 2006). Several proxies such as Mg/Ca, Mg/Li, B/Ca have been proposed for SST estimates but their robustness have not yet completely proved (Gagan et al., 2000; Oomori et al., 1983; Min et al., 1995; Mitsuguchi et al., 1996; Quinn and Sampson, 2002; Shen and Dunbar, 1995; Watanabe et al., 2001). Currently δ^{18}O isotopes, Sr/Ca and U/Ca are commonly used for paleo-temperature studies where Sr/Ca is considered to be the most promising proxy in reconstructing the past climate history. However, U/Ca proxy is still not very well established (Min et al., 1995). Proxy evidence of paleo-climate reconstruction helps a better understanding the climate system that allows analysis of the current climate into a broader context which improves projections of future climate. The use of multi-proxy approach improves the strength of paleo-climate reconstruction because it combines the information from different proxies that uses advantage of the strengths of one proxy and minimizes the limitations of some other proxies.

1.6. Oxygen isotopes ($\delta^{18}O$) in corals

Coral skeletal $\delta^{18}O$ isotopes are considered to be the most commonly used proxy for SST reconstruction. This is because the composition of this isotope in the aragonitic skeleton depends on water temperature and also isotopic composition of the sea water. The $\delta^{18}O$ isotopes of the aragonitic coral skeleton represent an inverse relationship with sea water temperature i.e. as the sea surface temperature increases the $\delta^{18}O$ values of the precipitated oxygen in the coral skeleton decreases due to temperature-dependent kinetic fractionation effects (Kim and O'Neil, 1997). However, significant variations exist between corals of different species or between different locations (e.g.Weber and Woodhead, 1972;Weil et al., 1981; Carriquiry et al., 1994; Wellington et al., 1996; Cardinal et al., 2001). Studies have shown that 1°C increase in sea water temperature corresponds to ~0.18‰ - 0.22‰ (slope) decrease of $\delta^{18}O$ precipitated in the *Porites* coral skeleton (Cahyarini et al., 2008; Cohen and Hart 2004; De Long et al., 2010; Evan et al., 1999; Felis et al., 2012; Grottoli, 2001; Corrège, 2006; McCulloch et al., 1994; Quinn et al., 1996; Wellington et al., 1996), some of these slopes are shown in the figure 6 below. In coral SST calibrations the slopes can vary depending on location, depth and coral species (Weber & Woodhead 1972; Wellington et al. 1996). Even if the calibration equations have the same slopes, the species difference or location difference might lead to erroneous SST estimation. It is therefore essential to be aware of the uncertainties that may arise if one fails to consider these contributing factors when attempting to accurately reconstruct paleo-climatic conditions.

It is also known that, the oxygen isotopic composition of sea water varies with local evaporation-precipitation balance i.e. the seawater $\delta^{18}O$ decreases as precipitation increases (Fairbanks et al., 1997). Therefore, large and significant precipitation can decrease the surface salinity and seawater $\delta^{18}O$ which is reflected in the coral skeleton. For example, study of Grottoli and Eakin, (2007) has indicated that, $\delta^{18}O$ isotopic composition of sea water decreases by 0.27‰ for each 1p.s.u. decrease in salinity depending on latitude, depth and ocean basin.

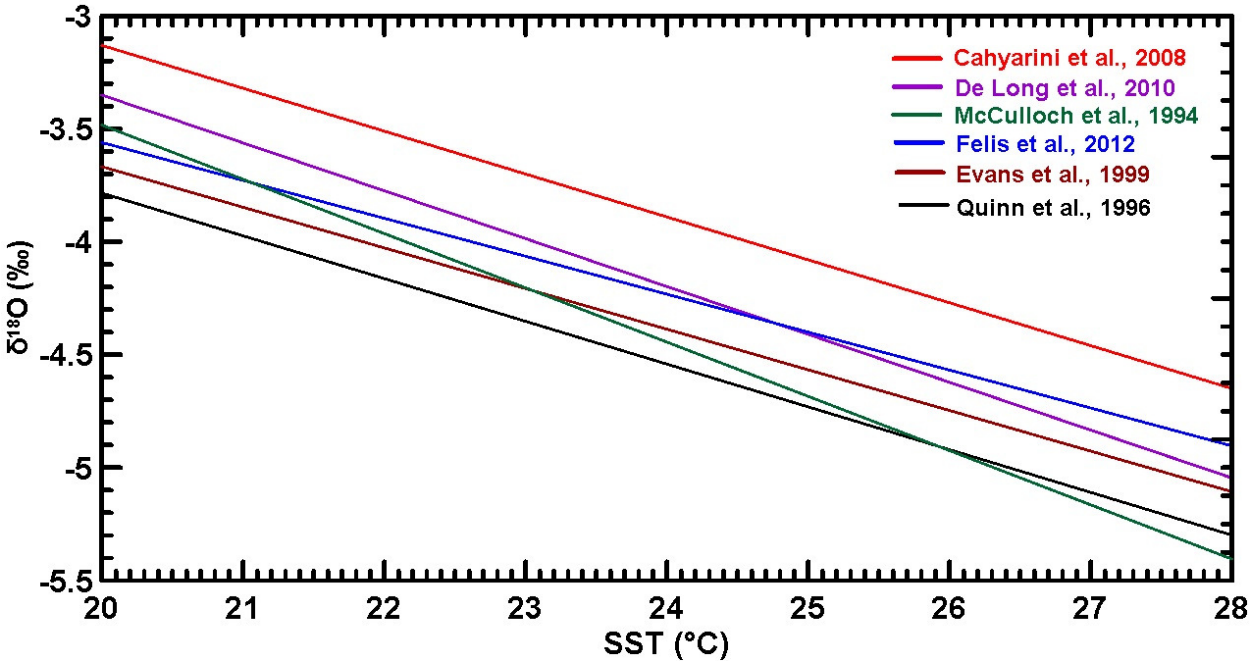

Figure 6: The δ^{18}O-SST calibrations (slopes) published from previous researches in Central and Southern Pacific Ocean using *Porites* sp.

Corals that live in regions where salinity is relatively constant throughout the year, coral δ^{18}O records are primarily recording SST variability. However, in regions where salinity varies significantly might dominate the δ^{18}O isotope signal of the sea water. In cases both SST and salinity are highly variable, the interpretation of this proxy might be challenging. Other factors such as skeletal extension rate, light intensity and feeding rate might also influence the skeletal δ^{18}O. However, there is still controversy concerning these factors (Corrège, 2006). In addition, the aragonite deposited by scleractinian corals is usually depleted in δ^{18}O isotope relative to equilibrium with ambient seawater. This disequilibrium is a control of the coral physiology related to zooxanthellae photosynthesis and algal and coral respiration which is generally referred to as "vital effect" (Allemand et al., 2004; McConnaughey, 1989).

1.7. Sr/Ca ratios in corals

The Sr/Ca ratio of the coral skeleton is considered as a more reliable proxy of paleo-temperature due to its strong temperature dependent in its incorporation into the coral skeletons. An increase in SST causes the decrease in the Sr/Ca ratio in the coral skeleton and vice versa (Beck et al., 1992; Gagan et al., 1998; McCulloch et al., 1994). Compared to δ^{18}O isotope, this proxy is not

influenced by salinity changes of the sea water hence it is considered as a direct tracer of the sea water temperature (Weber, 1973; Beck et al., 1992). In fact, the Sr/Ca in the coral skeleton is influenced by the Sr/Ca ratios of the ambient sea water during skeletal precipitation (Felis and Pätzold, 2004). Because of the long residence times of Sr (5.1 $x10^6$ yr) and Ca (1.1 $x10^6$ yr) in the oceans (Guilderson et al., 1994), Sr/Ca ratio has been assumed to remain essentially constant in the ocean on glacial-interglacial time scales (de Villiers, 1999; Edmond, 1992; Marshall and McCulloch, 2002). It has been reported that the Sr/Ca values from the surface oceans range between 8.5-8.7 mmol/mol (de Villiers et al., 1994; de Villiers, 1999; Kinsman, 1969). However the average value of the shallow water from Pacific and Atlantic Ocean is 8.539±0.0045 mmol/mol (de Villiers, 1999). This is considered to be the representative Sr/Ca ratio of the oceans. However, significantly high Sr/Ca ratios in the shallow waters are characteristic of upwelling zones of the oceans (de Villiers, 1999). Considering the SST estimates, the slopes of the calibration equations do not seem to vary markedly for individual corals inhabiting the same site. However, there are variations of slopes between the colonies from different locations (de Villiers et al., 1994). The slopes of Sr/Ca calibrations range between 0.0597 to 0.062 mmol/mol per 1°C (Gagan et al., 2000; Marshall and McCulloch, 2002; Felis and Pätzold, 2004).

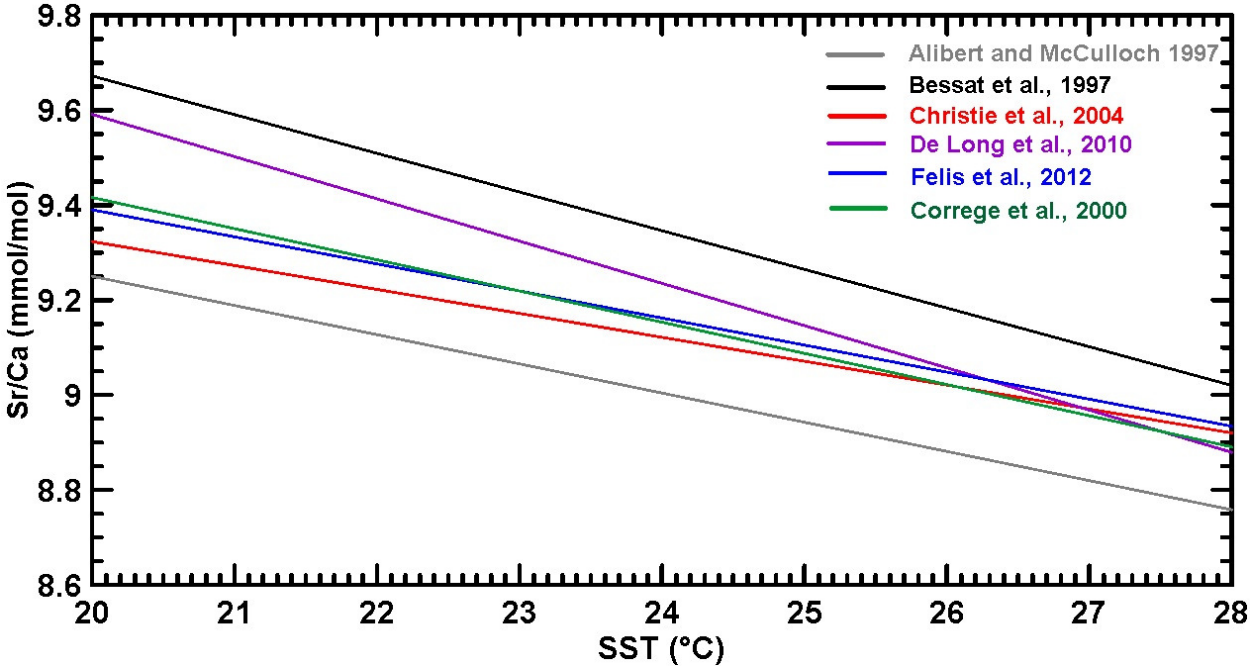

Figure 7: Sr/Ca-SST calibrations (slopes) published from previous researches in Central and Southern Pacific Ocean using *Porites* sp.

1.8. U/Ca ratios in corals

Skeletal U/Ca has been proposed to be a proxy for temperature (Min et al., 1995; Shen and Dunbar, 1995). This is because the incorporation of this proxy depends on the temperature of the ambient sea water. Despite its sensitivity to temperature, this proxy is still not well established and it is bound to many uncertainties (Min et al., 1995; Quinn and Sampson, 2002). For example, Quinn and Sampson, (2002) have reported that the strength of its correlation to temperature varies as a function of time. Previous studies (Min et al., 1995; Shen and Dunbar, 1995; Cardinal et al., 2001) have demonstrated that incorporation of this proxy in the corals skeleton is also influenced by SST, salinity, pH and uranium speciation. These facts bring questions to the potentiality of this proxy that led to suggestion that variations of this proxy not entirely as a function of temperature, but other environmental parameters might also influence the incorporation of uranium in coral aragonite. This is mainly due to the complex chemical behavior of uranium in seawater and to its relatively unknown mode of incorporation in aragonite (Min et al., 1995; Pingitore et al., 2002, Lazar et al., 2004). In general combination of different proxies (multi-proxy approach) in SST reconstruction is vital to a reliable SST estimation. This is because the combined information from different proxy types takes the advantage of the strengths of some proxies and minimizes the limitations of individual proxies.

1.9. Challenges in SST and sea level reconstruction in corals

Nowadays most of the researches in paleo-climatology are focusing on massive scleractinian corals (e.g. *Porites*) in paleo-climate reconstruction. This is because they live in the shallow waters of tropical and subtropical areas. In addition, modes of some elements which are incorporated during skeletal growth are linked to variation of environmental conditions (e.g. SST) of ambient sea water. However, modification in incorporation of these elements (by coral polyp) during skeletal formation known as "vital effects" (Allemand et al., 2011) which have crucial impact on the application of these proxies are still not fully constrained (e.g. Adkins et al., 2003; Meibom et al., 2006; Juillet Leclerc et al., 2009). There are still ongoing researches in order to understand this process (Tambutté et al., 2011). In addition species-specific variation in skeletal composition poses a limitation making it challenging to use of some proxies especially those ones which are not well established (Maier et al., 2004).

For Sr/Ca ratio as a paleo-SST proxy, there is still ongoing subject about Sr/Ca heterogeneity in a micro-scale level within a coral skeletal structure (Allison et al., 2001). To resolve this issue, a better understanding of incorporation mechanism of Sr^{2+} and Ca^{2+} within the skeleton is essential to determine the robustness of this proxy as a paleo-thermometer (Corrège, 2006). Two theories have been proposed about uptake mechanisms of these elements from the sea water to the coral skeleton (Corrège, 2006). One theory has suggested that Sr^{2+} and Ca^{2+} are transported into the coral skeleton by a similar active transport pathway (Ferrier-Pagès et al., 2002) while another theory suggested the passive transport (diffusion) of Sr^{2+} and active transport (using Ca^{2+}ATPase pump) for Ca^{2+} (Sinclair and Risk, 2006). Since Sr^{2+} is suggested to substitute for Ca^{2+} in its incorporation into the coral skeleton, Sr^{2+} ion incorporation might probably follow the same pathway as Ca^{2+}. Al-Horani et al., (2003) explained the light activation of coral Ca^{2+}ATPase pump during the day that favors Ca^{2+} over Sr^{2+} and therefore, in the day time the coral skeleton is Sr^{2+} depleted. During night time, the potential of Ca^{2+} transport by ATPase pump is reduced and therefore the passive pathway dominates which favors Sr^{2+} incorporation. Incorporation of uranium from the sea water into coral skeleton as either UO_2^{2+} (uranyl ion) as proposed by Broecker and Peng, (1982) or as $UO_2(CO_3)^{2-}$ (uranyl carbonate) by Shen and Dunbar, (1995) is unclear and still under debate.

There are also unresolved issues on variations of Sr/Ca ratio in different skeletal parts of the coral skeleton. Growth rate differences are also assumed to influence the uptake of Sr^{2+} in corals and subsequently affect the Sr/Ca SST proxy (de Villiers et al. 1995). Cohen and Hart (2004) found differences in Sr^{2+} uptake as a result of growth rate differences during winter and summertime within the same species of coral. However, some studies have documented that the amount of Sr/Ca is more representative of the ambient environmental conditions along the maximum growth axis of a skeleton (Alibert & McCulloch 1997; Gagan et al. 1998; Wei et al. 2000; Corrège et al. 2004). There are also differences in Sr/Ca ratio within the corals of the same species living in the same locality under the same conditions (de Villiers et al. 1995; Alibert and McCulloch 1997; Reynaud et al. 2004). Resolving these issues might be useful to determine the robustness of Sr/Ca and its important role in paleo-thermometry.

Post depositional change of coral chemistry (diagenesis) is considered as a major source of error in paleo-reconstruction studies (Enmar et al., 2000; McGregor and Gagan, 2003; McGregor and Abram, 2008) because it is violating the "closed system behavior". This is common in fossil corals which have been exposed to freshwater or sea water for a longer period of time but has also been documented in coral colonies that are less than 50 years old (Nothdurft and Webb, 2009). The main challenge to SST reconstruction is caused by early diagenesis (submarine secondary aragonite precipitation or dissolution of primary aragonite skeleton), because common methods like X-ray Diffraction fail to distinguish between primary and secondary aragonite phases (earliest diagenetic phase) since they have the same mineralogy as the primary aragonite. Studies have reported that inclusion of less than ~10% secondary aragonite yields cooling artifacts of up to -3°C and -2°C in the corresponding paleo-SST reconstructions for SST-Sr/Ca and SST-$\delta^{18}O$ respectively (Nurhati et al., 2009). Therefore, petrographic analysis of the samples prior to analysis might help to identify the incorporation of the secondary phase within the skeletal chemistry; otherwise the results might include some bias in SST estimates (Allison et al., 2007; McGregor and Gagan, 2003; Lazar et al., 2004).

For the islands of volcanic origin there are still some concerns about the subsidence rates of these islands in reconstructing the sea level. Few studies have focused on the assessment of the subsidence rates of the Society Islands mostly on Tahiti Island using GPS, satellite data, tide gauge measurements, model predictions, and coral reef stratigraphy (e.g. *Fadil et al.,* 2011), also coral chronology, $\delta^{18}O$ and diagenetic overprint of the uranium–thorium system (*Thomas et al.,* 2012). For Moorea, Huahine and Bora Bora, Pirazzoli et al., (1985) and Pirazzoli and Montaggioni, (1985) conducted a study based on petrological analysis of emerged reef conglomerate available on the shorelines of the islands. The analysis was based on the close inspection of thin sections of exposed coral reef conglomerates. They estimated the subsidence rate of 0.14mm/year for Moorea and 0.05mm/year for Bora Bora. However they argued that Huahine to have similar subsidence rate as Moorea (without specific estimate) although they are located 148km apart from each other. Considering the effect of differential geoid distortion as a function of the local gravitational field (Woodroffe et al., 2012) the island's specific subsidence rates should be available in order to have a precise reconstruction.

Chapter Two

2. Materials and methods

2.1. Study area and sample location

Society Islands are one among the five archipelagos (Marquesas, Toamotus, Gambier, Austral and Society Islands) of French Polynesia (Fig. 1a). This archipelago comprises more than ten islands and atolls elongated in 17°52'S 149°50'W and 15°48'S 154°50'W direction which spread 720km across the Pacific Ocean (Duncan and McDougall, 1976; Montaggioni, 2011; Peltier, 2002; Pirazzoli and Montaggioni, 1988).

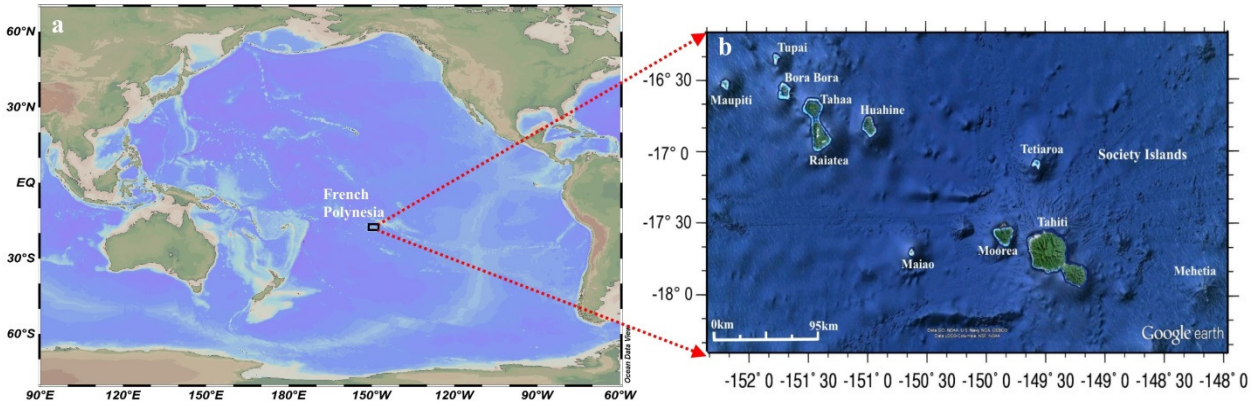

Figure 1a: Geographic location of French Polynesia in the Pacific Ocean where Society Islands are located. Figure 1b: Society Islands distribution relative to the volcanic hotspot (Mehetia).

Society Islands are volcanic in origin formed from hotspot which is currently located around Mehetia Island ~110 km east of Tahiti (Gripp and Gordon, 1990; Devey et al., 1990). These islands extend parallel to the present absolute motion of the Pacific plate which moves at with the rate of ~110mmyr^{-1} relative to the fixed hotspot plume (Blais et al., 2002; Neall and Trewick, 2008). Society Islands are subdivided into Windward and Leeward Islands based on the position of the islands relative to the dominant southeast trade winds. The Windward Islands comprise of Mehetia, Tahiti, Moorea, Maiao and Tetiaroa while the Leeward Islands are Huahine, Bora Bora, Raiatea, Tahaa, Maupiti, Tupai, Maupihaa, Motu One and Manuae (Fig. 1b). This islands chain shows an age progression from east to west direction for example, Mehetia is less than 1 Ma, Tahiti (~0.25–1.67 Ma), Moorea (1.36–2.15Ma), Huahine (2.06-3.08 Ma), Raiatea (~2.29–2.75 Ma old), Tahaa (~1.10–3.39 Ma), Bora Bora (3.1–3.5Ma) and

Maupiti is ~5 Ma (Blais et al., 2002; Duncan et al., 1994; Guillou et al., 2005; Uto et al., 2007; White and Duncan, 1996). Because of their volcanic origin, these islands tend to subside as they move away from the hotpots region (Fadil et al., 2011; Pirazzoli and Montaggioni, 1985; Scott and Rotondo, 1983). This is because as the Earth plate (Pacific plate) moves away from the asthenospheric bump (hotspot) it is progressively cooling and subsiding as it moves down the slope of asthenospheric bump with increasing age and distance (Scott and Rotondo, 1983). This could also explain the presence of as Tahiti a high island near the original hotspot and almost atoll islands (such as Bora Bora at ~400km away) and atolls (Tupai, Maupihaa, Motu One) on further increasing distance from the original hotspot. However, the rate of subsidence decreases with time and distance from the original hotspot (Scott and Rotondo, 1983).

2.1.1. Climate

The climate of the Society Islands is tropical characterized by two main seasons, the austral summer and austral winter. The austral summer is the warm and rainy season that spans from November to April. During this period, the conditions are hot and humid with the average SST in the order of ~28°C and 29°C (Delesalle et al., 1985; Boiseau et al., 1998). Heavy rains are mostly experienced during December and January which are the most intense rains along the coastline. The average rainfall is ~2753 mm/year (Cabioch et al., 1999; Neall and Trewick, 2008). The austral winter is normally from May to October. This period is marked by low sea surface temperature averages between 23°C and 25°C and rarely reaches below 19°C (Delesalle et al., 1985). The trade winds generally blow from East (South-East) and North-East direction. Westerly winds are infrequent and span for short duration. Tides are semi-diurnal and do not exceed 0.4 or 0.5m during spring tides (Delesalle et al., 1985; Seard et al., 2011). According to National Oceanic and Atmospheric Administration (NOAA) tide information, the average tidal amplitude for these islands is 0.5 m (NOAA, 2013).

2.2. Sample collection

Fossil coral samples were collected in 2009 during CHECKREFF expedition in the Southern Pacific. This area is characterized by emerged (exposed) coral platforms which are currently exposed above the modern sea level as a consequence of sea level fall (Late Holocene). Fossil samples of *Porites* and *Porites* micro atoll were taken (digged) from emerged coral platforms at

Moorea, Huahine and Bora Bora islands from their original growth position at the height between -1.5 m below the present mean sea level (bpmsl) to +1.5 m above the present mean sea level (apmsl) using hammer and chisel. The elevation of the collected coral samples was determined by triangulation of the coral´s position to the current position of the mean sea level. This was done by placing a laser on top of the sample with the beam pointing horizontally towards the water table. Using a meter rule, the measurement of the elevation was determined relative to the water level. The process was repeated up to 15 times where by each time the elevation and the local time are recorded. These elevations were also compared to our GPS measurement during each time. Using tide table and the local time, the elevation relative to the mean sea level was achieved.

2.2.1. Sample Processing

Using a wet disc saw the selected samples were cut into slabs along the growth direction. The slabs were washed with Milli-Q water and dried at room temperature in a clean lab fume hood. Then a hand held diamond saw was used for further cutting each sample into smaller blocks ($1cm^3$) within the parallel growth bands. In order to have pristine samples for analysis, parts that are visually free from any algal or carbonate infill of the pore volume were carefully selected for sampling. The sample blocks obtained were cut into two parts (pieces) which are mirror image to one another. One part was further cut into small chips and transferred into 15ml Teflon beaker for ultrasonic cleaning and another part of the block was kept for petrographic analysis.

2.2.2. Ultrasonic cleaning of samples (Ultra-sonification)

Ultrasonic cleaning started with an ultrasonic bath available in GEOMAR, Kiel. To perform this, each Teflon beaker containing chips were filled with ~8mls of 18.2MΩ Milli-Q water. The closed beakers were transferred into ultrasonic bath for 15 minutes. Milli-Q water was then discarded and the beaker is rinsed with Milli-Q water. The process was repeated again with fresh Milli-Q water for another 15 minutes. The Milli-Q water was then discarded and the clean samples were then transferred into a hot plate and dried at ~35°C overnight. Each sample was then ground into a fine powder using mortar and pestle. In order to avoid cross contamination, the mortar and pestle were cleaned with Milli-Q water and then with ethanol between each sample.

2.2.3. X-ray diffraction

For analysis of sample mineralogy ~100mg of homogenized powdered samples were analyzed using X-ray diffractometer (Philips X-ray diffractometer, goniometer with an automatic divergence slit and monochromator). The equipment uses a cobalt (Co) cube with 40kV and 35mA for the measurements. The measurements were done in steps of 0.01sec-1 at an angel (2θ) between 20° to 50°. Identification of crystalline compounds was done using XPowder (Ver. 2004. 04. 80 with PDF2 database provided by ICDD (International Center for Diffraction Data). Quantification of mineralogy (%) was done using the standard calibrations done at GEOMAR, Kiel. All the samples with detectable amounts of calcite were excluded from further analysis. For powdered samples with no detectable amounts of calcite ~50-100mg was taken for U/Th dating (age estimation), ~10-25mg for elemental analysis and a small part (~100µg) was taken for C and O isotopes measurements (described in section 2.5.2).

2.3. U/Th geochronology

The uranium and thorium isotopes of the powdered samples were used for age estimation. To achieve this 100µl of spike containing a mixture of $^{233}U/^{236}U/^{229}Th$ (commonly known as double spike, mixed spike or combined spike) was added into each sample, then each sample was dissolved in 10mls of 4.5HNO_3. The whole procedures involve the blanks (for tracing the whole procedure contamination) and HU1 standard (to calibrate for Th and U of the combined spike) which are added and treated as samples.

2.3.1. Separation of uranium and thorium (ion exchange separation)

Uranium and thorium separation from the sample matrix was done using vacuum columns and Eichrom-UTEVA resin filters at GEOMAR, Kiel. The whole procedure involves four main processes: Washing of the columns, conditioning of the columns, loading the sample solution into the columns and collection of thorium and uranium into the Teflon beakers. Separation was done via vacuum columns and Eichrom-UTEVA resin filters. Initially the columns have to be washed with 10 ml 4.5N HNO_3 followed by 10 ml 4.5N HCl and 10 ml 0.02N HCl, then the whole washing process was repeated. For conditioning, the columns were again flushed with 10 ml 4.5N HNO_3. Afterwards the 10 ml of the sample solutions were loaded into the columns and washed with another 10 ml 4.5N HNO_3. Now the thorium can be extracted from the filters by

running 8 ml 4.5N HCl. The acid with the dissolved thorium was then collected in clean Teflon beakers. To extract the uranium 6 ml 0.02N HCl were loaded and allowed to run through the columns.

2.3.2. Uranium/Thorium age determinations

Uranium series measurements of coral ages were performed at GEOMAR, Kiel, Germany. Determination of uranium and thorium isotope ratios was done using multi-ion-counting inductively coupled plasma mass spectroscopy (MC-ICP-MS: Axiom) using the approach of Fietzke et al. (2005). For isotope dilution measurements a combined $^{233}U/^{236}U/^{229}Th$-spike was used, with stock solutions calibrated for concentration using NIST- SRM 3164 (U) and NIST-SRM 3159 (Th) as combi-spike calibrated against CRM-145 uranium standard solution (formerly known as NBL-112A) for U-isotope composition, and against a secular equilibrium standard (HU-1, uranium ore solution) for the precise determination of $^{230}Th/^{234}U$ activity ratios. Whole-procedure blank values of this sample set were measured between 0.5 pg and 1 pg for thorium and between 10 pg to 20 pg for uranium. Both values are in the range typical of this method and the laboratory (Fietzke et al., 2005). The ages were calculated using the half-lives published by Cheng et al, (2000b) using the following equation:

$$[^{230}Th/^{238}U]_m - 1 = -e^{-\lambda_{230}t} + (\delta^{234}U_{measured}/1000)\,(\lambda_{230}/\lambda_{230} - \lambda_{234})\,(1 - e^{-(\lambda_{230} - \lambda_{234})t}) \quad (1)$$

Where m represents modern, t represents the age. The λ represents decay constants which are $9.1577 \times 10{-}6\ yr{-}1$ for ^{230}Th, $2.8263 \times 10{-}6\ yr{-}1$ for ^{234}U [Cheng et al., 2000], and $1.55125 \times 10{-}10\ yr{-}1$ for ^{238}U (Jaffey et al., 1971). The $\delta^{234}U$ represents $(^{234}U/^{238}U)$ activity ratio of a coral. The initial uranium activity ratio (i) during the coral formation can be calculated from the measured uranium activity ratio (m) using the relationship of radioactive production and decay assuming that diagenesis involving uranium has not occurred since the coral formation:

$$\delta^{234}U_m = (\delta^{234}U_i)\, e^{-\lambda_{230}t} \quad (2)$$

The initial ^{230}Th was corrected for any non-zero detrital ^{230}Th using the equation:

$$[^{230Th}/^{234}U]_{excess} = [^{232}Th/^{234}U] \times 0.6 \pm 0.2 \quad (3)$$

2.4. Microscopic observations

All sample blocks which are mirror images of the processed powders were observed using epi-fluorescence microscope (Type: Zeiss Axio Imager.M2, with the camera: Zeiss AxioCam MRm Rev.3 using a light source: HXP 120 V (D) and objective: EC Plan-Neofluar 10x/0.3 M27. For imaging the DAPI filter set with excitation 350/50 nm, emission 460/50 nm was used. This was aimed to observe the presence of infillings within the skeletal voids of the coral skeletons.

2.4.1. Micro-mill based sampling for diagenetic samples

The two samples (H-Tai-2 and HM4) detected with the presence of secondary aragonite needles (ingrowth) within the skeletal voids (from microscopic observation) were further taken for micro-mill based sampling to investigate the Sr/Ca ratios in the massive parts of the skeleton and the porous parts where the secondary ingrowths were found. To achieve these procedures following specifications were set: Depth per pass: 5 µm, number of passes 10 passes (that make the cut depth of 50 µm), Scan speed: 10 µm/sec with the plunge speed of 25 µm/sec. This was done by milling the powdered samples at the massive parts of the skeleton and also on the porous parts of the skeleton where the secondary aragonite needles were found. Samples with no secondary aragonite were also included and treated the same way as diagenetic samples for comparison. The powders obtained were taken for Sr/Ca geochemical analysis.

2.4.2. Electron Microprobe (EMP) element mappings of early diagenetic corals and investigation of Sr/Ca intra-skeletal variability within the primary coral skeleton.

The same samples (blocks) used for the micro-milling (H-Tai-2 and HM4) were polished and taken for the electron Microprobe mapping (EMP: JXA- 8200 JEOL) to investigate high-spatial resolution Sr/Ca variations within the primary coral skeleton and along the skeletal voids where the secondary aragonite needles have been detected. The EMP maps were obtained by wavelength dispersive spectrometry mode measuring simultaneously Sr (La, TAP) and Ca (Ka, PETJ). The electron beam was focused to a spot size of 2 µm, accelerating voltage set to 15 kV and beam current to 100 nA. A step size of 2 µm as well as an accumulation time of 10 ms was used and the map was repeated to gather 5 accumulations of the selected area. Standards (Calcite, Volcanic glass – VG-2 as well as KAN1 and Strontianite) were measured before and after mapping the sample to convert raw intensities into Sr/Ca ratios. In addition, the

investigation of intra-skeletal variability of Sr/Ca ratio was done using line analysis technique. This was achieved by using Sr/Ca maps from the EMP analysis and extracting values as a line where each point of a line is an average of 20 pixels in horizontal or vertical direction. In each map the values were taken as a line passing only the massive area of a skeleton, and a line starting from the massive area crossing the porous area where the secondary needles were observed.

2.5. Geochemical analysis

2.5.1. Sr/Ca analytical Procedures

2.5.1.1. Measurements of Sr/Ca ratios of the bulk samples powders

The Sr/Ca ratios of the bulk samples were measured using Varian 720-ES Inductively Coupled Plasma Optical Emission Spectrometry (ICP-OES) at the GEOMAR, Kiel. Prior to the analysis, the coral powder samples were weighed to approximately 20 to 30 mg in order to have total weight of the bulk sample. This weight is used to calculate the total calcium concentration of each sample. The sample solution was prepared by dissolving the coral powder in 10 ml of 2% ultrapure HNO_3. Accordingly the respective sample solutions was prepared by serial dilutions of the sample solution with 2% HNO_3 since all samples have to be measured in the same matrix with a Ca concentration level of 25 ppm. The internal standard (400µl Indium solution) was added in each sample in order to monitor the matrix effect and correcting for the machine drifts. The Sr and Ca lines used for this measurement were 407 and 370 nm, respectively. Respective element emission signals were simultaneously collected and subsequently drift corrected by sample-standard bracketing method done by measuring JCP-1 standard (Okai et al., 2002) after every two samples following the combination of previously published techniques (de Villiers et al., 2002; Schrag, 1999). The validity of this reference material has been proved by long term inter-laboratory comparisons of this standard (Hathorne et al., 2013b). Measurement results from this inter-laboratory standard were used for normalization of our Sr/Ca results.

2.5.1.2. Measurements of Sr/Ca ratios from the micro-mill sampling

Because the ICP-OES cannot precisely measure very small amounts of samples (<1 mg), Sr/Ca measurements from micro-mill samples were analyzed using the ICP MS-Quadrupole at GEOMAR, Kiel. Prior to analysis, the powdered samples were dissolved in 2% HNO_3 and

concentrations were adjusted to the Ca level of 25ppm. Indium was used as an internal standard for each sample to monitor the matrix effect and also to correct machine drifts. All the measured Sr/Ca values were normalized to the JCP-1 standard (Hathorne et al., 2013b) similar to the Sr/Ca values from the bulk sampling.

2.5.2. Determination of stable isotope ratios

The $\delta^{18}O$ ratios were measured following the standard procedure for carbonate samples at GEOMAR, Kiel. To achieve this ~100 µg of homogeneous carbonate powder was reacted with water-free Phosphoric acid in an automated carbonate device "Carbo Kiel" (Thermo Fischer Scientific Inc.) at 73°C to produce CO_2. The isotopic ratios of stable $\delta^{18}O$ were measured on a MAT 253 mass spectrometer (Thermo Fischer Scientific Inc.). The isotopic ratios of $\delta^{18}O$ are expressed as deviations in per mill relative to the Vienna-PeeDee Belemnite (VPDB) standard. The values of $\delta^{18}O$ isotopes are calculated as:

$$\delta^{18}O‰ = (\delta^{18}O/\ \delta^{16}O)_{\text{sample}} - (\delta^{18}O/\ \delta^{16}O)_{\text{standard}} \text{ x } 1000$$

The standard deviation of single samples reported are based on replicate analyses (n=30) of the laboratory standard

2.6. Focus of this thesis

Most of the climate studies in the past focused on the period after the Last Glacial Maximum about 18 ka where the temperature increase has resulted into massive deglaciation of the ice sheets that resulted into rise in sea levels. Information about Mid to Late Holocene sea level and temperature variability was rare because it was considered to be climatically stable with more or less stable temperatures and sea level variations. However, few recent studies indicate that the temperature and the sea level were rather fluctuating above and below the modern on different time scales (Flood and Frankel, 1989; Gagan et al., 1998; Pirazzoli et al., 1988; Montaggioni and Pirazzoli, 1984; Wanner et al., 2008; Woodroffe and Horton 2005). To evaluate these facts we used the fossil corals in growth position from the emerged platforms of the Society Islands (French Polynesia). Massive specimens of *Porites* were used for this study because this species

is considered to be the most reliable archive in reconstructing the past variability in climate (Corrège, 2006).

For reconstructing sea level variations previous studies from Society Islands used fossil reef conglomerates which are mostly consisting reworked samples which are replaced from their original growth positions (Montaggioni and Pirazzoli, 1984; Pirazzoli and Montaggioni, 1988; Pirazzoli and Pluet, 1991). Dating of these conglomerate samples were mostly based on ^{14}C which is associated with a number of uncertainties as a result of irregularity of the curves used to calibrate ^{14}C dates as well as the lack of information about ^{14}C residence time (Chappell and Polach, 1991; Eisenhauer et al., 1999; Grossman et al., 1998; Kench et al., 2009; Pirazzoli et al., 1988; Pirazzoli and Montaggioni, 1986; Scoffin and Le Tissier, 1998; Woodroffe and McLean, 1990). Elevations of samples relative to the mean local sea level were far less constrained due to lack of modern "Global Positioning System (GPS)". For volcanic islands, the Island's specific subsidence rates were not considered in reconstruction.

In case of SST reconstruction the impact of early marine diagenesis that leads to errors in SST estimates was far less considered (e.g. Stephans et al., 2004; Boiseau et al., 1998; Min et al., 1995; Kuhnert et al., 1999). This is because the sample screening method for mineralogy was entirely based only on the traditional X-ray Diffraction method which cannot distinguish between the primary aragonite and the aragonite which is secondary precipitated without the influence of coral itself. Errors of SST estimates from these studies were mostly considered to be originated from biological control (vital effect) of a coral (e.g. Stephans et al., 2004, Boiseau et al., 1998; Min et al., 1995).

This study aims on precisely constraining the sea level variations using massive fossil *Porites* sp. which were taken on growth positions from emerged (exposed) platforms of Society Islands. Since normal *Porites* have a larger range of growth depth (0-25m), the *Porites* micro atoll samples (few centimeters growth range) were also included to reduce the range of estimation. For accurate and more precise age estimation, we employed U/Th dating method for our samples. To better constrain of the elevation of the samples relative to the mean local sea level, we have compared our elevations to the Global Positioning System (GPS) and tidal datum of the

area (to reduce the tidal uncertainties). Because the volcanic islands tend to subside as a result of time and the distance from the hotspot, the island's specific subsidence rate was applied to correct for the current elevations of the samples for better constraint of the sample heights.

In addition we have used a multi-proxy approach (Sr/Ca, U/Ca and $\delta^{18}O$) to reconstruct SST variability from Mid to Late Holocene period. The results were compared to global temperature variation from solar activity reconstructed using ^{10}Be and ^{14}C production (Vonmoos et al., 2006) and with carbon dioxide concentration on the time window of our samples. To reduce the uncertainties (errors) of our SST estimates the petrographic analysis were applied to the samples in order to investigate the presence of the secondary aragonite needles or any secondary phase resulting from early marine diagenesis.

We have also used the Sr/Ca proxy to trace the shift of SST estimates on the areas where secondary aragonite needles are found. Micro-scale intra-skeletal variations of Sr/Ca within the samples were also assessed in order to investigate the distribution of Sr/Ca ratio within the massive area of the primary skeleton.

2.7. Thesis Structure

This thesis consists of three chapters. Chapter 1 describes basic theories applied for natural archives in paleo-climate reconstructions and the potential use of massive corals (*Porites*) in paleo-climate studies. In this section anatomy, nature of the corals, calcification, reef growth and development, habitat and their distribution have also been explained. In addition, the concept behind U/Th dating in corals and the potential use of corals as tracers of sea level change has been explained. Furthermore, the three important coral proxies used for paleo-thermometry (Sr/Ca, $\delta^{18}O$ and U/Ca) have been discussed including challenges which are faced in application of these proxies in SST reconstruction.

The detailed descriptions of the study area that include nature of the islands, location, climatic conditions and tidal amplitudes have been explained in chapter 2. This is followed by the methodology and approach used to accomplish this study.

Chapter 3 is designed in a paper format: This is a manuscript which was published as: Rashid, R., Eisenhauer A., Stocchi P., Liebetrau V., Fietzke J., Rüggeberg A., and Dullo, C. 2014. Constraining Mid to Late Holocene relative sea level change in the southern equatorial Pacific Ocean relative to the Society Islands, French Polynesia. Geochemistry, Geophysics, Geosystems, 15, 2601–2615. This paper aimed to reconstruct Mid to Late Holocene Sea level change from the exposed fossil coral platforms (*Porites* and *Porites* micro atoll from growth position) which are currently exposed above the mean sea level as a consequence of sea level regression on far-field areas (e.g. tropical Pacific) caused by ocean siphoning effect. The results were also compared to geophysical models from GIA induced ice sheet chronologies (ICE-5G+VM2 and the RSES-ANU+VKL) to see whether the empirical data agree with model predictions of our area of study.

Chapter 4 is also designed as a manuscript: This is a manuscript is in the process to be submitted as: Rashid R., Eisenhauer A., Liebetrau V., Fietzke J., Böhm F., Wall M., Krause S., Goos M., Rüggeberg A., and Dullo C. 2014. Early Diagenetic imprint on temperature proxies in Holocene Corals: A case study from French Polynesia. This article aims to reconstruct sea surface temperature variability in the Mid to Late Holocene period using Sr/Ca, $\delta^{18}O$ and U/Ca together with analyzing diagenetic impact caused by the early marine diagenesis in SST estimates. Furthermore, it attempts to investigate the micro-scale intra-skeletal variation of Sr/Ca ratios that reflects the variability of incorporation of Sr/Ca ratios during skeletal formation.

Chapter 5 provides the general conclusion together with recommendation and future perspectives suggested from this thesis.

Chapter Three

3. Constraining Mid to Late Holocene Relative Sea Level Change in the Southern Equatorial Pacific Ocean Relative to the Society Islands, French Polynesia

(Published as *Rashid et al., 2014, G^3, 15, 2601–2615*)

Rashid Rashid[1], Eisenhauer Anton[1], Stocchi Paolo[2], Liebetrau Volker[1], Fietzke Jan[1], Rüggeberg Andres[3], Dullo Christian[1].

[1]GEOMAR, Helmholtz Zentrum für Ozeanforschung Kiel, Kiel Germany. [2]NIOZ Royal Netherlands Institute for Sea Research, Texel, Netherlands. [3]Department of Geosciences, University of Fribourg, Fribourg, Switzerland.

Abstract

Precisely quantifying the current climate-related sea level change requires accurate knowledge of long-term geological processes known as Glacial Isostatic Adjustments (GIA). Although the major post-glacial melting phase is likely to have ended ~6-4 ka (before present), GIA is still significantly affecting the present-day vertical position of the mean sea surface and the sea bottom. Here we present empirical rsl (relative sea level) data based on U/Th dated fossil corals from reef platforms of the Society Islands, French Polynesia, together with the corresponding GIA-modelling. Fossil coral data constrains the timing and amplitude of rsl-variations after the Holocene sea level maximum (HSLM). Upon correction for isostatic island subsidence, we find that local rsl was at least ~1.5±0.4 m higher than present at ~5.4 ka. Later, minor amplitude variations occurred until ~2 ka, when the rsl started dropping to its present position with a rate of ~0.4 mm/year. The data match with predicted rsl curves based on global ice-sheet chronologies confirming the role of GIA-induced ocean siphoning effect throughout the mid to late Holocene. A long lasting Late Holocene highstand superimposed with second order amplitudinal fluctuations as seen from our data suggest that the theoretical predicted timing of rsl change can still be refined pending future calibration.

Key words: fossil coral record, U-Th geochronology, sea level highstand, micro atolls

3.1. Introduction

The Intergovernmental Panel on Climate Change (IPCC) predicts a mean sea level rise in the order of ~3.5mm/year as a consequence of greenhouse warming (Richard Alley et al., 2007). This is likely to contribute to a sea level rise between 29 and 82 centimeters by the end of the century [*IPCC report,* 2013]. Since about 10% of human population inhabit low coastal regions and islands (McGranahan et al., 2007), it is fundamental to understand the frequency and amplitude of the several natural and anthropogenic mechanisms which contribute to sea level variations. In particular, the knowledge of present-day and future sea level changes strongly relies on our understanding of the past sea level variations (Houghton, 1996). Geological data show that during the Quaternary period, glacial and interglacial climate conditions have been characterized by a transfer of ~3% of the global ocean water volume between the continental ice sheets and the oceans (Bard et al., 2010; Blanchon et al., 2009; Eisenhauer et al., 1996; Montaggioni et al., 1996; Montaggioni, 2005; Woodroffe and Horton, 2005). During the Last Glacial Maximum (LGM; ~21 ka) 120-130 m of equivalent sea level were stored in form of large continental ice-sheets over North America, Eurasia, Greenland and Antarctica (Denton and Hughes). The post-LGM sea level change was punctuated by short-term periods of slower and faster rise, with higher rates of up to 10 to 15 m/ka (Bard et al., 1996; Deschamps et al., 2012; Woodroffe and Horton, 2005) during melt-water pulse 1A (14.6-14.3 ka). Before and after the Younger Dryas event (12.9-11.6 ka) [*Carlson,* 2010], the rate of sea level rise was at its maximum (Bard et al., 1996; Fairbanks, 1989) and caused coral reefs to drown (Camoin et al., 2012; Dullo et al., 1998).

Although the trend and rate of global mean sea level (msl) change (commonly known as eustatic sea level change) follows the rate of melting/growth of continental ice masses, several coeval mid to late Holocene sea level indicators based on fossil coral reefs found in different regions show that the timing and amplitude of post-glacial sea level variations are not uniform, but strongly depend on the geographical position and varies considerably as a function of the distance from the formerly glaciated areas (Lambeck et al., 2002; Milne et al., 2009; Mitrovica and Milne, 2002; Mitrovica and Peltier, 1991). Because the msl is an equipotential surface of gravity, it does not only vary in time as a function of addition/removal of ocean water, but also spatially according to the differential variations of the Earth's gravity potential which are

triggered by the continental ice-sheet fluctuations (Mitrovica and Peltier, 1991; Peltier, 2002). Hence, as far as ice-sheets fluctuations are concerned, the oceans do not behave like a bathtub as the eustatic model would imply as it was described in the pioneering study of (Suess and Waagen, 1888). When an ice-sheet melts, in fact, the lack of gravitational pull which was previously exerted by ice mass on the ocean water results in a sea level drop nearby the formerly glaciated area and in a sea level rise higher than the eustatic value at the opposite end (Mitrovica and Milne, 2002; Woodward, 1888). Hence, the ocean averaged sea level change exactly corresponds to the eustatic change (Suess and Waagen, 1888), but the local sea level change may be significantly different, or even opposite in sign.

Furthermore, a time-dependent contribution to the msl variation from the ice-sheets fluctuations exists because of the deformability of the solid Earth with respect to ice and ocean surface mass displacements. In fact, during and after the melting of an ice sheet, the formerly glaciated areas undergo isostatic rebound (rise of the land mass) in order reach new isostatic equilibrium. At the same manner, the uplifted area surrounding the formerly glaciated area subsides, as well as the ocean sea-floor because of the addition of melt water (Mitrovica and Milne, 2002). This implies that the solid Earth response is both immediate and delayed and can be approximated by a Maxwell viscoelastic body. The solid Earth deformations behave like density variations and directly affect the shape of the geoid and the msl, respectively. However, and more importantly, since both the msl and the solid Earth surface deform during and after the melting of an ice sheet, any land based marker (sea level indicator like coral reef corals) would record the msl change with respect to the sea bottom, i.e., the local rsl. The feedbacks described so far drive GIA processes and result in rsl changes which depart from eustasy as a function of the distance from the formerly glaciated areas, of the shape of the ocean basins and of the rheology of the solid Earth.

Geological evidences from South Pacific and Indian Ocean islands show that the last 6.5 ka were characterized by a 1-3 m rsl drop (Banerjee, 2000; Deschamps et al., 2012; Eisenhauer et al., 1993; Grossman et al., 1998; Woodroffe and Horton, 2005) which can be explained by the GIA-induced ocean siphoning effect and the migration of ocean water towards the subsiding peripheral forebulges that surrounded the formerly glaciated areas in the Northern and Southern

Hemispheres (Milne and Mitrovica, 1998; Mitrovica and Milne, 2002; Mitrovica and Peltier, 1991). As a morphological consequence to Mid and Late Holocene regression, the coral reefs from Indian and Pacific Ocean islands developed extended emerged fossil reef platforms which are currently 1-3 m above the msl (Eisenhauer et al., 1999; Eisenhauer et al., 1993; Grossman et al., 1998; Montaggioni and Pirazzoli, 1984; Pirazzoli et al., 1988; Woodroffe and Horton, 2005). Because of the geographical location, the late Holocene sea level regression observed at the Indo-Pacific islands is clearly in contrast with the almost eustatic rsl change recorded at the Caribbean islands (Fairbanks, 1989; Woodroffe and Horton, 2005). Furthermore, superimposed to the general rsl drop, the Indo-Pacific islands show second order rsl fluctuations in the range of 0.1-1.0 m (Flood and Frankel, 1989; Pirazzoli et al., 1988; Scoffin and Le Tissier, 1998; Woodroffe et al., 1990; Young et al., 1993) which may be attributed to sea surface temperature (SST) variations in the order of 1 to 2 °C (Goelzer et al., 2012; Levermann et al., 2013).

In general, tropical Pacific areas remain far less understood than their Atlantic counterparts (Camoin and Davies, 1998; Kennedy and Woodroffe, 2002; Montaggioni, 2005). Also, published rsl records from Indo-Pacific regions and, in particular, from the Society Islands (Montaggioni and Pirazzoli, 1984; Pirazzoli and Montaggioni, 1988; Pirazzoli and Pluet, 1991) are mostly based on radiocarbon dating and consequently carry higher uncertainty due to the lack of information about the ^{14}C residence time (Chappell and Polach, 1991; Eisenhauer et al., 1999; Grossman et al., 1998; Kench et al., 2009; Pirazzoli et al., 1988; Pirazzoli and Montaggioni, 1986; Scoffin and Le Tissier, 1998; Woodroffe and McLean, 1990). Furthermore, the geographical position provided in earlier studies as well as the corresponding elevation above mean sea level are less constrained due to the lack of modern “Global Positioning System (GPS)” and improved tidal and atmospheric pressure corrections. More robust estimates of mid to late Holocene rsl fluctuations in the Indo-Pacific region can be gained by the comparison of U/Th dated corals from different islands and atolls. In particular, the U/Th dating method is independent of any reservoir ages and provides high precision values ranging from ~2 year old sample up to ~600,000 year old sample (c.f., (Stirling et al., 2001). However, diagenetic changes related to the recrystallization of aragonite to calcite may obscure the actual age of the samples (Eisenhauer et al., 1993; Scholz and Mangini, 2007).

The present study aims at better constraining the amplitude and timing of mid to late Holocene rsl changes by means of U/Th dating of fossil corals sampled from emerged platforms of the Society Islands (French Polynesia, South Pacific Ocean). The rsl record presented here is compared to theoretical predictions of GIA-induced rsl changes computed for two available global ice-sheet chronologies (Lambeck et al., 1998; Peltier, 2004) by solving the gravitationally self-consistent Sea Level Equation formalism (SLE) (Farrell and Clark, 1976; Mitrovica and Peltier, 1991; Spada and Stocchi, 2007). Any difference between empirically determined sea level records and theoretical predictions will help to constrain the geophysical models and basic parameters as well as to determine the timing of the post-glacial melting of the three major ice reservoirs in North-America, Europe and Antarctica.

3.2. Samples and Methods

3.2.1. Sample location

Samples for this study were collected from Society Islands, French Polynesia (Figure 1A and B) because these islands are characterized by extended Holocene emerged fossil reef platforms (Davies and Marshall, 1980; Montaggioni and Pirazzoli, 1984; Pirazzoli and Montaggioni, 1986) being a direct consequence of the decline of the Late Holocene sea level highstand after ~6.5 ka. According to the model for epicontinental reef growth (Davies and Marshall, 1980), the presence of these platforms provide suitable sampling localities for mid to late Holocene sea level variations studies (Eisenhauer et al., 1993; Montaggioni and Pirazzoli, 1984; Pirazzoli et al., 1988; Pirazzoli and Montaggioni, 1986; Yu et al., 2010). The Society archipelago comprises more than ten islands and atolls elongated in 17°52'S 149°50'W and 15°48'S 154°50'W direction which spread across 720km of the Pacific Ocean (Duncan and McDougall, 1976; Montaggioni, 2011; Peltier, 2002; Pirazzoli and Montaggioni, 1988). The islands are elongated in the direction which is virtually parallel to the present absolute motion of the Pacific plate (Blais et al., 2002; Gripp and Gordon, 1990; Uto et al., 2007). These islands are thought to have originated from a volcanic hotspot presently located around the island of Mehetia about 110 km east of Tahiti (Binard et al., 1991; Binard et al., 1993; Blais et al., 2002; Devey et al., 1990; Nolasco et al., 1998).

According to published chronological studies, the ages of the islands increase with the distance from a hotspot ranging in age from Mehetia (less than 1 Ma old), to Tahiti (~1.67– 0.25 Ma old), to Moorea (~2.15-1.36 Ma old), to Huahine (~3.08– 2.06 Ma old), to Tahaa (~3.39–1.10 Ma old), to Raiatea (~ 2.75–2.29 Ma old) and to Maupiti ~5 Ma old (Duncan et al., 1994; Guillou et al., 2005; Uto et al., 2007; White and Duncan, 1996).

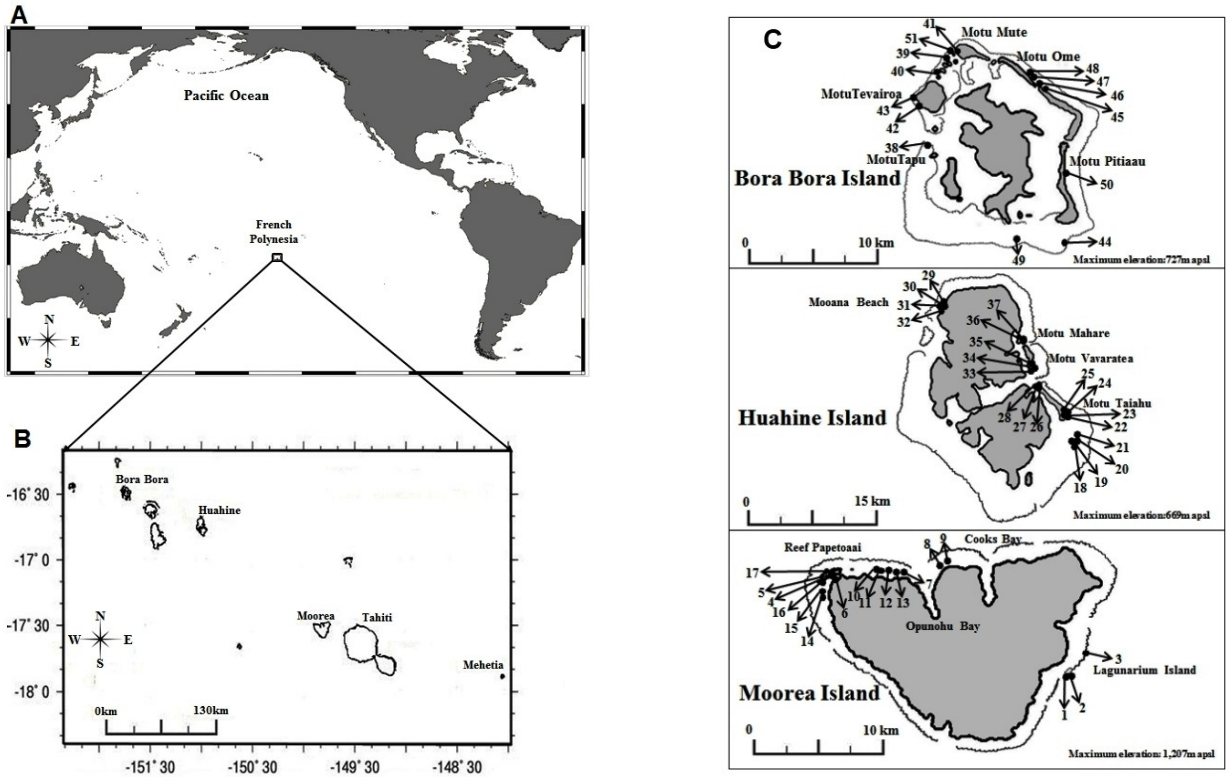

Fig. 1: Location of the French Polynesia where Society Islands are located (A) and the islands of Moorea, Huahine and Bora Bora in particular (B). Figure 1C shows the sample sites along the shore lines of Moorea, Huahine and Bora Bora. Arrows pointing towards numbers refer to Tab. 1 and 2.

The studies have also shown that, as volcanic islands move away from the hotspot, the oceanic crust becomes progressively cooler and denser and gradually subsiding from the level of its formation. In this case these Society Islands slowly subside as they move further from its point of origin (Neall and Trewick, 2008). The Holocene subsidence rate of Society Islands has been determined to be ~0 to a maximum of ~0.5 mm/year (Bard et al., 1996; Fadil et al., 2011; Lepofsky et al., 1996; Pirazzoli et al., 1985; Pirazzoli and Montaggioni, 1988). The climate of the Society Islands is tropical with two main seasons. The warm and rainy season (austral summer) runs from November to April. During this period, the conditions are hot and rainy, with

the average SST in the order of ~28°C whereas the heavy rains are mostly experienced during December and January. These are the most intense rains along the coastline exposed to the trade winds that usually blow from East (South-East) and North-East direction. During May to October (austral winter), the climate is relatively less humid, with a SST in the order of ~25°C. The available information indicates the tidal range is between 0.3 and 0.4m [*Bongers and Wyrtki,* 1987*; Tylor,* 1979; *Yates et al.,* 2013]. This is in general accord with the NOAA tide book indicating an average of 0.5m for the Society Islands (Seard et al., 2011).

3.2.2. Sample collection and preparation

The samples were collected during April to May 2009 during the CHECKREEF expedition to the Holocene emerged reef platforms at Moorea, Huahine and Bora Bora (Tab. 1; Fig. 1 B and C).

Table 1A: Information of sampling locations on Moorea

Map code	Sampling Location	Coordinates		Height apsl (m)	Island	Comments
Lagunarium Island					**Moorea**	
1	L1-2	17°33' 7.62"S	149°46'33.46"W	0.75±0.40	Moorea	*in situ*
2	LI-4	17°33' 7.62"S	149°46'33.46"W	0.75±0.40	Moorea	*in situ*
White Light House					**Moorea**	
3	WL1	17°32' 31.00"S	149°45'54.69"W	0.75±0.40	Moorea	*in situ*
Reef Papetoaai					**Moorea**	
4	CB10	17°29' 27.4"S	149°55'15.4"W	1.80±0.40	Moorea	Conglomerate
5	CB11	17°29' 18.8"S	149°54'52.6"W	1.80±0.40	Moorea	Conglomerate
6	CB12	17°29' 29.07"S	149°54'32.9"W	1.80±0.40	Moorea	Conglomerate
7	CB5	17°29' 08.9"S	149°54'07.6"W	1.80±0.40	Moorea	Displaced
8	RP2	17°29' 12.59"S	149°53'7.57"W	0.00±0.40	Moorea	*in situ*
9	RP4	17°29' 12.59"S	149°53'7.57"W	-0.80±0.40	Moorea	*in situ*
10	MCM1	17°29' 7.62"S	149°54'9.74"W	1.10±0.40	Moorea	*in situ*
11	MCM2	17°29' 7.62"S	149°54'9.74"W	1.10±0.40	Moorea	*in situ*
12	MCM5	17°29' 7.62"S	149°54'9.74"W	1.10±0.40	Moorea	*in situ*
13	MCM10	17°29' 8.86"S	149°54'7.64"W	1.10±0.40	Moorea	*in situ*
14	CM1	17°29' 34.89"S	149°55'19.98"W	0.75±0.40	Moorea	*in situ*
15	CM2	17°29' 34.89"S	149°55'19.98"W	0.75±0.40	Moorea	*in situ*
16	CM4	17°29' 26.29"S	149°55'14.83"W	0.75±0.40	Moorea	*in situ*
17	CM7	17°29' 18.84"S	149°54'52.60"W	0.75±0.40	Moorea	*in situ*

Note: the numbers shown in this table indicate the sampling points shown on the map.

Table 1B: Information of sampling locations on Huahine

Map code	Sampling Location	Coordinates		Height apsl (m)	Island	Comments
Motu Taiahu					**Huahine**	
18	H-Tai-1	16°47' 0.50"S	150°56'54.26"W	0.50±0.40	Huahine	*in situ*
19	H-Tai-2	16°47' 0.50"S	150°56'54.26"W	0.50±0.40	Huahine	*in situ*
20	H-Tai-3	16°47' 0.50"S	150°56'54.26"W	-0.80±0.40	Huahine	*in situ*
21	H-Tai-5	16°47' 0.50"S	150°56'54.26"W	1.00±0.40	Huahine	*in situ*
22	H-Tai-7	16°46' 31.94"S	150°56'54.89"W	-0.25±0.40	Huahine	*in situ*
23	H-Tai-8	16°46' 31.94"S	150°56'54.89"W	0.30±0.40	Huahine	*in situ*
24	H-Tai-9	16°46' 31.94"S	150°56'54.89"W	0.00±0.40	Huahine	Micro atoll
25	H-Tai-10	16°46' 31.94"S	150°56'54.89"W	0.00±0.40	Huahine	Micro atoll
26	H-Tai-11	16°45' 12.13"S	150°57'53.39"W	0.75±0.40	Huahine	*in situ*
27	H-Tai-12	16°45' 12.13"S	150°57'53.39"W	-0.20±0.40	Huahine	*in situ*
28	H-Tai-13	16°45' 12.13"S	150°57'53.39"W	-0.20±0.40	Huahine	*in situ*
Mooana Beach					**Huahine**	
29	H-M-1	16°42' 1.51"S	151°2'18.68"W	0.50±0.40	Huahine	*in situ*
30	H-M-2	16°42' 1.51"S	151°2'18.68"W	0.30±0.40	Huahine	*in situ*
31	H-M-4	16°42' 1.51"S	151°2'18.68"W	0.10±0.40	Huahine	*in situ*
32	H-M-5	16°42' 1.51"S	151° 2'18.68"W	0.00±0.40	Huahine	*in situ*
Motu Vavaratea					**Huahine**	
33	H-MT-1	16°44' 29.66"S	150°58'16.10"W	1.10±0.40	Huahine	*in situ*
34	H-MT-2	16°44' 29.66"S	150°58'16.10"W	0.75±0.40	Huahine	*in situ*
35	H-V-1	16°44' 28.80"S	150°58'15.66"W	0.25±0.40	Huahine	*in situ*
Pass Tiare (Motu Mahare)					**Huahine**	
36	H-PT-1-A	16°43' 14.08"S	150°58'37.37"W	0.00±0.40	Huahine	*in situ*
37	H-PT-1-2	16°43' 14.08"S	150°58'37.37"W	0.75±0.40	Huahine	*in situ*

Note: the numbers shown in this table indicate the sampling points shown on the map.

Table 1C: Information of sampling locations on Bora Bora

Map code	Sampling Location	Coordinates		Height apsl (m)	Island	Comments
Motu Tapu					**Bora Bora**	
38	BB-MP 3/2	16°29' 43.99"S	151°46'46.92"W	1.10±0.40	Bora Bora	*in situ*
Motu Mute					**Bora Bora**	
39	BB-MP 4/2	16°26' 48.49"S	151°46'3.18"W	1.10±0.40	Bora Bora	*in situ*
40	BB-MP 2/2	16°27' 22.49"S	151°46'20.20"W	1.10±0.40	Bora Bora	*in situ*
41	BB-MP 5/3	16°26' 36.14"S	151°45'52.75"W	-1.30±0.40	Bora Bora	*in situ*
Motu Tevairoa					**Bora Bora**	
42	BB-MP 6/6	16°28' 30.24"S	151°46'55.51"W	-1.30±0.40	Bora Bora	*in situ*

Map code	Sampling Location	Coordinates		Height apsl (m)	Island	Comments
43	BB-MP 6/5	16°28' 17.90"S	151°47'4.26"W	-1.30±0.40	Bora Bora	*in situ*
Motu Pitiaau					**Bora Bora**	
44	BB-MX 1/2	16°33' 6.35"S	151°42'20.01"W	1.30±0.40	Bora Bora	*in situ*
		Motu Ome			**Bora Bora**	
45	BB-MX 3/2	16°27' 54.67"S	151°42'44.50"W	0.95±0.40	Bora Bora	Micro atoll
46	BB-MX 4/2	16°27' 54.67"S	151°42'44.50"W	1.40±0.40	Bora Bora	*in situ*
47	BB-MX 5/1	16°27' 50.86"S	151°42'49.35"W	0.95±0.40	Bora Bora	*in situ*
48	BB-MX 5/3	16°27' 49.99"S	151°42'50.70"W	0.95±0.40	Bora Bora	*in situ*
		Motu Pitiaau			**Bora Bora**	
49	BB-MX 6/3	16°33' 7.49"S	151°44'1.36"W	0.95±0.40	Bora Bora	*in situ*
50	BB-MX 7/2	16°30' 42.07"S	151°42'4.73"W	1.40±0.40	Bora Bora	*in situ*
		Motu Mute			**Bora Bora**	
51	BB-MM-13	16°26' 36.03"S	151°45'53.24"W	0.65±0.40	Bora Bora	*in situ*

Note: the numbers shown in this table indicate the sampling points shown on the map.

The main targets for sampling have been *in situ Porites* in general and *Porites* micro atolls in specific. Criteria for *in situ* sampling have been that fossils corals were found upright in growth position and not showing any indications for later displacement. Samples considered being reworked and transported (conglomerates) in Tab. 1 and 2 are not considered for the rsl-curve. The position of the corals above the present mean sea level (apmsl) was determined by triangulation of the coral´s position to the current position of the mean sea level. To achieve this, the laser was placed on top of the sample with the beam pointing horizontally towards the water table. Using a meter rule, the measurement of the elevation was determined relative to the laser beam and the water level. This process was repeated up to 15 times where by the local time is recorded. Using tide table and the local time, the elevation relative to the mean sea level was achieved. These elevations were also compared to our GPS measurement during each time. Certainly, this method is burdened with uncertainties because the sea level position is not well defined due to wave action but careful positioning and repeated measurements allowed the determination of coral positions in the order of ±0.4 m. Note, concerning the reconstruction of a Late Holocene sea level curve not only the present day position apmsl rather its past position during corals life time is of certain importance. The past position has to be determined and reconstructed from the individual subsidence rate of the particular island. Local subsidence rates are known (see section 2.4 below) and assumed to be linear. However, the accuracy of the

subsidence rate is also burdened with some unknown uncertainty and may also not be linear rather than abrupt and discontinuously. Hence, the uncertainty of about ±40 cm attributed to our samples may account for the present day position but also for the uncertainty induced by the subsidence correction. In addition, the height of sea level may also be obscured by the uncertainty of corals position below sea surface. In order to circumvent at least this problem micro-atolls are of certain interest.

In particular the elevation of micro atolls (sample no. 24, 25 and 45 in Tab. 1 and 2) above the sea level put distinct constraints on the position of a past sea level because normally the sea level is only a few centimeters above micro-atolls surface during their formation (Chappell, 1983; Flora and Ely, 2003; Larcombe et al., 1995; Scoffin et al., 1978; Smithers and Woodroffe, 2001; Woodroffe and McLean, 1990; Woodroffe, 2005). Selected fossil coral samples were taken out of the platforms using hammers and chisels. The elevation interval from which the samples were taken ranges from -1.5 m to less than ~2 m apmsl, respectively. The uncertainty of the sample's elevation determination relative to the present msl was conservatively estimated to be in the order of ±0.4m.

Selected samples were cut into slabs (~1 cm thick) along the growth direction. Afterwards, the slabs were washed with Milli-Q water and dried at room temperature in a clean lab fume hood. Using a diamond saw, samples were further cut into smaller blocks within the parallel growth bands by selecting the best parts visually free from any algal or carbonate infill of the pore volume. These blocks were then cut into small pieces (chips) and transferred into teflon beakers for further cleaning using ultra-sonification method (Cheng et al., 2000). Cleaned sample were then transferred into a hot plate and dried at ~35°C overnight. Each sample was then crushed into powder and the mineralogy of the samples in terms of aragonite or Mg-calcite was determined by X-Ray diffraction (XRD) method.

3.2.3. Uranium and thorium isotope measurements

Uranium series measurements of coral ages were performed at GEOMAR, Helmholtz Centre for Ocean Research Kiel, Germany. In brief, separation of uranium and thorium from the sample matrix was done using Eichrom-UTEVA resin followed previously published methods

(Blanchon et al., 2009; Douville et al., 2010; Fietzke et al., 2005). Determination of uranium and thorium isotope ratios was done using the multi-ion-counting inductively coupled plasma mass spectroscopy (MC-ICP-MS) approach using the method of (Fietzke et al., 2005). The ages were calculated using the half-lives published by Cheng et al, [2000b]. For isotope dilution measurements, a combined $^{233}U/^{236}U/^{229}Th$ spike was used with stock solutions calibrated for concentration using NIST-SRM 3164 (U) and NIST-SRM 3159 (Th) as combi-spike, calibrated against CRM-145 uranium standard solution (formerly known as NBL-112A) for uranium isotope composition and against a secular equilibrium standard (HU-1, uranium ore solution) for the precise determination of $^{230}Th/^{234}U$ activity ratios. Whole-procedure blank values of this sample set were measured between 0.5 pg and 1 pg for thorium and between 10 pg to 20 pg for uranium. Both values are in the range typical of this method and the laboratory (Fietzke et al., 2005).

3.2.4. Correction for the subsidence of the islands

Few studies have been focusing on the assessment of the subsidence rates of the Society Islands (e.g. [*Fadil et al.,* 2011; *Thomas et al.,* 2012]) mostly on Tahiti Island. For Moorea, Huahine and Bora Bora, Pirazzoli et al., [1985] and Pirazzoli and Montaggioni, [1985] conducted a study based on petrological analysis of emerged reef conglomerate available on the shorelines of the islands. The analysis was based on the close inspection of thin sections of exposed coral reef conglomerates. In their study they have found different layers of the conglomerates corresponding to different diagenetic sequences. The lower sequence exhibit earlier generations of diagenesis developed within marine phreatic zone corresponding to sub tidal environment (e.g. Magnesian Calcite, Pelleted micrite) within inter-particle pore spaces. The upper part exhibit the later generation of diagenesis developed in the marine vadose zone corresponding to mid littoral zone (e.g. irregular rims of truncated aragonite fibres and pendant microstalactites) or the splash zone. Using radiocarbon dating, the type of diagenetic imprint and the stratigraphic elevation of the conglomerates specimen, they have been able to calculate the subsidence rates of the Islands. Based on this study we have directly applied the subsidence rates of Moorea and Huahine (0.14mm/year) and Bora Bora (0.05mm/year) islands for correction of the elevations of our samples.

3.3. Results and Discussion

3.3.1. U/Th-Age Dating

Table 2 summarizes all measured uranium and thorium data and the calculated U/Th ages. For uranium and thorium isotope analysis only samples with no detectable traces of calcite were used for measurements. The data show that ^{238}U concentrations vary between 2.055±0.001 ppm (No. 50, BB-MX7/2) and 4.26±0.01 ppm (No. 26, H-Tai-11) with a mean ^{238}U concentration of 2.986±0.005 ppm. The concentrations of ^{232}Th vary from 0.0045±0.0001 ppb (No. 18, HTai-1) to 0.91±0.01 ppb (No. 11, MCM2) with an average value of 0.163±0.004 ppb. Both the measured ^{232}Th and ^{238}U values are in typical range for young corals from oceanic islands (Chen et al., 1991; Edwards et al., 1988; Yokoyama and Esat, 2004). The $\delta^{234}U(T)$ values (Tab. 2, Fig. 2) show lowest values for sample No. 6 of 139±3‰ and highest value of 151±3‰ for sample No. 3 and 33. The $\delta^{234}U(0)$ values range from 138±3‰ (sample No. 6) to 150±3‰ for sample No. 3 and 9.

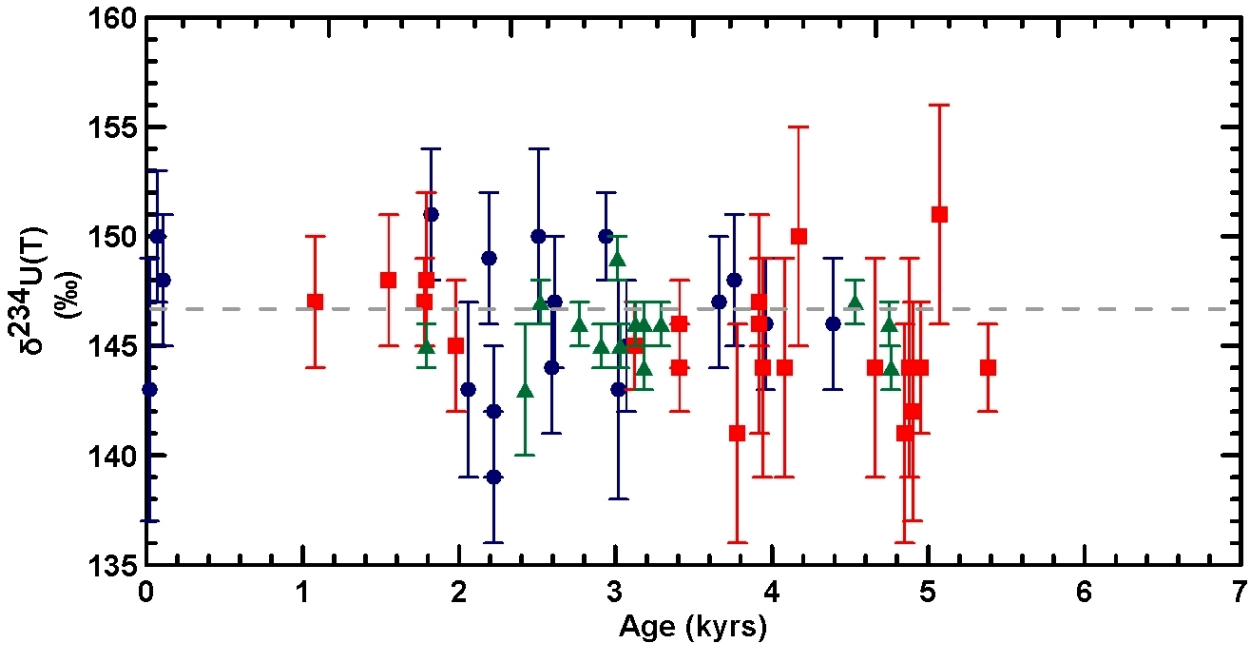

Fig. 2: The decay corrected uranium activity ratios, reported as $\delta^{234}U(T)$ as a function of their corresponding ages. The dashed grey line marks the interval of reported modern sea water uranium isotopic composition 146.8±0.1‰ [*Andersen et al.,* 2010]. Most of our data within uncertainties are plotting within this range. The values below or above this range suggest some marginal open system behavior of these samples [*Andersen et al.,* 2010].

Taking the $\delta^{234}U$ isotope value of the sea water into account from Fig. 2 it is obvious that most of the $\delta^{234}U(T)$ values fall within their statistical uncertainties in the range of the presently most precise $\delta^{234}U$ seawater value of 146.8±0.1‰ [*Andersen et al.,* 2010]. Twelve samples (marked with * in the tables 2A, B and C) are slightly but significantly lower and three samples (marked with **) are significantly higher than this expected value in average by about 3.7±0.6‰. This deviation from the expected value probably suggests a marginal open system behavior of these samples. A difference of 1‰ in the $\delta^{234}U(T)$ value is expected to change a 4.5 ka old coral in the order of about 5 years.

Table 2: Uranium/Thorium isotopic composition and ages of fossil corals from Moorea (2A), Huahine (2B) and Bora Bora (2C), Society Islands.

Table 2A: Uranium/Thorium isotopic composition and ages of fossil corals from Moorea

Sample Number	Island	Sample Label	^{238}U (ppm)	$\delta^{234}U(0)$ (‰)	$\delta^{234}U(T)$ (‰)	^{232}Th (ppb)	$^{230}Th/^{238}U$ (dpm/dpm)	$^{230}Th/^{232}Th$ (dpm/dpm)	Age (ka)	Sampling elevation (m)	Subsidence corrected elevation (m)
1	Moorea	**LI-2	2.877±0.004	148±2	150±2	0.0161±0.0001	0.0304±0.0002	16800±160	2.94±0.03	0.75±0.40	1.16±0. 40
2	Moorea	LI-4	3.215±0.004	144±3	145±3	0.0094±0.0001	0.0316±0.0001	33200±400	3.07±0.02	0.75 ±0. 40	1.18±0. 40
3	Moorea	**WL1	2.230±0.003	150±3	151±3	0.0437±0.0003	0.0189±0.0001	3000±30	1.82±0.02	0.75±0. 40	1.01±0. 40
4	Moorea	CB 10	3.481±0.007	142±4	143±4	0.505±0.011	0.0214±0.0011	400±20	2.06±0.11	1.80±0. 40	2.09±0. 40
5	Moorea	CB11	2.994±0.005	143±3	144±3	0.0556±0.0002	0.0267±0.0001	4500±20	2.59±0.02	1.80±0. 40	2.16±0. 40
6	Moorea	*CB12	2.695±0.005	141±3	142±3	0.331±0.003	0.0229±0.0003	600±10	2.22±0.03	1.80±0. 40	2.11±0. 40
6	Moorea	*CB12 no.2	2.734±0.002	138±3	139±3	0.336±0.004	0.0229±0.0003	600±10	2.22±0.03	1.80±0. 40	2.11±0. 40
7	Moorea	CB 5	2.433±0.007	143±6	143±6	0.313±0.007	0.00025±0.00002	6±1	0.021±0.002	1.80±0. 40	1.80±0. 40
8	Moorea	RP2	2.265±0.003	148±3	148±3	0.0225±0.0002	0.00115±0.00003	400±10	0.109±0.003	0.00±0. 40	0.02±0. 40
9	Moorea	RP4	2.390±0.004	150±3	150±3	0.365±0.003	0.00078±0.00003	20±1	0.072±0.003	-0.80±0. 40	-0.79±0. 40
10	Moorea	MCM1	3.470±0.011	142±5	143± 5	0.093±0.006	0.0311±0.0002	4000±200	3.02±0.04	1.10±0. 40	1.52±0. 40
11	Moorea	MCM2	2.597±0.005	146±3	147±3	0.910±0.007	0.0271±0.0001	200±2	2.61±0.02	1.10±0. 40	1.47±0. 40
12	Moorea	MCM5	3.292±0.005	149±4	150±4	0.024±0.006	0.0260±0.0001	10900±3000	2.51±0.02	1.10±0. 40	1.45±0. 40
13	Moorea	MCM10	2.684±0.004	149±3	149±3	0.089±0.007	0.0227±0.0002	2100±200	2.19±0.02	1.10±0. 40	1.41±0. 40
14	Moorea	CM1	3.469±0.005	144±3	146±3	0.0099±0.0001	0.0451±0.0002	48900±700	4.39±0.04	0.75±0. 40	1.37±0. 40
15	Moorea	CM2	3.607±0.006	145±3	146±3	0.059±0.0003	0.0407±0.0002	7800±40	3.96±0.03	0.75±0. 40	1.31±0. 40
16	Moorea	CM4	2.934±0.005	146±3	147±3	0.1583±0.005	0.0378±0.0002	2200±70	3.66±0.03	0.75±0. 40	1.26±0. 40
17	Moorea	CM7	2.598±0.005	147±3	148±3	0.276±0.007	0.0388±0.0002	1100±20	3.76±0.04	0.75±0. 40	1.28±0. 40

Table 2B: Uranium/Thorium isotopic composition and ages of fossil corals from Huahine

Sample Number	Island	Sample Label	^{238}U (ppm)	$\delta^{234}U(0)$ (‰)	$\delta^{234}U(T)$ (‰)	^{232}Th (ppb)	$^{230}Th/^{238}U$ (dpm/dpm)	$^{230}Th/^{232}Th$ (dpm/dpm)	Age (ka)	Sampling elevation (m)	Subsidence corrected elevation (m)
18	Huahine	H-Tai-1	3.892±0.006	145±2	146±2	0.0045±0.0001	0.0351±0.0001	94900±1500	3.41±0.02	0.50±0. 40	0.98±0. 40
18	Huahine	**H-Tai-1 no 2*	3.95±0.02	143±2	144±2	0.0045±0.0001	0.0352±0.0003	102900±78200	3.41±0.03	0.50±0. 40	0.98±0. 40
19	Huahine	H-Tai-2	3.367±0.004	144±2	145±2	0.116±0.002	0.0321±0.0003	2900±40	3.12±0.03	0.50±0. 40	0.94±0. 40
20	Huahine	H-Tai-3	3.532±0.009	142±5	144±5	0.628±0.006	0.0477±0.0002	800±10	4.66±0.05	-0.80±0. 40	-0.15±0. 40
21	Huahine	H-Tai-5	3.99±0.01	140±5	142±5	0.105±0.007	0.0499±0.0003	5800±400	4.90±0.06	1.00 ±0. 40	1.69±0. 40
22	Huahine	*H-Tai-7	3.579±0.008	139±5	141±5	0.098±0.007	0.0495±0.0003	5600±400	4.85±0.06	-0.25±0. 40	0.43±0. 40
23	Huahine	H-Tai-8	2.656±0.008	142±5	144±5	0.076±0.007	0.0404±0.0003	4400±400	3.94±0.05	0.30±0. 40	0.85±0. 40
24	Huahine	H-Tai-9	2.964±0.009	142±5	144±5	0.053±0.006	0.0419±0.0012	7200±900	4.08±0.14	0.00±0. 40	0.57±0. 40
25	Huahine	*H-Tai-10	2.966±0.007	140±5	141±5	0.113±0.008	0.0387±0.0015	3100±200	3.78±0.17	0.00±0. 40	0.53±0. 40
26	Huahine	H-Tai-11	4.26±0.01	142±4	144±5	0.039±0.006	0.0498±0.0003	16900±2700	4.88±0.06	0.75±0. 40	1.43±0. 40
27	Huahine	H-Tai-12	3.44±0.01	149±5	150±5	0.050±0.007	0.0430±0.0004	9100 ±1300	4.17±0.07	-0.20±0. 40	0.38±0. 40
28	Huahine	H-Tai-13	2.645±0.007	144±5	146± 5	0.020±0.005	0.0403±0.0003	16800±4500	3.92±0.05	-0.20±0. 40	0.35±0. 40
29	Huahine	H-M-1	2.596±0.006	144±4	147±2	0.055±0.001	0.0402±0.0002	5900±60	3.92±0.04	0.50±0. 40	1.05±0. 40
30	Huahine	H-M-2	2.293±0.002	146±2	147±2	0.0109±0.0001	0.0402±0.0001	26200±300	3.92±0.02	0.30±0. 40	0.85±0. 40
31	Huahine	HM-4	3.639±0.006	147±3	148±3	0.011±0.004	0.0161±0.0001	15900±6000	1.55±0.02	0.10±0. 40	0.32±0. 40
32	Huahine	HM-5	3.183±0.005	147±3	147±3	0.119±0.005	0.0113±0.0001	900±40	1.08±0.02	0.00±0. 40	0.15±0. 40
33	Huahine	H-MT-1	2.593±0.007	149±5	151±5	0.084±0.001	0.0520±0.0002	5000±30	5.07±0.05	1.10±0. 40	1.81±0. 40
34	Huahine	*H-MT-2	3.082±0.004	142±2	144±2	0.156±0.001	0.0547±0.0002	3300±20	5.38±0.03	0.75±0. 40	1.50±0. 40
35	Huahine	H-V-1	2.579±0.003	147±2	147±2	0.0679±0.0003	0.0184±0.0001	2200±10	1.78±0.01	0.25±0. 40	0.50±0. 40
35	Huahine	*H-V-1 no 2*	2.736±0.002	147±4	148±4	0.0713±0.0007	0.0187±0.0002	2400±200	1.79±0.02	0.25±0. 40	0.50±0. 40
36	Huahine	H-PT-1-A	2.807±0.004	144±3	145±3	0.490±0.002	0.0205±0.0002	400±3	1.98±0.02	0.00±0. 40	0.28±0. 40
37	Huahine	H-PT-1-2	3.937±0.005	142±3	144±3	0.215±0.001	0.0505±0.0002	2900±10	4.95±0.02	0.75±0. 40	1.44±0. 40

Table 2C: Uranium/Thorium isotopic composition and ages of fossil corals from Bora Bora

Sample Number	Island's Name	Sample Name	^{238}U (ppm)	δ^{234}U (0) (‰)	δ^{234}U(T) (‰)	^{232}Th (ppb)	^{230}Th/^{238}U (dpm/dpm)	^{230}Th/^{232}Th (dpm/dpm)	Age (ka)	Sampling elevation (m)	Subsidence corrected elevation (m)
38	Bora Bora	BB-MP 3/2	2.047±0.001	146±1	147±1	0.055±0.005	0.0261±0.0003	3000±300	2.52±0.03	1.10±0. 40	1.23±0. 40
39	Bora Bora	*BB-MP 4/2	3.142±0.002	144±1	145±1	0.730±0.006	0.0301±0.0002	400±4	2.91±0.02	1.10±0. 40	1.25±0. 40
40	Bora Bora	BB-MP 2/2	3.021±0.001	144±1	146±1	0.201±0.006	0.0324±0.0002	1500±40	3.13±0.02	1.10±0. 40	1.26±0. 40
41	Bora Bora	BB-MP 5/3	3.326±0.002	145±1	147±1	0.177±0.005	0.0466±0.0002	2700±80	4.53±0.02	-1.30±0. 40	-1.07±0. 40
42	Bora Bora	BB-MP 6/6	3.090±0.002	144±1	146±1	0.714±0.005	0.0488±0.0002	700±5	4.75±0.02	-1.30±0. 40	-1.06±0. 40
43	Bora Bora	*BB-MP 6/5	3.094±0.002	142±1	144±1	0.147±0.007	0.0488±0.0002	3200±150	4.76±0.03	-1.30±0. 40	-1.06±0. 40
44	Bora Bora	*BB-MX 1/2	3.505±0.002	144±1	145±1	0.107±0.007	0.0313±0.0002	3200±200	3.03±0.02	1.30±0. 40	1.45±0. 40
45	Bora Bora	BB-MX 3/2	2.767±0.001	145±1	146±1	0.140±0.006	0.0287±0.0002	2000±70	2.77±0.02	0.95±0. 40	1.09±0. 40
46	Bora Bora	BB-MX 4/2	2.858±0.001	145±1	146±1	0.058±0.005	0.0341±0.0002	5200±400	3.29±0.02	1.40±0. 40	1.56±0. 40
47	Bora Bora	BB-MX 5/1	2.493±0.001	145±1	146±1	0.021±0.004	0.033±0.0002	12300±2600	3.18±0.02	0.95±0. 40	1.11±0. 40
48	Bora Bora	**BB-MX 5/3	2.160±0.001	148±1	149±1	0.055±0.006	0.0312±0.0003	3800±400	3.01±0.03	0.95±0. 40	1.10±0. 40
49	Bora Bora	*BB-MX 6/3	2.815±0.002	142±1	144±1	0.033±0.006	0.0328±0.0002	8600±1700	3.18±0.03	0.95±0. 40	1.11±0. 40
50	Bora Bora	*BB-MX 7/2	2.055±0.001	144±1	145±1	0.102±0.007	0.0186±0.0003	1200±70	1.79±0.03	1.40±0. 40	1.49±0. 40
51	Bora Bora	*BB-MM-13	2.661±0.005	142±3	143±3	0.0049±0.0001	0.0249±0.0001	41900±700	2.42±0.02	0.65±0. 40	0.77±0. 40

Note for table 2: The δ^{234}U(0) indicates the measured ^{234}U/^{238}U ratios from our samples and the δ^{234}U(T) represents the decay corrected activity ratio calculated from the measured ^{234}U(0). All statistical errors are two standard deviations of the mean (2σ mean). * indicates the samples with δ^{234}U(T) slightly lower, and ** indicates the values slightly higher than δ^{234}U seawater value of 146.8±0.1‰ [*Andersen et al.,* 2010]. For the correction of subsidence of the Islands, we have used 0.14 mm/year for Moorea and Huahine according to Pirazzoli et al., [1985]. For Bora Bora Island we have used 0.05 mm/year [*Pirazzoli and Montaggioni,* 1985]. All samples have been corrected for initial ^{230}Th by using a ^{230}Th/^{232}Th activity ratio of 0.6±0.2 [*Fietzke et al.,* 2005].

Hence, the average absolute difference of those samples slightly off the accepted value results in an age uncertainty of about ±20 years. Latter value is within the age uncertainty of our samples being in the order of about 20 to 30 years and can therefore be considered to be negligible.

3.4. Society Island Relative Sea level Curve, Subsidence Correction and Statistical Age Distribution

3.4.1. *In situ* Corals and Micro-atolls

For establishing an empirical relative sea level curve based on observation only those corals which can be considered to be *in situ* and being not displaced have to be taken into account. Following this approach we neglect sample Nos. 4, 5, 6 (Tab. 1 and 2; marked by dashed circles in Fig. 3A) originating from Moorea which were already considered to be conglomerate during the field expedition in 2009. Sample No. 7 (Tab. 1 and 2; marked with a dashed circle in Fig. 3A) was originally considered to be *in situ*, however, this sample show an age of ~20 years and is actually supposed to be located at the modern msl rather than an elevation of ~1.8 m apmsl. Hence, we consider this exceptional sample to be not *in situ* rather displaced or being a sampling artifact. Therefore, these samples as well as the samples considered to be conglomerate are arbitrarily neglected for further discussion. For later reconstruction of the apparent past sea level, the age and the elevation apmsl of micro-atolls is of certain interest (marked by squares in Fig. 3). Sample No. 24 (H-Tai-9) and No. 25 (H-Tai-10) from Huahine as well as sample 45 (BB-MX 3/2) from Bora Bora represent such micro-atolls.

3.4.2. Subsidence Correction

These Society Islands are volcanic in origin and tend to subside as they move away from the asthenospheric bump and as a result of lithospheric cooling with age (McNutt and Menard, 1978). Therefore, the islands near hotspot tend to subside more rapidly as they move down the slope of the asthenospheric bump compared to the islands which are further away from the hotspot region (McNutt and Menard, 1978; Scott and Rotondo, 1983a, b). In Fig. 3A it can be seen that the Moorea and Bora Bora corals tend to have the highest elevation whereas the Huahine corals tend to be at the most shallow positions apmsl.

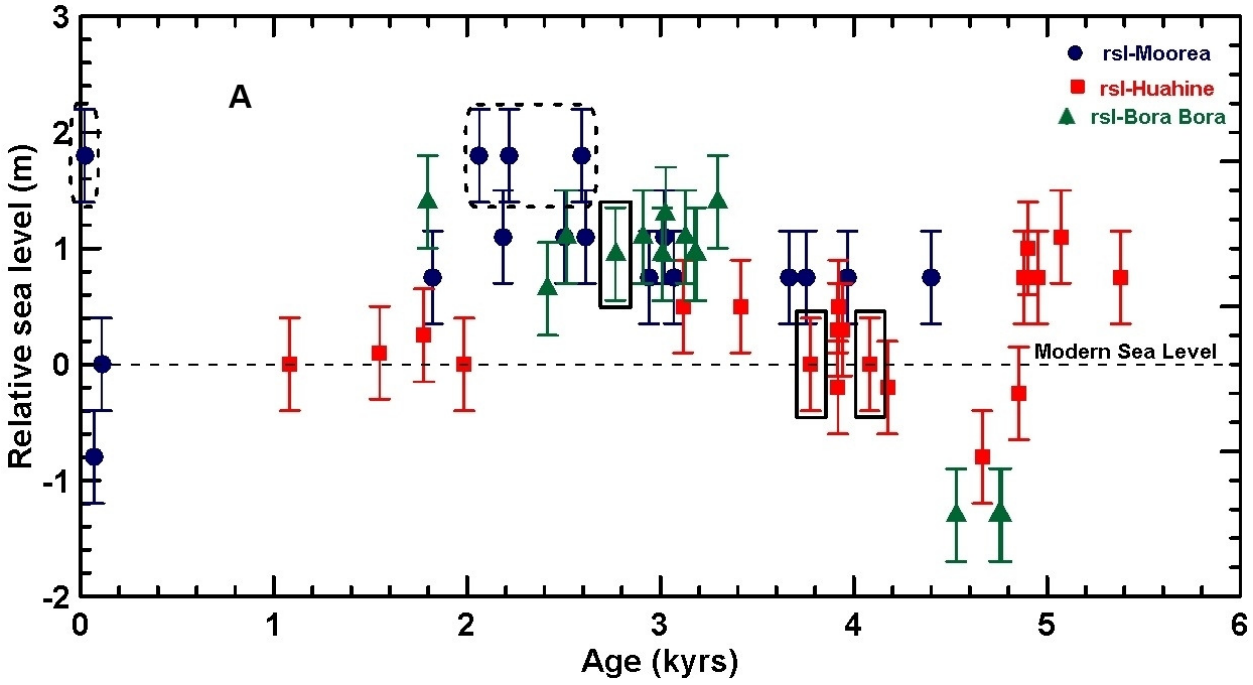

Fig. 3A: The heights apmsl of the samples are plotted as a function of their corresponding ages. In Fig. 3A dashed circles mark the corals which are either conglomerate or being displaced from their original positions. Samples marked with squares represent micro-atolls.

Latter observation may reflect differential subsidence rates of the three islands relative to each other as a function of the islands individual cooling which is assumed to be a function of the distance to the former volcanic hotspot. In order to approach the original sea level position during live time of the corals ("paleo-sea level"), the measured elevations of our samples have to be corrected by the subsidence of the studied islands. For Moorea island which is located ~130 km from the hotspot region (Blais et al., 2002), we have applied a subsidence rate of 0.14 mm/year according to Pirazzoli et al., [1985]. For Bora Bora island which is located ~390 km away from the hotspot region the height apmsl is corrected by 0.05 mm/year only which is the minimum subsidence rate of the Leeward islands in the Society Islands group (Pirazzoli et al., 1985). Although Huahine is located ~140 km from Moorea, petrological analysis has claimed that Huahine have similar subsidence rate as Moorea island [*Pirazzoli et al.,* 1985], therefore, the same correction for the subsidence rate was used for this island (Fig. 3B, 4A and B).

However, after correction, although they overlap within the error, Huahine corals still tend to indicate slightly shallower sea level positions compared to the other two islands. This may

indicate that the Huahine subsidence rate is probably slightly higher than the applied rate of 0.14 mm/year used here for corrections.

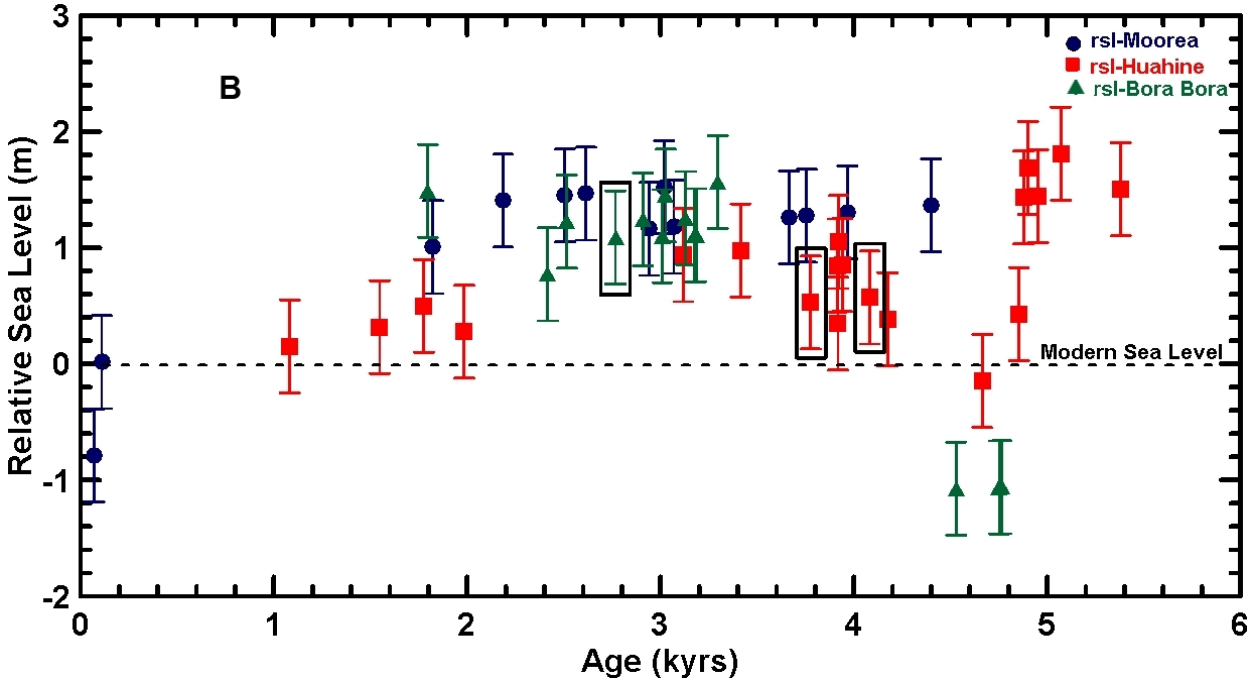

Fig. 3B: All values (heights apmsl) have been corrected for their island specific subsidence rate.

Note that, our correction and their related uncertainty involves only the uncertainty of our measured sample elevations, because the information about uncertainties concerning the subsidence rates was not available from the cited studies of Pirazzoli and Montaggioni, [1985] and Pirazzoli et al., [1985]. In Fig. 3B after subsidence correction the oldest sample data (No. 34, 5.38±0.03 ka) has reached an elevation of ~1.50±0.40 m apmsl at Huahine island slightly below the highest coral at a position of 1.81 m apmsl of a coral from Huahine island (No. 33). The micro atoll samples No. 24, 25 from Huahine show a subsidence corrected paleo-elevations of 0.57±0.40 m and 0.53±0.40 m apmsl (Fig. 3) which is compatible to the paleo-elevation of the micro-atoll sample 45 from Bora Bora of 1.09±0.40 m apmsl. In particular for the micro-atoll, the position of the sea level is expected to be within few centimeters of the micro-atoll position (Smithers and Woodroffe, 2000).

To our knowledge there are only a few measurements by Pirazzoli and Montaggioni, [1988] from Bora Bora and Huahine which are directly pertinent to our study. We compare these older ^{14}C-based data with our data presented here after transformation of the ^{14}C ages to U/Th calendar

year using the Calib radiocarbon calibration Program (Calib 6.11 program-Marine09) (Fairbanks et al., 2005). Note, that U/Th ages are calendar year ages (2014) whereas ^{14}C ages are stratigraphic ages which have to be converted to calendar year ages by using a well-known ^{14}C-U/Th calibration curve by (Fairbanks et al., 2005). The converted U/Th ages (in ka) for Bora Bora are: (2BB1: 2.97±0.39 (+0.5 m), 2BB7: 3.26±0.36 (+0.4 m), 2BB5: 2.80±0.31 (+0.6 m)) and for Huahine (2HU1: 3.92±0.41 (+0.3 m), 2HU9: 3.55± 0.40 (+0.3 m)). For conversion to calendar years reservoir age corrections have been applied between 350 and 400 years according to the geographical locations (Fairbanks et al., 2005). All these earlier measurements are in general accord with our data presented here.

3.5. Numerical Modeling of the Society Island Sea level Curve(s)

3.5.1. Geophysical model

To compute the mid to late Holocene GIA-induced rsl changes at the Society Islands we solve the gravitationally self-consistent Sea Level Equation (SLE; [*Farrell and Clark,* 1976; *Mitrovica and Peltier,* 1991]) by means of the program SELEN (Spada and Stocchi, 2007). Solving the SLE for a prescribed continental ice-sheet chronology and solid Earth rheology yields the space- and time-dependent rsl change on a global scale (Wu and Peltier, 1983). The solution of the SLE implies that the gravitational potential of the sea surface is always constant, i.e., that the sea surface corresponds to the equipotential surface of gravity named geoid (Farrell and Clark, 1976; Spada and Stocchi, 2007; Wu and Peltier, 1983). This implies that ice-sheet thickness variations are compensated by equivalent ocean-averaged sea level variations (eustatic solution), and that the gravity vector is everywhere perpendicular to the sea surface. The two main ingredients of the SLE are (i) the ice-sheet chronology, which describes the ice-sheets thickness variation through time, and (ii) the solid Earth rheological model, which describes the response of the solid Earth and of the geoid to ice-sheets thickness variation. We solve the SLE by means of the pseudo-spectral method, which allows a direct and fast spectral analysis (Milne and Mitrovica, 1998; Mitrovica et al., 1994; Mitrovica and Peltier, 1991). For this purpose, the solid Earth and geoid deformations are implemented by means of the “Normal Modes Technique” as introduced by (Peltier, 1974). The latter assumes a spherically symmetric, self-gravitating, rotating and radially stratified solid Earth model (Spada et al., 2006; Spada et al., 2012). The latter is a 1-D linear model and does not include lateral heterogeneities. The outer shell is elastic and mimics

the lithosphere. Between the lithosphere and the inner inviscid core is the mantle. The latter can be discretized into *n* Maxwell viscoelastic layers. In this work we discretize the Earth´s mantle into two layers, namely the upper mantle, and the lower mantle. The lithosphere thickness and the viscosity of the mantle layers are the free parameters.

We employ and compare ICE-5G (Peltier, 2004) and RSES-ANU in global ice-sheets chronologies for the post-LGM deglaciation. The ice-sheets models describe the Late Pleistocene ice-sheets thickness variations until present-day and have been constrained by means of geological and archaeological rsl data as well as present-day instrumental observations like GPS-derived vertical and horizontal crustal velocities and Satellite Gravimetry (Peltier, 2004). Both ice-sheet models depend on the solid Earth rheological, in particular on the thickness of the elastic lithosphere as well as on the number and on the viscosity of Mantle viscoelastic layers which have been employed within the iterative process (Lambeck et al., 1998). Hence, each ice-sheet model should be employed within the SLE with the accompanying Earth model (Lambeck et al., 1998; Peltier, 2004; Tushingham and Peltier, 1992). Consequently we combine ICE-5G chronology with VM2 viscosity profile. The latter is characterized by a 100 km-thick elastic lithosphere and by an upper mantle viscosity of 5.0×10^{20} Pa and a lower mantle viscosity of 5.0×10^{21} Pa (Peltier, 2004). At the same manner we employ RSES-ANU ice-sheets model with a VKL mantle profile. The latter is characterized by a 65 km-thick elastic lithosphere and by an upper mantle viscosity of 3.0×10^{20} Pa and a lower mantle viscosity of 10.0×10^{21} Pa (Lambeck et al., 2004). Hereafter, we refer to the solutions for ICE-5G and VM2 as ICE-5G+VM2, and for RSES-ANU and VKL as RSES-ANU+VKL. We use ETOPO1 model for the initial topography and allow for the self-consistent variation of coastlines as well as for the near-field meltwater damping function (Milne and Mitrovica, 1996, 1998). Also, we include the rsl variations associated with fluctuations of the Earth's rotation vector (Milne and Mitrovica, 1998).

3.5.2. Predicted rsl Curves

3.5.2.1. Eustatic Sea level Change

We compare the rsl curves as predicted for Bora Bora according to RSL-ICE-5G+VM2 (red solid line) and RSL-RSES-ANU+VKL (black solid line), respectively (Fig. 4A). The red and black dashed curves represent the eustatic solutions according to ICE-5G and RSES-ANU,

respectively. According to ICE-5G (red dashed line), the global mean sea level rises to almost the present position at ~4.5 ka although some minor fluctuations occur still later (Fig. 4A).

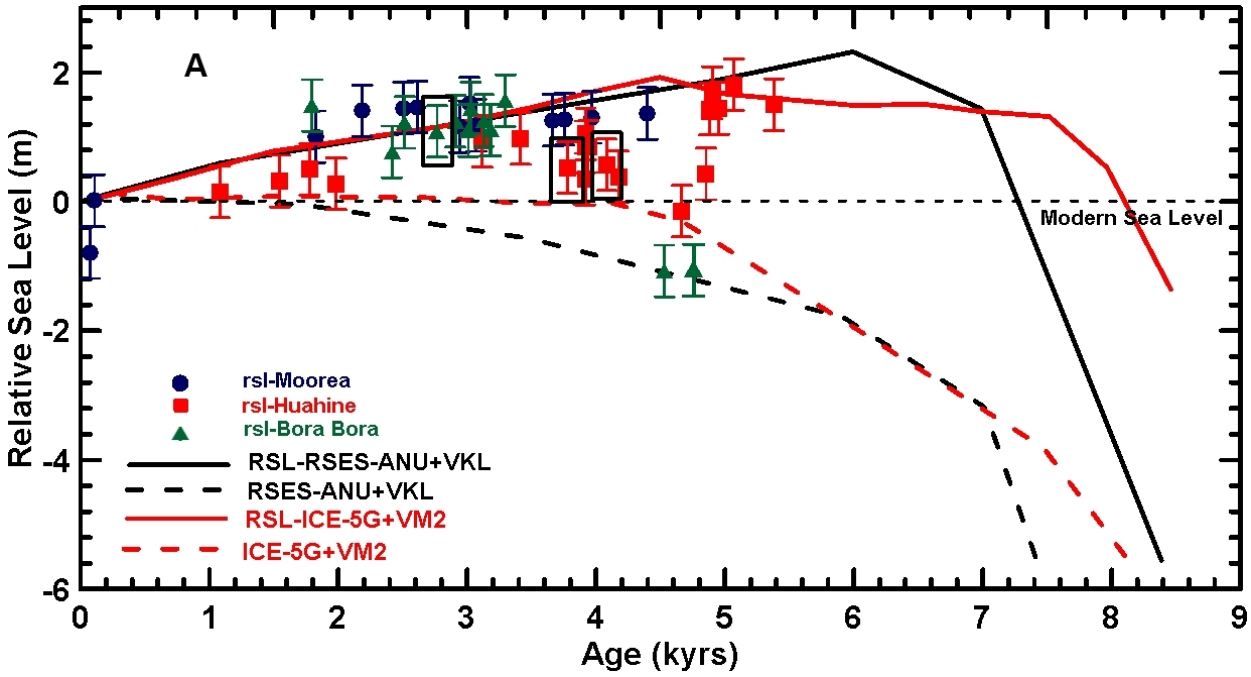

Fig. 4: In Fig. 4A the theoretical predicted rsl-curves are compared with empirical observations. The solid black curve represents the predicted rsl according to RSL-RSES-ANU+VKL (ice sheet model and Mantle profile) and the red solid curve represents the predicted rsl according to RSL-ICE-5G+VM2 (ice sheet chronology and the viscosity profile). The dashed lines represent the eustatic sea levels. In general solid curves represent the full result of the sea level equations which incorporates all the solid Earth and gravitational as well as rotational feedback. The dashed curves represent the hypothetical eustatic sea level change for each ice sheet model. It can be seen that there is a general accord between theoretical predictions and observations. In particular the micro-atoll positions are in general accord with the predictions.

A different trend is expected according to RSES-ANU deglaciation, which results in a monotonous sea level rise until present (black dashed line, Fig. 4A). For the period under consideration, the main difference between the two eustatic curves depends on the different deglaciation of the Antarctic ice-sheet component in the two global ice-sheets chronologies. While the melting of the Antarctic ice-sheet ends at 4.5 ka in ICE-5G, in RSES-ANU it continues until present-day.

3.5.2.2. Predicted RSL at Society Islands

Both ice-sheets models result in a ~2.0 m rsl highstand which is then followed by a drop until present mainly driven by the ocean siphoning effect. In particular, RSL-RSES-ANU+VKL (black solid line in Fig. 4A) results in a more peaked highstand at ~6 ka, which is then followed by an almost linear rsl drop. The latter is almost specular to the eustatic curve, implying that the local GIA response is significantly stronger than the rate of meltwater release. The RSL- ICE-5G+VM2 model (red solid line) instead, results in an almost stable highstand from about 7.5 ka until 5.0 ka, which is then followed by a short term rise peaking up at 4.5 ka, when most of the melting ceases. Despite the differences in ice-sheets models and mantle viscosity profiles, our modelled rsl curves show an almost undistinguishable rsl drop after 4.0 ka as a function of the ocean siphoning effect. While for RSL-ICE-5G+VM2 the rsl drop starts by the very end of the melting phase (4.5 ka), the regression predicted according to RSL-RSES-ANU+VKL starts earlier when ~1.8 m of equivalent sea level are still to be released to the oceans from Antarctica. Our GIA modeling results confirm the strength of the ocean siphoning effect, summed to the increase of ocean area due to ice-sheets waxing and flooding of coastal areas, is large enough to fully cloak the eustatic rise.

3.6. Comparison between theoretical data and empirical observations

3.6.1. Factors influencing sea level height observations

In general, *Porites* corals grow from very close to sea level to ~25 m below sea level (Cabioch et al., 1999; Carpenter et al., 2008; Pratchett et al., 2013). Therefore, fossil coral reef cores do not necessarily provide precise constraints on the position of local sea level because of their considerable range of vertical growth. From these arguments it is clear that we cannot unambiguously establish the actual local sea level curve from sea level observations derived from corals alone. However, we can infer that the Late Holocene sea level curve must have reached a significant height above the present sea level position at this locality and that the true sea level must lie above the corals position. Micro-atolls are the exception because micro-atolls are formed at the actual sea level position and may even fall dry during low tides. Following this approach we infer that any theoretical predicted sea level curve as modeled in the frame of this project must lie at certain distance above the dated corals but with an almost zero distance for a micro-atoll. The comparison of our data with our numerical modeling predictions (Fig. 4A)

shows in general good agreement. In particular, the micro-atoll sample No. 45 from Bora Bora lies directly along both predicted rsl curves, while Huahine micro-atolls Nos. 24 and 25 are situated 0.3 m below the theoretical curve.

The scatter in the sea level amplitude as seen from our data may therefore be a function of the differences in the coral´s position relative to the sea surface and the differences in the subsidence rate. Considering the micro atolls in our study, they seem to best serve as natural and precise recorders of the sea level. For example, in our data, we can clearly see that, after subsidence correction the micro atoll No. 45 from Bora Bora Island clearly marks the sea level around 2.77±0.02 ka (Figure 3B, 4A and B). For Huahine Islands, although the micro atolls No. 24 and 25 overlap within the uncertainty with the normal *Porites* (Sample No.s 15 (3.96±0.03 ka), 16 (3.66±0.03 ka) and 17 (3.76±0.04 ka) from Moorea but they are plotted slightly lower in elevation (Fig. 3B, 4A and B). From the micro atoll study of Christmas island, Woodroffe et al., [2012] have observed that although micro atolls mark the sea level within few centimeters, they still may show significant differences in elevation as a function of their position in the island. This is probably caused by a differential geoid distortion as a function of the local gravitational field varying as a function between different parts of the island or attenuation of tidal amplitude of the samples collected in the lagoonal areas. Our data can neither support nor preclude the presence of tidal attenuation or geoidal gradient in French Polynesia.

3.6.2. Comparison of empirical to modeled data

The model-based amplitudes are in general accord with the empirical data concerning the maximum amplitude of ~2m and the timing of the rsl at least for the decline of the Holocene sea level from the highstand to the present day position. Note, from our rsl data we cannot distinguish which of the ice-models (RSL-ICE-5G+VM2 or RSL-RSES-ANU+VKL), fits best the observations. This is because there are no data available older than ~5.5 ka necessary for such a specific model verification. Although most of the samples lie below the predicted rsl curves, a few data mostly from Moorea and Bora Bora lie slightly above the predictions. We may argue the applied subsidence correction of 0.14 mm/year for the Moorea corals has been over estimated and the smaller rate is more suitable. We may also argue that the GIA model should be improved by changing the solid Earth model parameters taking into account the local distortions

of the geoid, i.e. mantle viscosity values, lithospheric thickness, or even the ice-sheets chronology, or that these corals are not *in situ* and rather have been displaced from their original positions. In contrast, the applied subsidence correction for Huahine which is also pending independent verification is in general agreement with the theoretical predictions and the other empirical data in general.

In Fig. 4B we also compare the empirical data of this study with earlier model predictions of Mitrovica and Peltier, [1991] who employed ICE-3G ice-sheet chronology. According to ICE-3G, the post-glacial rsl reached modern position approximately 2.5 ka later and resulted in a highstand which is ~1m higher than suggested in this study.

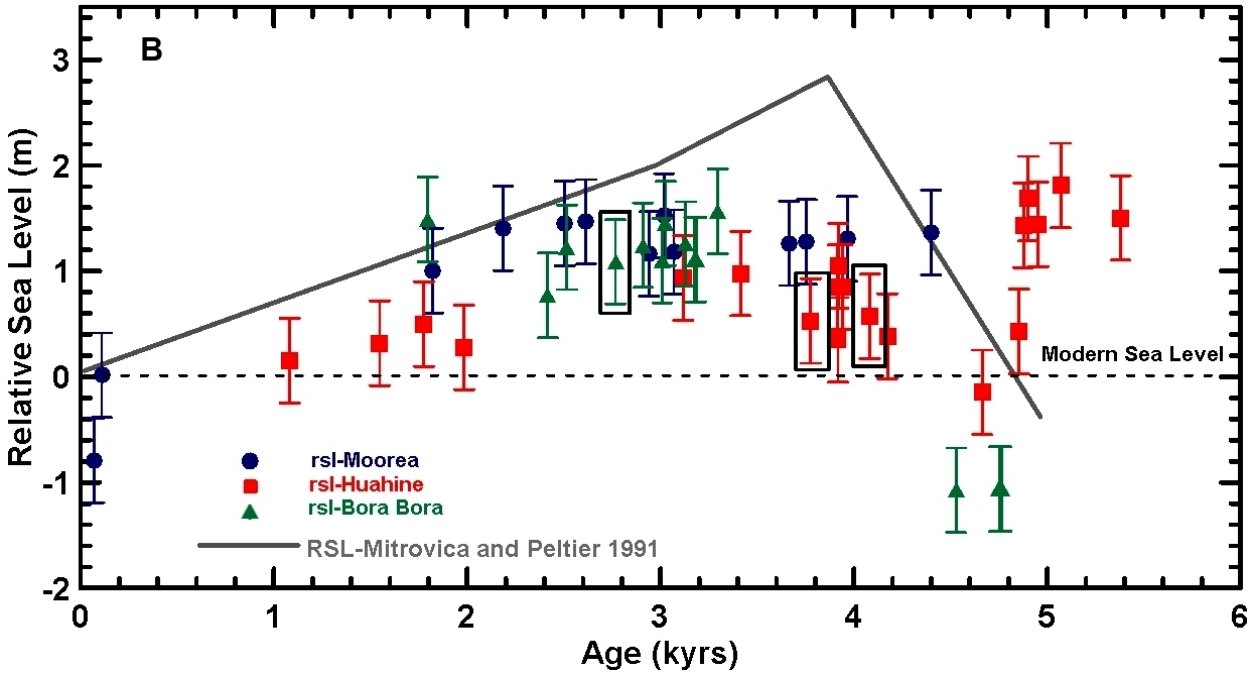

In Fig. 4B our empirical observations are compared with an earlier model of Mitrovica and Peltier, [1991]. However, there is a general disagreement between the empirical data and this earlier model prediction.

It can be seen that most of the empirical data fall within the frame provided by the Mitrovica and Peltier, [1991] curve and are in general accord with our findings. However, none of the micro-atoll positions (Nos. 24, 25, 45, marked by squares) are on or close to the Mitrovica and Peltier, [1991] model curve indicating that the rsl amplitude may be overestimated at these points. In addition all Huahine corals older than about ~4.5 ka (Nos. 21, 22, 26, 33, 34, 37) are also

plotting outside the predicted rsl-frame being in contrast to our expectations. Our results support the improvements occurred from the earlier ICE-3G [*Tushingham and Peltier,* 1992] to the more recent ICE-5G ice-sheet model [*Peltier,* 2004].

3.7. Conclusions

Collected *in situ* fossil corals from the Society Islands, French Polynesia clearly indicate that the local Late Holocene sea level there was higher between at least 5.4 ka until the recent past.

Reconstruction of sea level positions based on dated corals is hampered by the relative wide depth range for coral growth in the water, the subsidence rate of the islands where sample are collected and the gravitational geoid deformation of the local sea level height. Both the predicted rsl curves RSL-ICE-5G+VM2 and RSL-RSES-ANU+VKL (Fig. 4A) are in general accord with our empirical data concerning sea level amplitude and timing. In particular the available micro-atoll age (No. 45) from Bora Bora is in full support of both model curves after the Holocene sea level highstand.

The available empirical data cannot distinguish between ICE-5G+VM2 and the RSES-ANU+VKL ice-sheet model because no age data are available for corals older than 5.5 ka due to island subsidence.

Both empirical data and modeling indicate that Society Island sea level dropped by ~2 m since the Holocene maximum at ~4.5 ka corresponding to a rate of about 0.4 mm/year. This value has to be considered when sea level rise due to modern global climate change is considered.

Acknowledgements

The program funding was provided by the ESF funded CHECKREEF project (EI272/22-1, DU129/141-1) and also by GEOMAR, Helmholtz Zentrum für Ozeanforschung, Kiel. The PhD work of Rashid Rashid was financially supported by the Tanzania Ministry of Education and Vocational Training (MoEVT) in collaboration with DAAD (German Academic Exchange Service) fellowship. We gratefully acknowledge Ana Kolevica, Jutta Heinze, Brendan Ledwig, Patrick Reichert and Jeroen van der Lubbe for their assistance in sample processing and data analysis.

Chapter Four

4. Early Diagenetic imprint on temperature proxies in Holocene Corals: A case study from French Polynesia

Rashid Rashid[1], Anton Eisenhauer[1], Volker Liebetrau[1], Jan Fietzke[1], Florian Böhm[1], Marlene Wall[1], Stefan Krause[1], Andres Rüggeberg[1,2] and Wolf-Christian Dullo[1]

[1]GEOMAR Helmholtz Centre for Ocean Research Kiel, 24148 Kiel, Wischhofstr.1-3, Germany.

[2]University of Fribourg, Chemin du Musée 6, CH-1700 Fribourg, Switzerland.

Abstract

Coral based reconstructions of sea surface temperatures (SST) using Sr/Ca, U/Ca and $\delta^{18}O$ ratios are important tools for quantitative analysis of past climate variability. However, post-depositional alteration of coral aragonite due to early diagenesis is restricting the accuracy of calibrated proxies even on young corals. Here we present Mid to Late Holocene SST reconstructions using well dated (U/Th: ~70yr to 5.4ka) fossil *Porites* collected from the Society Islands, French Polynesia.

For a few coral samples microscopic observations and electron microprobe mapping reveal the presence of aragonite needles inside coral pores. Coral sections with identified secondary aragonite show on average a 25-30% higher Sr/Ca ratio than corresponding massive parts. Sections with secondary aragonite are characterized by Sr/Ca values above 10 mm/mol. We interpret this value as the threshold between diagenetically altered and unaltered coral material. The observed intra-skeletal variability of 5.4 to 9.9 mmol/mol probably reflects the physiological control of the corals on its trace metal uptake and the individual variability controlled by the rates of $CaCO_3$-precipitation. The Sr/Ca, U/Ca and $\delta^{18}O$ values are well correlated. However, we observe a significant offset between Sr/Ca, U/Ca, and $\delta^{18}O$ based SST reconstructions of up to ±7°C and a trend towards cooler temperatures. Latter shifts mostly reflect trace element specific diagenetic alteration due to partial dissolution and re-precipitation of secondary aragonite. This process tends to amplify temperature extremes and hence increase the SST-U/Ca and SST-Sr/Ca gradients and consequently their apparent temperature sensitivity.

A relative SST reconstruction is still feasible by normalizing our records to their individual mean value defined as ΔSST. This approach shows that the ΔSST records derived from different proxies are in phase with an amplitudinal variability of up to ±2°C with respect to their Holocene mean value. The ΔSST-values which are higher than mean SSTs (Holocene warm periods) are observed between ~1.8ka to ~2.8ka (Interval I), between ~3.7 and 4.0ka (Interval III) as well as before ~5ka. Lower ΔSSTs (Holocene cold periods) are observed between ~2.8 to ~3.7ka (Interval II) and ~4.0 to ~4.9ka (Interval IV). The corresponding SST periodicity of ~1500yrs in the Society Island record is in phase with the solar activity reconstructed from ^{10}Be and ^{14}C production [*Vonmoos et al.,* 2006] emphasizing the role of the solar activity for the climate variations in the Late Holocene. In particular, the observed Late Holocene SST variability reconciles empirically determined sea level variations [*Rashid et al.,* 2014] linking higher Late Holocene sea levels than predicted from numerical modelling that considered only "Glacial Isostatic Adjustment" into account to time intervals of higher SST values.

4.1. Introduction

Paleoclimate reconstruction is a scientific challenge for times that go beyond historical archives and instrumental climate recordings [*Gagan et al.*, 2000; *Grottoli*, 2001]. Among natural archives (e.g. tree rings, ice or sediment cores) used for climate reconstruction, scleractinian corals are one of the best recorder of environmental history of shallow water tropical oceans by providing windows to the climate in the past [*Beck et al.*, 1992; *de Villiers et al.*, 1995; *McCulloch et al.*, 1996; *Min et al.*, 1995; *Mitsuguchi et al.*, 1996; *Schrag*, 1999; *Shen et al.*, 1996; *Zinke et al 2004*]. This is because the trace element and isotope (TEI) ratios incorporated during biomineralization of the coral skeleton are sensitive recorders of environmental changes (proxies) providing continuous and undisturbed records with annual and even seasonal chronology due to their relatively high growth rates of up to several cm/year [*Corrège*, 2006]. These characteristics guarantee high temporal resolution down to a week and even better as well as undisturbed records free of bioturbation [*Corrège*, 2006]. Following this approach TEI proxies preserved in coral skeleton are essential for determining the evolution of the chemical history of seawater and its temperatures [*Beck et al.*, 1992; *Cohen and Hart*, 2004; *Corrège*, 2006; *Hathorne et al.*, 2011; *Marchitto et al.*, 2010]. In particular, the records of Sr/Ca, U/Ca and of δ^{18}O became most important proxies for the reconstruction of climatic history from sclerectinian

corals [*de Villiers et al.*, 1995; *Hathorne et al.*, 2011; *McGregor and Gagan*, 2003; *Weber*, 1973; *Yu et al.*, 2004]. However, coral TEI records cannot simply be transferred into environmental and climatic information; they need a species specific calibration to the environmental parameter (e.g. temperature) which is done by both field experiments and by culturing studies under controlled laboratory conditions. Experiments have shown that biogenic and inorganic precipitated aragonite ($CaCO_3$) is different. For example coral Sr/Ca ratios are about 10 to 15% lower when compared to inorganic Sr/Ca ratios precipitated at the same temperature [*Dietzel et al.,* 2004]. This observation refers to the so called "vital effect" and the strong physiological control of the coral´s metabolism on the uptake of trace metals from seawater for $CaCO_3$ precipitation. These processes are subject to intensive biomineralization studies and have to be considered for paleo-reconstructions [*Cohen and Gaetani, 2010; McConnaughey, 1989; Cohen and McConnaughey,* 2003].

A more general precondition that corals reliably record environmental conditions is that they preserve the TEI primary ratios of the original skeletal aragonite ("closed system behavior"). This is not always the case because under natural conditions aragonite is thermodynamically unstable and hence susceptible to dissolution and recrystallization to calcite (diagenetic alteration). This process generates a reorganization of the chemical composition and may violate the closed system behavior superimposing and obscuring original TEI compositions. The latter process in particular affects Sr/Ca and U/Ca ratios because both proxies tend to show considerably lower ratios in calcite than in aragonite [*Reeder et al.,* 2000]. In addition, exposure of fossil corals to meteoric water and groundwater cause dissolution of primary biological aragonite and re-precipitation of inorganic secondary calcite. Secondary inorganic aragonite precipitation is typical for marine diagenetic environment [*Enmar et al.*, 2000]. Dolomitization and cementation are processes further violating closed system behavior [*Enmar et al.*, 2000; *Land*, 1973; *McGregor and Gagan*, 2003; *McGregor and Abram*, 2008; *Tucker and Wright*, 2009] challenging the use of TEI in fossil scleractinian coral as a reliable TEI archive [*Allison et al.*, 2007; *McGregor and Abram*, 2008; *Müller et al.*, 2001; *Nothdurft and Webb*, 2009].

The magnitude and the type of diagenesis does not necessarily correlate with the age of a coral, but generally the type of environmental exposure, corals species and coral porosity are supposed

to be the controlling factor for diagenesis [*Dullo, 1986; Enmar et al.*, 2000; *Hendy et al.*, 2007; *McGregor and Gagan*, 2003]. For example, diagenesis can occur in a coral immediately post mortem, whereas fossil corals as old as 125 ka being unaffected of diagenesis [*Nothdurft and Webb*, 2009]. Studies have shown that precipitation of secondary aragonite within the pores of a coral skeleton is related to marine environments where the pores are saturated by sea water [*Longman*, 1980; *Tribble et al.*, 1990]. Calcite diagenesis is mainly associated with fossils being exposed to fresh water [*Longman*, 1980].

Reconstructions may be associated with uncertainties that are difficult to detect. For example, different phases of early diagenesis such as submarine secondary aragonite precipitation or dissolution of primary aragonite skeleton could cause inaccuracy of the reconstruction [*Hendy et al.*, 2007; *McGregor and Abram*, 2008]. This is because common methods like X-Ray Diffraction fail to distinguish between primary and secondary aragonite phases (earliest diagenetic phase) because it has the same mineralogy as the primary aragonite. It has been suggested that very small diagenetic changes might obscure any paleoclimate estimates [*McGregor and Gagan*, 2003]. For Sr/Ca proxy, which has been found to be strongly affected by diagenesis [*Sayani et al.*, 2011], it has been shown that the presence of ~1% of calcite in the skeletal pores could result in about 1-2°C warmer SST estimates [*McGregor and Gagan*, 2003]. About 2% of early diagenetic secondary aragonite is able to shift the SST estimates into cooler temperatures by 0.4 and 0.9°C [*Allison et al.*, 2007]. In contrast, the $\delta^{18}O$ isotope ratio has been known to be at least less susceptible to diagenesis and also less impacted by calcite precipitation compared to the Sr/Ca proxy [*McGregor and Gagan*, 2003]. Despite the recent increase of coral studies few studies have focused on sampling strategies to avoid diagenetically altered skeletal parts in order to extract reliable proxy information.

The present study attempts to show the impact of early diagenetic imprint on SST proxies in Holocene corals by analyzing areas within a single sample that are affected by diagenesis and compare them with areas where the original signature of primary aragonite is observed. The sampling methods used to achieve these results contribute into the understanding of achieving most precise paleoclimate reconstructions. Furthermore, this study is also focusing on constraining the Mid to Late Holocene climate history of the Society Islands, French Polynesia,

using Sr/Ca, U/Ca ratios and $\delta^{18}O$ isotopes from fossil *Porites* corals that are exposed to subaerial conditions during Late Holocene sea level regression [*Rashid et al.,* 2014].

4.2. Methodology

4.2.1. Study Area

The Society archipelago lies in the tropical South Pacific Ocean of French Polynesia between 17°52'S 149°50'W and 15°48'S 154°50'W (Fig. 1). The archipelago consists of more than ten islands lying along the distance of 720km from Southeast to Northwest of the area [*Duncan and McDougall,* 1976; *Montaggioni,* 2011]. The islands are volcanic in origin formed by a distinct hotspot (Teahiti'a-Mehetia) which is currently located around Mehetia region as the Pacific plate moves over the hotspot in North West direction [*Gripp and Gordon*, 1990].

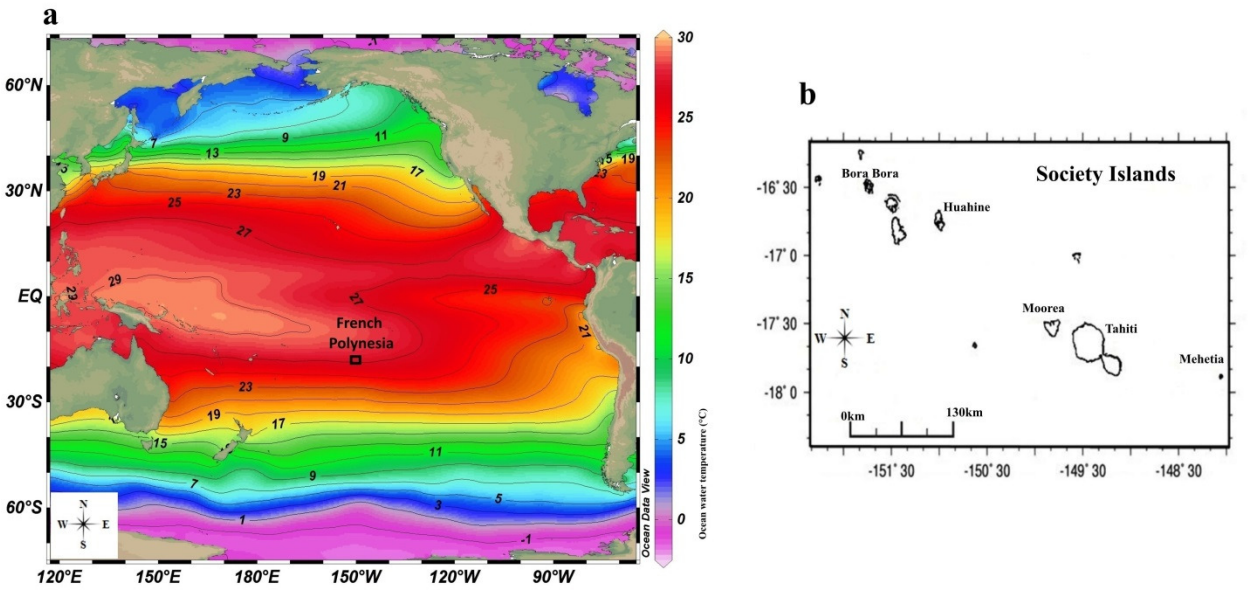

Fig. 1: (a) The map of French Polynesia where the Society Islands are located, together with the SST contour lines showing temperature distribution, b) The map of Society Islands where samples were collected.

They are characterized by extended emerged reef platforms currently exposed above the present sea level [*Rashid et al.,* 2014]. The geochronology of these islands is described in several studies (e.g. [*Blais et al.*, 1998; *Blais et al.*, 2000; *Duncan and McDougall*, 1976; *Duncan et al.*, 1994; *Guillou et al.*, 2005; *White and Duncan*, 1996]. They have shown that the ages of these islands increase towards northwest as they move away from the hotspot. For example, Mehetia (<1 Ma),

Tahiti (1.67–0.25 Ma), Moorea (2.15–1.36 Ma), Huahine (3.08–2.06 Ma), Raiatea (2.75–2.29 Ma), Tahaa (3.39–1.10 Ma), Bora Bora (3.83–3.10 Ma) and 5 Ma for Maupiti. The climate of the Society Islands is tropical with two main seasons. The austral summer is the warm and rainy season that spans from November to April. During this period, the conditions are hot with average SSTs between 28°C and 29°C [*Delesalle et al.,* 1985; *Boiseau et al.,* 1998]. Heavy rains are mostly experienced during December and January mainly affecting the coastline. Average rainfall is ~2753 mm/year [*Cabioch et al.*, 1999]. The austral winter spans from May to October. This period is marked by low SST averaging between 23°C and 25°C and rarely dropping below 19°C [*Delesalle et al.,* 1985]. Trade winds blow from East (South-East) and North-East direction. Tides are semi-diurnal and their amplitude averages 0.5 m [*Seard et al.*, 2011].

4.2.2. Coral sampling

In situ fossil *Porites* corals were collected between -1.5m below present mean sea level (bpmsl) and ~1.8m above the present mean sea level (apmsl) using hammer and chisel from the exposed shores of Moorea, Huahine and Bora Bora Island (Fig. 1) French Polynesia in 2009 [*Rashid et al.,* 2014]. The samples were cut into ~1cm thick slabs parallel to the growth axis visually selecting pristine areas for further processing. The selected samples were rinsed several times with deionized water and dried in the clean laminar floor hood under room temperature (~20°C) for about 24 to 36 hours. After drying a diamond saw was used to cut small cubes (~1cm^3) out of a distinct growth layer. Greatest care was taken for each subsample to avoid sampling of material of different ages. Subsequently, each cube was equally divided into two parts. One part was cut into small chips and placed in Teflon beakers with deionized water for ultra-sonification. The chips were then dried on the hot plate (35°C) for about 12-24 hours. Using motor and pestle they were and gently ground into a homogeneous powder which was used for X-ray Diffraction (XRD) and geochemical analysis. The other half of the cube was prepared for microscopic analysis (for visible diagenetic alterations, e.g. infillings, secondary precipitates) and high-spatial resolution geochemical analyses by micro-milling and electron microprobe mapping.

4.2.3. Investigation of early diagenetic alteration

4.2.3.1. X-Ray diffraction (XRD) and microscopic observations

Detection and quantification of mineralogy of sample powders in terms of aragonite or Mg-calcite was done using X-Ray diffraction (XRD) at the University of Kiel, Germany. Microscopic observations of all samples (the sample cubes which are the mirror images of crushed samples) were done using epi-fluorescence microscope (Type: Zeiss Axio Imager.M2, with the camera: Zeiss AxioCam MRm Rev.3 using a light source: HXP 120 V (D) and objective: EC Plan-Neofluar 10x/0.3 M27. For imaging we used the DAPI filterset with excitation 350/50 nm, emission 460/50 nm. This observation was aimed identify samples which are affected by secondary diagenetic alterations by having infills within or a distinct rim around the pores.

4.3. Bulk sample analysis

This was done for only samples with no detectable traces of calcite from XRD analysis. The bulk Sr/Ca analysis was performed using Varian 720-ES Inductively Coupled Plasma Optical Emission Spectrometry (ICP-OES) at GEOMAR, Kiel. Respective element emission signals were simultaneously collected and subsequently drift corrected by sample-standard bracketing method done by measuring JCP-1 after every two samples. The sample solution was prepared by dissolving 10 to 30 mg of coral powder in 10 ml of 2% ultrapure HNO_3. The working solution was prepared by dilution of the sample solution with 2% HNO_3 to a Ca concentration of ~25ppm. An internal Indium standard was added in each sample in order to monitor the matrix effect and also to correct for machine drifts. The Sr and Ca lines used for this measurement were 407nm and 370 nm, respectively. Over the entire measurement period of 3 days, the JCP-1 reference material gave an average Sr/Ca ratio of 8.7±0.1 mmol/mol (2σ, n=13). This is in agreement with certified Sr/Ca of Hathorne et al., [2013] and in reasonable agreement with average value of 8.9 ± 0.2 mmol/mol measured in this study using ICP-MS Quadrupole. U/Ca was analyzed using the ICP-MS (Quadrupole) at GEOMAR Kiel using the same solution and standards prepared for ICP-OES. All measured U/Ca ratios were also normalized to the inter-laboratory JCP-1 standard results of Hathorne et al., [2013]. The average of the JCP-1 for the U/Ca is 1.18±0.09 µmol/mol (2σ, n=13).

The $\delta^{18}O$ ratios were measured according to the standard procedure for carbonate samples at GEOMAR, Kiel. In this analysis ~100 µg of homogeneous powdered sample material was reacted in water-free phosphoric acid in the automated carbonate device "Carbo Kiel" (Thermo Fischer Scientific Inc.) at 73°C. The isotope ratios of $\delta^{18}O$ were measured on a MAT 253 mass spectrometer (Thermo Fischer Scientific Inc.) and are expressed as deviations in per mill relative to the Vienna-PeeDee Belemnite (VPDB) standard**.** External precision (2σ) for $\delta^{18}O$ throughout the analysis was ±0.09‰ (n=30).

4.4. Analysis of Sr/Ca ratio in early diagenetic samples

4.4.1. Micro-milling of diagenetic samples

Micro-milling of the samples affected by early diagenetic alteration was done in Geomar, Kiel, Germany. To achieve this we set depth per pass: 5 µm, number of passes: 10, Scan speed: 10 µm/sec with the plunge speed of 25 µm/sec). Using this method we carefully took the samples (powder) from primary skeletal parts and also along the porous parts where secondary diagenetic infillings were detected. Note that, the porous parts may partly include some traces of the massive part because the secondary aragonite needles were too small to be sampled alone. We also included the preserved sample for comparison. These samples were then polished and prepared for the electron Microprobe (EMP) analysis.

4. 4.1.2. Sr/Ca analysis of diagenetic samples

The Sr/Ca measurements of these samples were done using the ICP MS-Quadrupole at GEOMAR, Kiel (Germany). The powdered samples were dissolved in 2% nitric acid and adjusted to a Ca concentration of 25ppm. An internal Indium standard was added to each sample in order to monitor the matrix effect and also to correct machine drifts. The measured Sr/Ca ratios were normalized to the JCP-1 coral standard. This geochemical reference material has been prepared by the Geological Survey of Japan by homogenizing a massive *Porites* sample [Okai et al., 2002]. The Sr/Ca ratio of this standard is known from long term inter-laboratory comparisons [*Hathorne et al.,* 2013] and was taken as fixed value for normalization. In our study the JCP-1 was measured after every two samples following the combination of previously published techniques [*de Villiers et al.*, 2002; *Schrag*, 1999]. The average of the JCP-1 was

8.864±0.205 mmol/mol (2σ, n=12) which is in agreement with the certified value of 8.838±0.009 mmol/mol [*Hathorne et al.,* 2013].

4.4.2. Electron Microprobe mapping (EMP)

Electron Microprobe mapping (EMP: JXA- 8200 JEOL) was used to investigate micrometer scale resolution Sr/Ca variations within primary and secondary skeleton. The EMP maps were obtained by wavelength dispersive spectrometry mode measuring simultaneously Sr (La, TAP) and Ca (Ka, PETJ). The electron beam was focused to a spot size of 2 µm, accelerating voltage set to 15 kV and beam current to 100 nA. A step size of 2 µm as well as an accumulation time of 10 ms was used and the map was repeated to gather 5 accumulations of the selected area. Standards (Calcite, Volcanic glass – VG-2 as well as Kan1 and Strontianite) were measured before and after mapping the sample to convert raw intensities into Sr/Ca ratios.

4.5. Intra-skeletal variability of Sr/Ca ratios in the primary aragonitic corals

The microprobe Sr/Ca maps were used to investigate Sr/Ca variations by line analysis. The lines span over different skeletal regions with a step size of 2µm. However, each point reflects the average of 20 adjacent pixels in horizontal or vertical direction. In each map we consider values from lines passing only the massive part of a skeleton. This was then compared with a line starting from the massive part crossing the porous parts where the secondary needles were observed.

4.6. Chronology

Chronology of the coral samples were performed following the established methods reported in very detail in Rashid et al., [2014]. Briefly, measurements of U and Th isotope ratios was done using the multistatic and multi-ion-counting MC-ICP-MS following the method of Fietzke et al., [2005].The mixed spike ($^{233}U/^{236}U/^{229}Th$) applied in the samples was calibrated for concentration using NIST-SRM 3164 (U) and NIST-SRM 3159 (Th), also against CRM-145 uranium standard solution (NBL-112A) for U isotope composition and against a secular equilibrium standard (HU-1) for the precise determination of $^{230}Th/^{234}U$ activity ratios. The whole blank procedure values were ranging between 0.5-1 pg for Th and between 10-20 pg for U. These values are in the range

typical of this method and the laboratory [Fietzke et al., 2005]. In this study the sample ages are provided in Table 1 and 2.

4.7. Results and discussion

4.7.1. Diagenetic alteration and coral skeletal system behavior

The primary part (aragonite) of Porites skeleton is considered to have elemental signatures which were incorporated during coral skeletogenesis which reflects elemental composition of ambient sea water, temperature controlled distribution coefficient and the vital effect. XRD results indicate that out of 55 samples, 4 samples contain detectable amounts of calcite (CM3: 3%, WL2: 3%, H-Tai-4: 7%, HV-3A: 12%) therefore, these samples were not included in the SST estimates because the observed recrystallization criteria is violating "closed system behavior". All other samples show that aragonite is the dominant $CaCO_3$-polymorph and that the amount of calcite is below the detection limit. However, the presence of pure aragonite is not necessarily an indication of negligible alteration rather the presence of "secondary aragonite" significantly interferes with any SST-Sr/Ca calibration, because secondary inorganic aragonite tends to show between 10% to 15% higher Sr/Ca ratio than coral aragonite [*Dietzel et al.*, 2004] resulting in apparently lower SST values. The presence of voids or any other pore space is important for the formation of secondary aragonite. Microscopic observations indicate the presence of secondary aragonite needles within the skeletal voids of H-Tai-2 (Fig. 2a: Age: 3.12±0.03ka) and HM4 (Fig. 2b: Age: 1.55±0.02ka) samples.

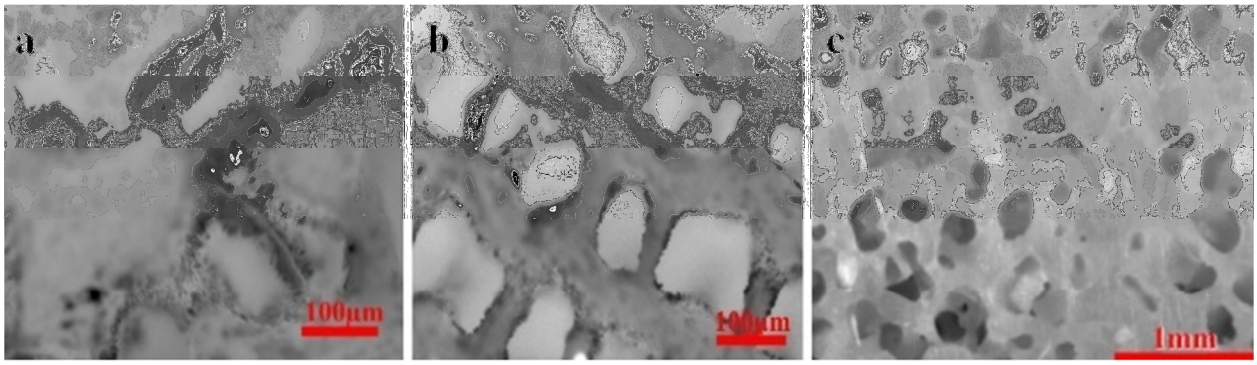

Fig. 2a-c: Microscopic images of samples (a): H-Tai-2, (b): HM4 and (c): WL1. The (a) and (b) samples show secondary aragonite needles within the skeletal voids as a sign of diagenetic alteration. The (a) sample shows larger pores and larger needles while (b) has very small needles with smaller pores. The (c) sample is considered as pristine and shows no secondary aragonite needles within the pores.

The H-Tai-2 shows few large pores with aragonite needles of a length of ~10-50µm. For sample HM4 small pores are more abundant with comparably short aragonite needles in the order of ~5-10µm. Differences in needle size probably reflect gaining secondary aragonite with age or increasing the amount of pore water percolating in the skeleton characterized by larger pore volumes [*Enmar et al.,* 2000]. For comparison, sample WL1 (1.82±0.02ka) exhibits that the original skeletal structure is still preserved (Fig. 2c).

4.7.2. Geochemical analysis of the bulk samples

The results of Sr/Ca, $\delta^{18}O$, and U/Ca analysis together with the paleo-SST reconstructions are summarized in Table 1 and shown in the Fig. 3. All values are presented with 2σ-standard deviation (SD).

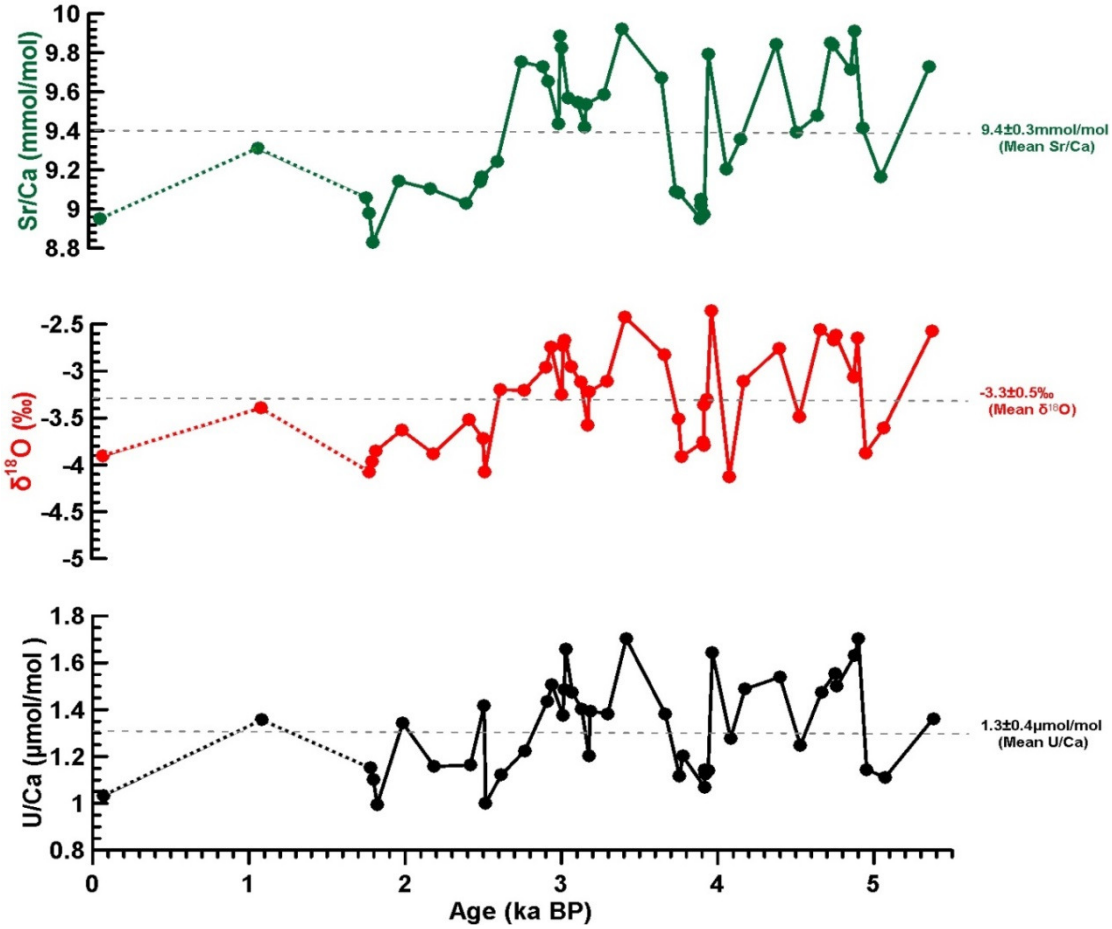

Fig. 3: The measured isotope ratios of Sr/Ca, $\delta^{18}O$ and U/Ca plotted as a function of their corresponding ages. All three records show similar patterns from Mid to Late Holocene. The grey broken line shows the average value of each proxy and the dotted lines of the curves (connecting the data) indicate a data gap.

The Sr/Ca ratios range between 8.83±0.01 mmol/mol and 9.92±0.02 mmol/mol corresponding to the average ratio of 9.4±0.3 mmol/mol. The Sr/Ca ratios of two samples H-Tai-2 and HM4 are 10.14±0.03 mmol/mol and 10.06±0.03 mmol/mol respectively. These are the samples which are detected with secondary diagenetic carbonate infill within the skeletal pores from the microscopic observations. Therefore, we exclude these samples from SST estimation. The $\delta^{18}O$ isotopes ratios range between -4.13±0.03 ‰ and -2.35±0.05 ‰ with an average value of -3.3±0.5 ‰. The U/Ca ratios range between 0.99±0.02 µmol/mol and 1.70±0.02 µmol/mol corresponding to an average ratio of 1.3±0.4 µmol/mol. Sr/Ca, $\delta^{18}O$ and U/Ca are all significantly correlated (Sr/Ca and $\delta^{18}O$: $R^2 = 0.99$, $n = 43$, $p < 0.005$; U/Ca and Sr/Ca: $R^2 = 0.98$, $n = 43$, $p < 0.005$; U/Ca and $\delta^{18}O$: $R^2 = 0.98$, $n = 43$, $p < 0.005$).

Table 1: Sampling locations, age (ka), the ratio of Sr/Ca (mmol/mol), $\delta^{18}O$ (‰), U/Ca (µmol/mol) with their reconstructed SSTs (°C).

Sample Location	Sample Name	Age (ky)	Sr/Ca (mmol/mol)	$SST_{Sr/Ca}$ (°C)	$\delta^{18}O$ (‰)	SST $\delta^{18}O$ (°C)	U/Ca (µmol/mol)	$SST_{U/Ca}$ (°C)
Moorea	RP4	0.072±0.003	8.95±0.01	26.87±0.04	-3.90±0.04	25.0±3.3	1.03±0.02	26.0±0.3
Huahine	HM5	1.08±0.02	9.31±0.02	25.57±0.06	-3.39±0.05	22.8±3.0	1.36±0.02	20.0±0.4
Huahine	H-V-1	1.78±0.01	9.06±0.02	26.48±0.08	-4.07±0.01	25.7±3.4	1.15±0.03	23.8±0.5
Bora Bora	BB-MX 7/2	1.79±0.03	8.98±0.01	26.77±0.03	-3.97±0.05	25.2±3.3	1.10±0.07	24.7±1.3
Moorea	WL1	1.82±0.02	8.83±0.01	27.29±0.04	-3.85±0.04	24.7±3.3	0.99±0.02	26.7±0.4
Huahine	H-PT-1-A	1.98±0.02	9.14±0.01	26.18±0.04	-3.63±0.04	23.8±3.1	1.34±0.01	20.3±0.2
Moorea	MCM10	2.19±0.02	9.10±0.02	26.32±0.06	-3.88±0.04	24.9±3.3	1.16±0.01	23.7±0.3
Bora Bora	BB-MM-13	2.42±0.02	9.03±0.01	26.58±0.02	-3.52±0.01	23.3±3.0	1.16±0.03	23.6±0.5
Moorea	MCM5	2.51±0.02	9.14±0.02	26.18±0.06	-3.72±0.02	24.2±3.2	1.42±0.02	18.9±0.4
Bora Bora	BB-MP-3/2	2.52±0.03	9.17±0.01	26.10±0.04	-4.08±0.04	25.7±3.4	1.00±0.01	26.6±0.2
Moorea	MCM2	2.61±0.02	9.24±0.01	25.82±0.05	-3.20±0.04	21.9±2.9	1.12±0.02	24.4±0.3
Bora Bora	BB-MX-3/2	2.77±0.02	9.75±0.04	23.99±0.13	-3.20±0.04	21.9±2.9	1.23±0.01	22.5±0.3
Bora Bora	BB-MP-4/2	2.91±0.02	9.73±0.01	24.08±0.05	-2.96±0.04	20.9±2.8	1.43±0.02	18.6±0.3
Moorea	LI-2	2.94±0.03	9.65±0.03	24.35±0.09	-2.74±0.03	19.9±2.7	1.51±0.03	17.3±0.5
Bora Bora	BB-MX-5/3	3.01±0.03	9.44±0.02	25.12±0.08	-3.25±0.04	22.1±3.0	1.37±0.03	19.7±0.5
Moorea	MCM1	3.02±0.04	9.89±0.01	23.52±0.03	-2.73±0.03	19.9±2.7	1.49±0.02	17.6±0.4
Bora Bora	BB-MX-1/2	3.03±0.02	9.83±0.02	23.73±0.07	-2.67±0.04	19.6±2.7	1.66±0.01	14.5±0.2
Moorea	LI-4	3.07±0.02	9.57±0.03	24.65±0.11	-2.95±0.03	20.8±2.8	1.47±0.01	17.9±0.3
Bora Bora	BB-MP-2/2	3.13±0.02	9.55±0.01	24.73±0.05	-3.12±0.04	21.6±2.9	1.40±0.04	19.2±0.8
Bora Bora	BB-MX-5/1	3.18±0.02	9.42±0.02	25.19±0.08	-3.57±0.04	23.5±3.1	1.20±0.02	22.8±0.4
Bora Bora	BB-MX-6/3	3.18±0.03	9.54±0.03	24.77±0.09	-3.22±0.04	22.0±2.9	1.39±0.03	19.3±0.5
Bora Bora	BB-MX-4/2	3.29±0.02	9.59±0.02	24.58±0.09	-3.11±0.04	21.5±2.9	1.38±0.02	19.6±0.3
Huahine	H-Tai-1	3.41±0.02	9.92±0.02	23.38±0.07	-2.42±0.03	18.5±2.6	1.70±0.02	13.7±0.3

Sample Location	Sample Name	Age (ky)	Sr/Ca (mmol/mol)	$SST_{Sr/Ca}$ (°C)	$\delta^{18}O$ (‰)	SST $\delta^{18}O$ (°C)	U/Ca (µmol/mol)	$SST_{U/Ca}$ (°C)
Moorea	CM4	3.66±0.03	9.67±0.02	24.28±0.07	-2.82±0.06	20.3±2.9	1.38±0.01	19.6±0.2
Moorea	CM7	3.76±0.04	9.09±0.03	26.36±0.09	-3.51±0.02	23.3±3.1	1.12±0.01	24.4±0.2
Huahine	H-Tai-10	3.78±0.17	9.08±0.03	26.39±0.09	-3.91±0.02	25.0±3.3	1.20±0.01	22.9±0.3
Huahine	H-M-2	3.92±0.02	8.95±0.01	26.86±0.04	-3.75±0.01	24.3±3.2	1.07±0.01	25.3±0.3
Huahine	H-M-1	3.92±0.04	9.05±0.01	26.51±0.04	-3.79±0.03	24.5±3.2	1.12±0.02	24.3±0.4
Huahine	H-Tai-13	3.92±0.05	9.02±0.02	26.63±0.07	-3.36±0.03	22.6±3.0	1.14±0.03	24.0±0.6
Huahine	H-Tai-8	3.94±0.05	8.971±0.005	26.79±0.02	-3.30±0.03	22.4±3.0	1.14±0.01	24.0±0.2
Moorea	CM2	3.96±0.03	9.79±0.02	23.85±0.07	-2.35±0.05	18.2±3.0	1.64±0.02	14.8±0.3
Huahine	H-Tai-9	4.08±0.14	9.20±0.02	25.96±0.08	-4.13±0.03	25.9±3.4	1.28±0.01	21.5±0.3
Huahine	H-Tai-12	4.17±0.07	9.36±0.02	25.40±0.07	-3.11±0.07	21.5±3.0	1.49±0.03	17.6±0.6
Moorea	CM1	4.39±0.04	9.84±0.02	23.66±0.05	-2.76±0.04	20.0±2.7	1.54±0.03	16.7±0.5
Bora Bora	BB-MP-5/3	4.53±0.02	9.39±0.01	25.28±0.04	-3.49±0.04	23.2±3.1	1.25±0.03	22.0±0.6
Huahine	H-Tai-3	4.66±0.05	9.48±0.06	24.97±0.21	-2.55±0.03	19.1±2.6	1.48±0.02	17.9±0.4
Bora Bora	BB-MP-6/6	4.75±0.02	9.85±0.02	23.64±0.06	-2.67±0.04	19.6±2.7	1.56±0.02	16.4±0.4
Bora Bora	BB-MP-6/5	4.76±0.03	9.84±0.01	23.69±0.04	-2.62±0.04	19.4±2.7	1.50±0.02	17.4±0.4
Huahine	H-Tai-11	4.88±0.06	9.71±0.01	24.13±0.05	-3.06±0.05	21.3±2.9	1.63±0.04	15.0±0.7
Huahine	H-Tai-5	4.90±0.06	9.91±0.03	23.42±0.10	-2.64±0.03	19.5±2.6	1.70±0.01	13.6±0.2
Huahine	H-PT-1-2	4.95±0.02	9.41±0.02	25.21±0.07	-3.87±0.08	24.8±3.4	1.14±0.03	23.9±0.5
Huahine	H-MT-1	5.07±0.05	9.16±0.02	26.10±0.06	-3.61±0.03	23.7±3.1	1.11±0.01	24.6±0.2
Huahine	H-MT-2	5.38±0.03	9.73±0.03	24.08±0.11	-2.58±0.03	19.2±2.6	1.36±0.01	19.9±0.2
**Huahine	**H-Tai-2	3.12±0.03	10.14±0.03	22.61 ± 0.11	-2.72±0.02	19.8±2.6	1.54±0.03	16.7±0.5
**Huahine	**HM4	1.55±0.02	10.06±0.03	22.88 ± 0.10	-2.91±0.02	20.6±2.7	1.56±0.05	16.4±0.9

Note: **indicate samples affected by early diagenesis (samples having secondary aragonite), these samples were not used for SST estimates.

4.7.3. Proxy Calibration

The $\delta^{18}O$ - SST estimates were performed using the calibration equation by Boiseau et al., [1998] of modern *Porites* from Moorea Island. The calibration equation is represented by a linear regression equation and rearranged for SST values:

(1) **SST (°C) = -4.35** x **$\delta^{18}O$** (‰ VPDB) **+8.00**

The Sr/Ca - SST estimates were carried out using the calibration equation for *Porites* from Moorea Island [*Cohen and Hart,* 2004]:

(2) **SST (°C) = -3.58** x **Sr/Ca** (mmol/mol) **+ 58.93**

For U/Ca - SST estimation, we have used the calibration equation of Min et al., [1995] for *Porites* from Tahiti Island:

(3) **SST (°C) = – 18.40** x **U/Ca** (µmol/mol) **+ 45.00**

The SST values calculated from analyzed samples are also shown in Table 1. Note that, the uncertainties of the reported SST estimates here are based on the analytical uncertainties only.

4.7.4. Early secondary diagenesis and its implications on SST estimates

4.7.4.1. Micro-mill based analysis

Micro-mill based sampling was applied on the early diagenetic samples to compare the Sr/Ca ratios of the massive and the porous parts where aragonite needles are found (Fig. 4a). For H-Tai-2, the sample taken from the massive part of the primary skeleton has a Sr/Ca ratio of 9.7±0.3 mmol/mol and two samples taken from porous parts have Sr/Ca ratios of 10.5±0.2 mmol/mol and 10.7±0.05 mmol/mol. For HM4, the sample taken from the massive part has a Sr/Ca ratio of 9.9±0.1 mmol/mol and the two samples taken from the porous parts have Sr/Ca ratios of 10.1±0.1 mmol/mol and of 10.1±0.3 mmol/mol.

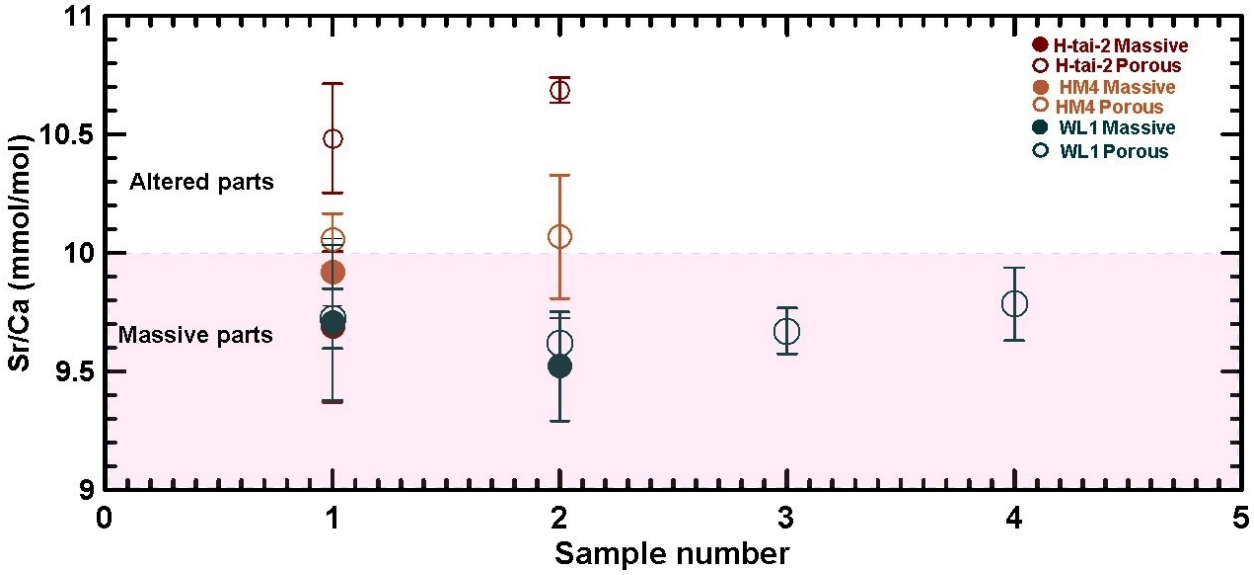

Fig. 4a: The Sr/Ca results from the micro-mill sampling. This includes samples taken from massive and porous parts of diagenetic samples (H-Tai-2 and HM4). In general, the samples taken from the massive parts are lying in the area below the selected threshold value of 10mmol/mol (for our samples) and the samples taken from the porous parts are located in the area above 10mmol/mol. Note that, for WL1 (well preserved sample) the massive part has Sr/Ca ratio located below this threshold value.

For HM4 the difference between porous and massive part of the skeleton overlap within the error, this is probably because, the secondary aragonite precipitation for this sample is in a very

early stage such that the secondary aragonite needles are small compared to H-Tai-2, therefore the Sr/Ca might be less in these needles with insignificant impact the SST estimates. Note that, although this method considers sampling either at porous or massive areas of the skeleton, the samples of the porous areas contain some traces of the massive (preserved) areas. In general we observe that all samples from massive parts tend to have Sr/Ca ratios below 10 mmol/mol, while those samples taken from porous areas where there is early diagenetic imprint lie above 10 mmol/mol. This observation is similar to the bulk sampling results for the diagenetic samples. For this reason, we suggest the value of 10 mmol/mol as a threshold for diagenetic alteration in our samples.

Obviously diagenesis in terms of secondary aragonite precipitation tends to shift the original Sr/Ca signature of the coral towards higher Sr/Ca ratios by introducing aragonite marked by increased Sr/Ca ratios which interferes with the primary material and distorts proxy reconstructions [*Allison et al.*, 2007; *McGregor and Gagan*, 2003]. For example 2.5-3% of secondary aragonite precipitation within the skeletal voids found in our diagenetically influenced corals has shifted the SST estimates from the bulk sampling to cooler temperatures by 0.5 - 1.6°C. This estimate was obtained by taking the difference between the Sr/Ca ratios of the bulk sample – the average Sr/Ca ratio of the sample from the micro-milling results. The results obtained were estimated for SST shift from SST-Sr/Ca calibration equation. The secondary aragonite precipitation is probably due to the fact that pores of the coral skeletons which are connected to the external environment act as an open system and allow the sea water to percolate through the skeleton thereby precipitating inorganic aragonite without any influence of the coral polyp. The biogenic carbonate precipitation (precipitation with the influence of a coral polyp) slightly modifies the Sr/Ca ratios incorporated into the coral skeleton and hence the Sr/Ca is less compared to aragonite precipitation (Cohen et al., 2002; Cohen and Gaetani, 2010).

4.7.4.2. Electron microprobe (EMP) analysis

Electron microprobe analysis of the H-Tai-2 (Fig. 4b.1) and HM4 (Fig. 4b.2) sample have revealed high concentration of Sr and Ca around the pore areas and along the aragonite needles compared to the massive parts of the coral skeleton. However, the preserved sample (WL1) shows no shift of Sr/Ca in its skeleton (Fig. 4b.3).

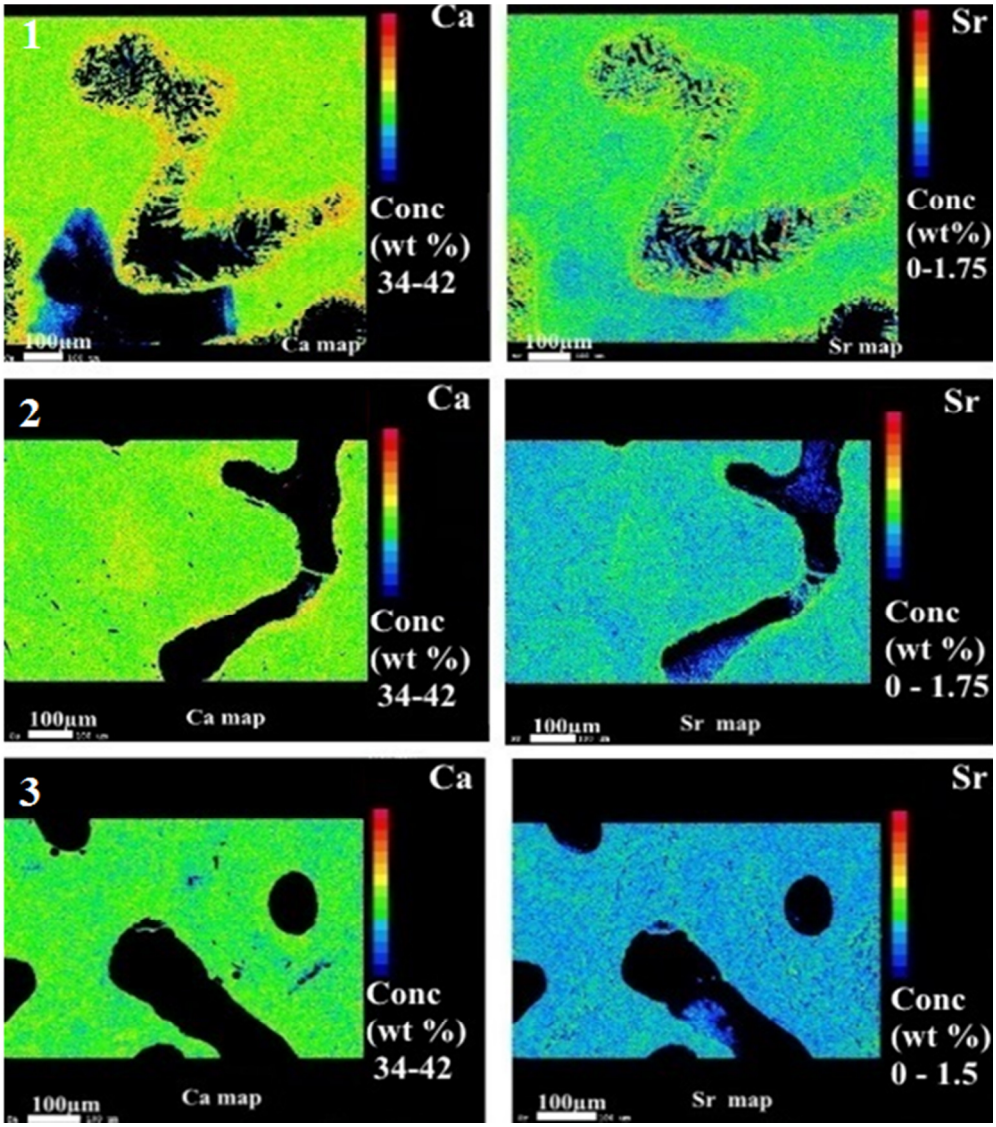

Fig. 4b: The Sr and Ca concentration distribution maps from EMP analysis. The figures (4b1) shows the Ca and Sr map of WL1 sample, (4b2) shows the Ca and Sr map of HM4 sample and (4b3) shows the Ca and Sr map of H-Tai-2 sample. Diagenetic samples show a shift of elemental concentrations towards higher values at the rim and within the aragonite needles. For the pristine sample (4b1), the elemental maps show no shift of elemental concentration along the skeletal voids.

Point analysis (spot analysis) of the primary massive skeletal aragonite of H-Tai-2 sample shows an average Sr/Ca ratio of 8.6±0.2 mmol/mol and considerably higher ratio of ~14.7±0.6 mmol/mol for the aragonite needles and around the pore areas (Fig. 4c). On the other hand, HM4 shows a ratio of 8.7±0.3 mmol/mol in the primary massive skeletal area and a higher ratio of ~10.3±0.7 mmol/mol around the porous parts. The high Sr/Ca ratio of H-Tai-2 (14.7±0.6

mmol/mol) compared to HM4 (10.3±0.7 mmol/mol) on the area of the skeletal pores is probably due to larger pores and longer secondary aragonite needles. The preserved sample (WL1) has an average Sr/Ca ratio of 8.6±0.5 mmol/mol.

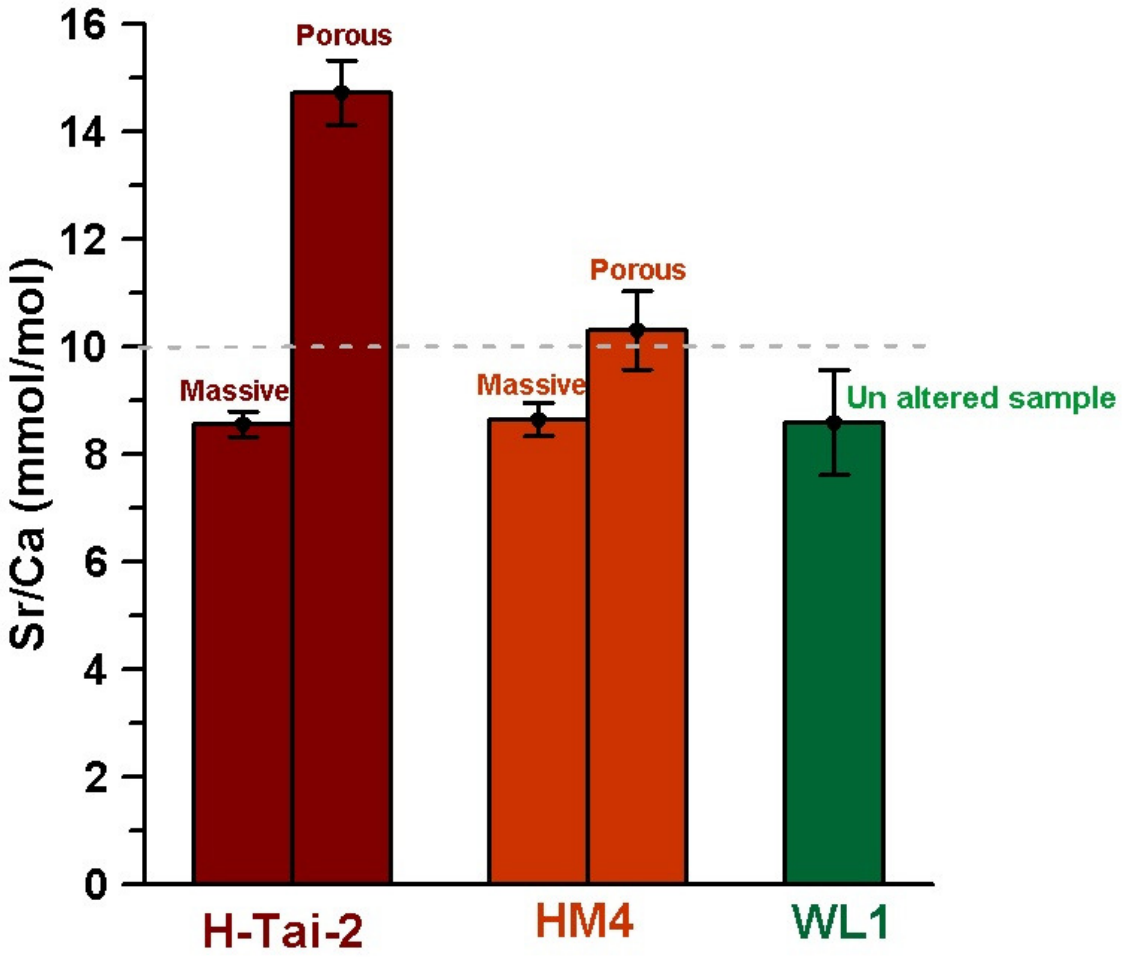

Fig. 4c: The Sr/Ca (mmol/mol) results from point analysis of the electron microprobe maps for samples H-Tai-2, HM4 on the massive and porous parts of the samples. The H-tai-2 (8.6±0.2 massive and 14.7±0.6 porous). The HM4 (8.6±0.3 massive and 10.3±0.7 porous). For WL1 we have sampled only the massive part which has Sr/Ca ratio of 8.59±0.98mmol/mol. In general, the samples taken from the massive parts are lying in the area below the value of 10mmol/mol and the samples taken from the porous parts are located in the area above 10mmol/mol. Therefore we take this value as a threshold of diagenetic alteration for our samples.

This method shows even higher Sr/Ca (up to ~14.7±0.6 mmol/mol) for H-Tai-2 porous, compared to the micro-mill based results. This is because the point analysis method considers only the pixels with secondary aragonite (seen from the EMP map), while the micro-mill

samples on the porous areas might possibly contain some traces of primary phases. However, the general results show the higher Sr/Ca ratios in the porous areas as shown by the micro-mill results.

4.7.5. Intra-skeletal variability of Sr/Ca ratios in the primary aragonitic corals

In the EMP line analysis we have observed that on a micrometer fine scale the Sr/Ca is not homogeneously distributed within the preserved massive primary skeleton (Fig. 5a, b, c) varying between 5.4 mmol/mol and 9.9 mmol/mol.

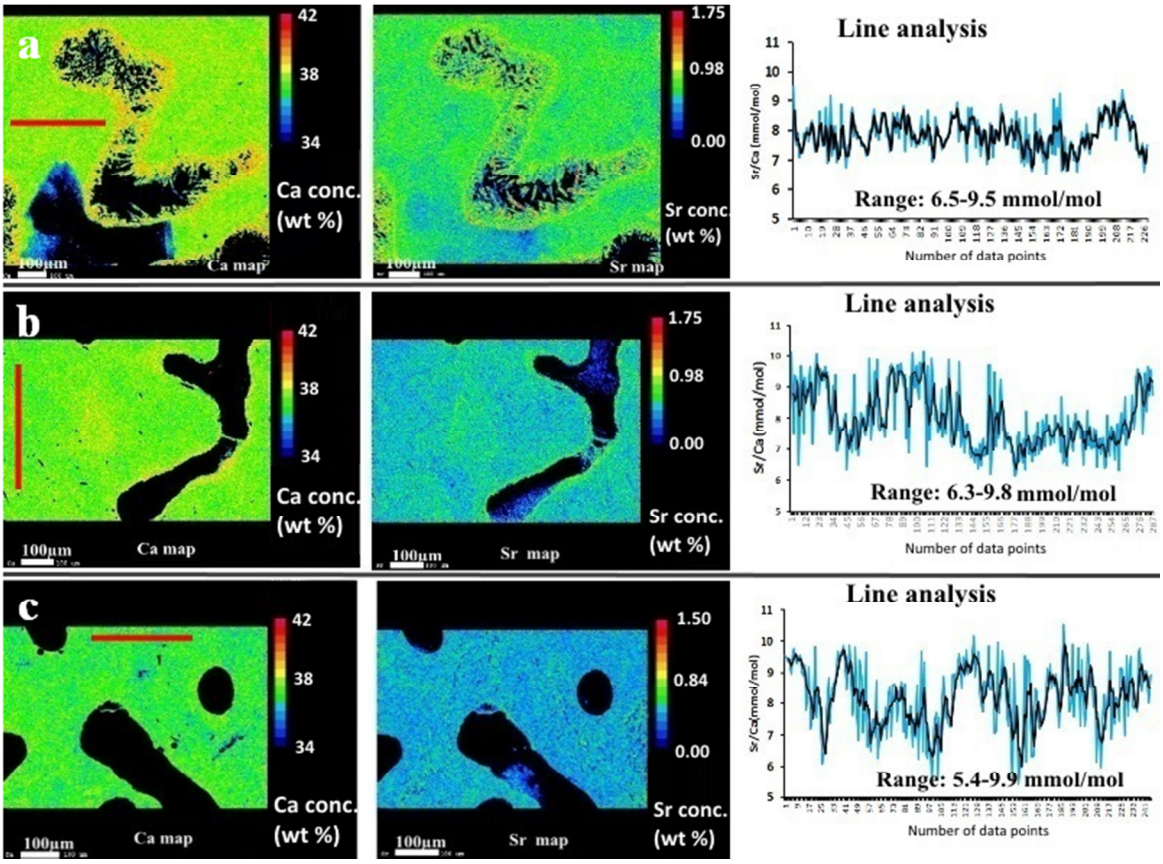

Fig. 5a-c: The line analysis of Sr/Ca from Ca and Sr concentration maps that indicate intra-skeletal variability of Sr/Ca within the coral skeleton. (5a) represents the Ca and Sr maps and the line analysis for H-Tai-2, (5b) is for HM4 and (5c) for WLI. The Sr/Ca ratios of the line analysis were obtained by taking the values (single line) from Sr map and divide by Ca values of exactly the same cells of a line after their respective calibrations. Red line in the map marks the trace of the transect line. Note, the values in the maps are in weight percent. These values have been converted to mmol/mol (Sr/Ca) in the line analysis diagram. In the line analysis the blue lines indicate the single values and the black lines indicate the three-point running mean. The diagrams show that the Sr/Ca ratios within the coral skeletons ranges between 5.4 and 9.9 mmol/mol for our samples.

Latter variation may reflect the physiological control of the corals on its trace metal uptake and the rates of $CaCO_3$ precipitation. Taking the average Sr/Ca of all measured data points through line analyses (Fig. 5d) on the massive parts of H-Tai-2, HM4 and WL1, they result into 7.98±0.04 mmol/mol, 8.10±0.08 mmol/mol, and 7.91±0.10 mmol/mol respectively. These ratios are close or overlapping within error with the values of point analysis performed at the massive parts shown in figure 4c.

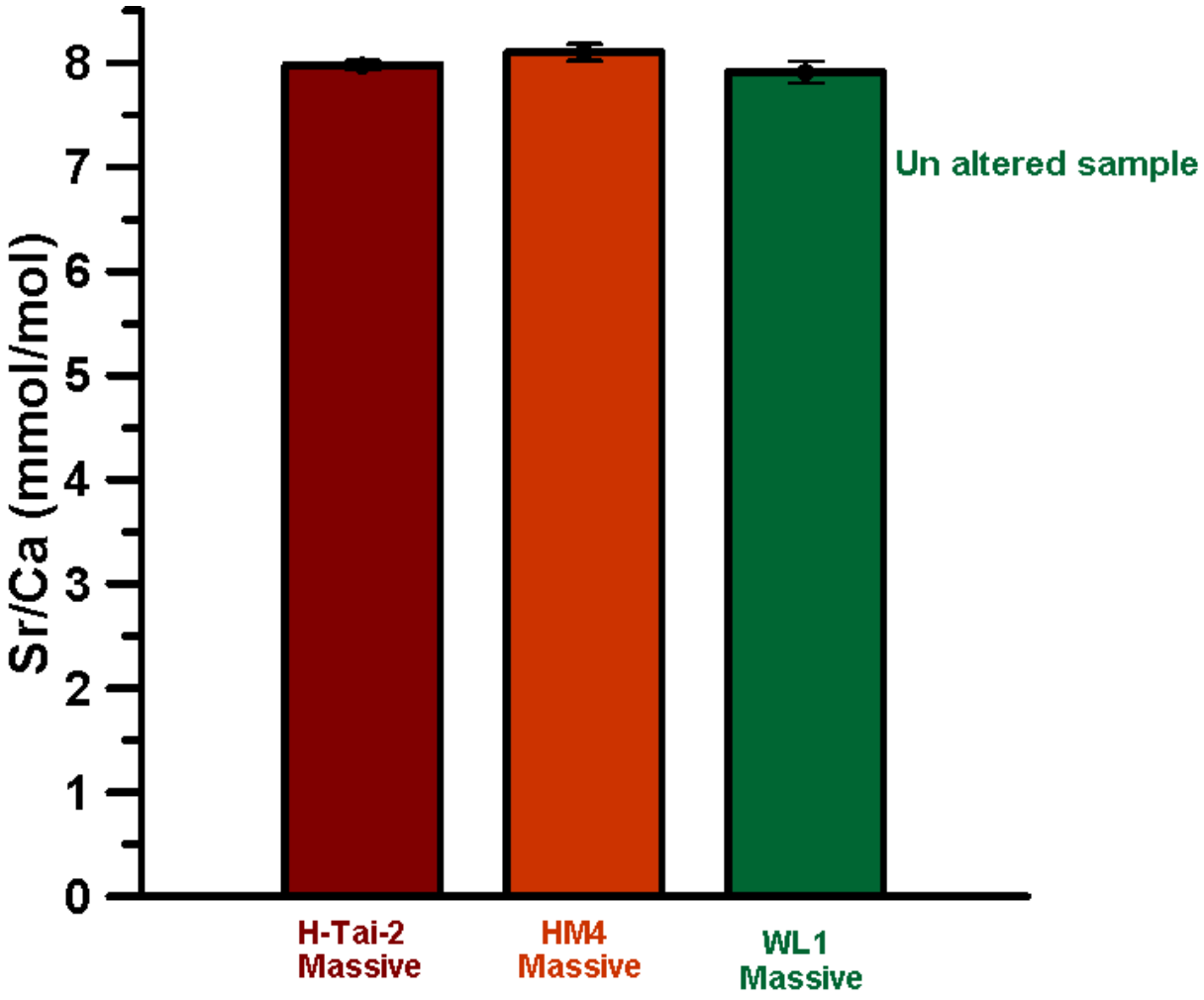

Fig. 5d: The mean Sr/Ca values of line analysis of massive parts of H-Tai-2, HM4 and WL1. Each mean value of a sample was obtained by averaging values of different lines (of more than one map) representing the whole sample. Note that, to obtain representative Sr/Ca estimates of a sample one has to consider lines that cover different areas within the massive part of the sample (map).

4.7.6. Sea surface temperature reconstructions (SST-Sr/Ca, SST-U/Ca, SST-δ^{18}O)

Our data provide the SST record from the Mid Holocene (5.4ka) to ~70 years (Table 1). The record shows a clear SST pattern of high and low temperatures recorded by coral skeleton (Fig. 6). The paleo-SST-Sr/Ca estimates range between 23.38±0.07°C and 27.29±0.04°C (with the average of 25.2±0.2°C). The SST-δ^{18}O range is between 18.2±3.0°C to 25.9±3.4°C (with the mean value of 22.3±0.3°C). The SST-U/Ca estimates show the apparent temperature range between 13.6±0.2°C and 26.7±0.4°C (with the mean value of 20.6±0.6°C).

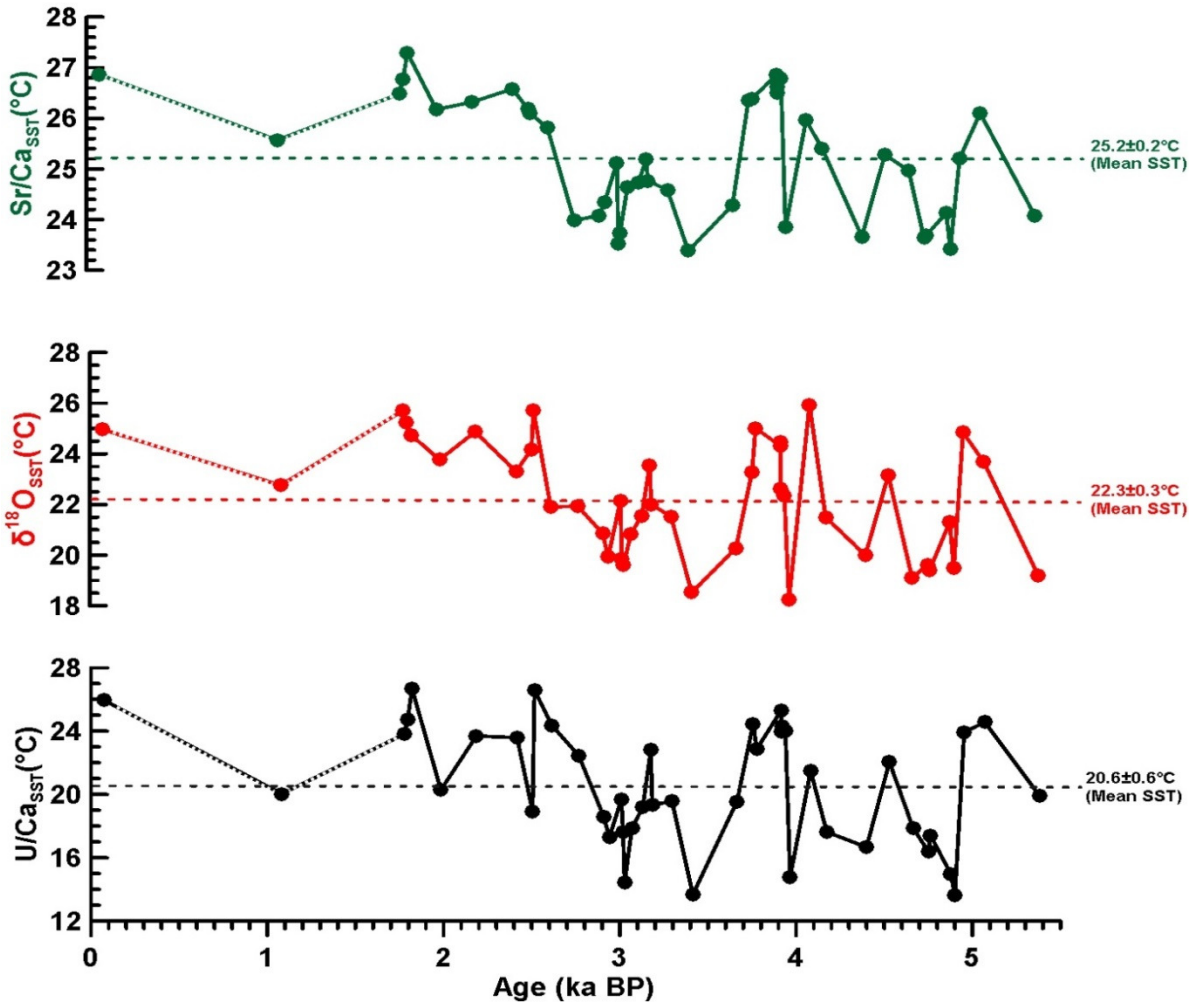

Fig. 6: Proxy temperature records of SST-Sr/Ca, SST-δ^{18}O and SST-U/Ca for the Mid to Late Holocene period. All three proxy records are significantly correlated (see text), they are in phase and show comparable amplitudinal pattern. The broken lines show the mean SST value for each proxy. However, the calculated mean values of all three proxies are significantly different and range from 20.6 to 25.2 °C.

There is an offset with an average of 3.0±0.2 °C for Sr/Ca and $\delta^{18}O$. Similarly between Sr/Ca and U/Ca the offset correspond to 4.5±0.5°C and to 1.5±0.4°C for $\delta^{18}O$ and U/Ca. Although the absolute values are significantly different, the general trends are similar in the three records. The application of the student t-test shows that average SST-Sr/Ca, SST-$\delta^{18}O$, and SST-U/Ca are all significantly different ($p < 0.0001$). This means that either proxy calibrations are not correct; the measured data also are influenced by other factors than temperature, or the offset is caused by uncertainties of the calibrations which were not indicated in the literatures of applied calibrations.

Concerning the statistical distribution of the SST-Sr/Ca, SST-U/Ca and SST-$\delta^{18}O$ values we would expect to see a Gaussian like distribution around a certain mean value distinctively between the modern seasonal extreme values. However, from the histogram plot of Fig. 7a it can be seen that the SST-Sr/Ca shows a kind of bimodal data distribution where the low SST-Sr/Ca peak at about 23.5 °C closely corresponding to the long term austral winter SST at the study area (see above). Whereas the higher austral summer temperatures in between 28 to 29°C in the study area are not reflected in the SST-Sr/Ca data**.** Either such high SST values did not occur in the Late Holocene and average SSTs were shifted more toward lower values or Sr/Ca temperature calibration is not correct having a distinct offset towards lower values of about 1°C. Alternatively early diagenesis e.g. precipitation of secondary aragonite shifted the Sr/Ca ratios to higher values and hence systematically to lower temperatures. Concerning the latter statement a back envelope calculation assuming a seawater Sr/Ca value of 8.541 mmol/mol and assuming that secondary aragonite is precipitating with a partitioning coefficient 15% higher than for coral aragonite implies a contribution of about 20% of secondary aragonite to the original coral carbonate. Although we have detected secondary aragonite precipitation in the pores some of samples (see above) we have not observed a systematic distribution of secondary aragonite and in particular no secondary aragonite present in the massive part of the corals. Rather the massive parts have been assumed to follow closed system.

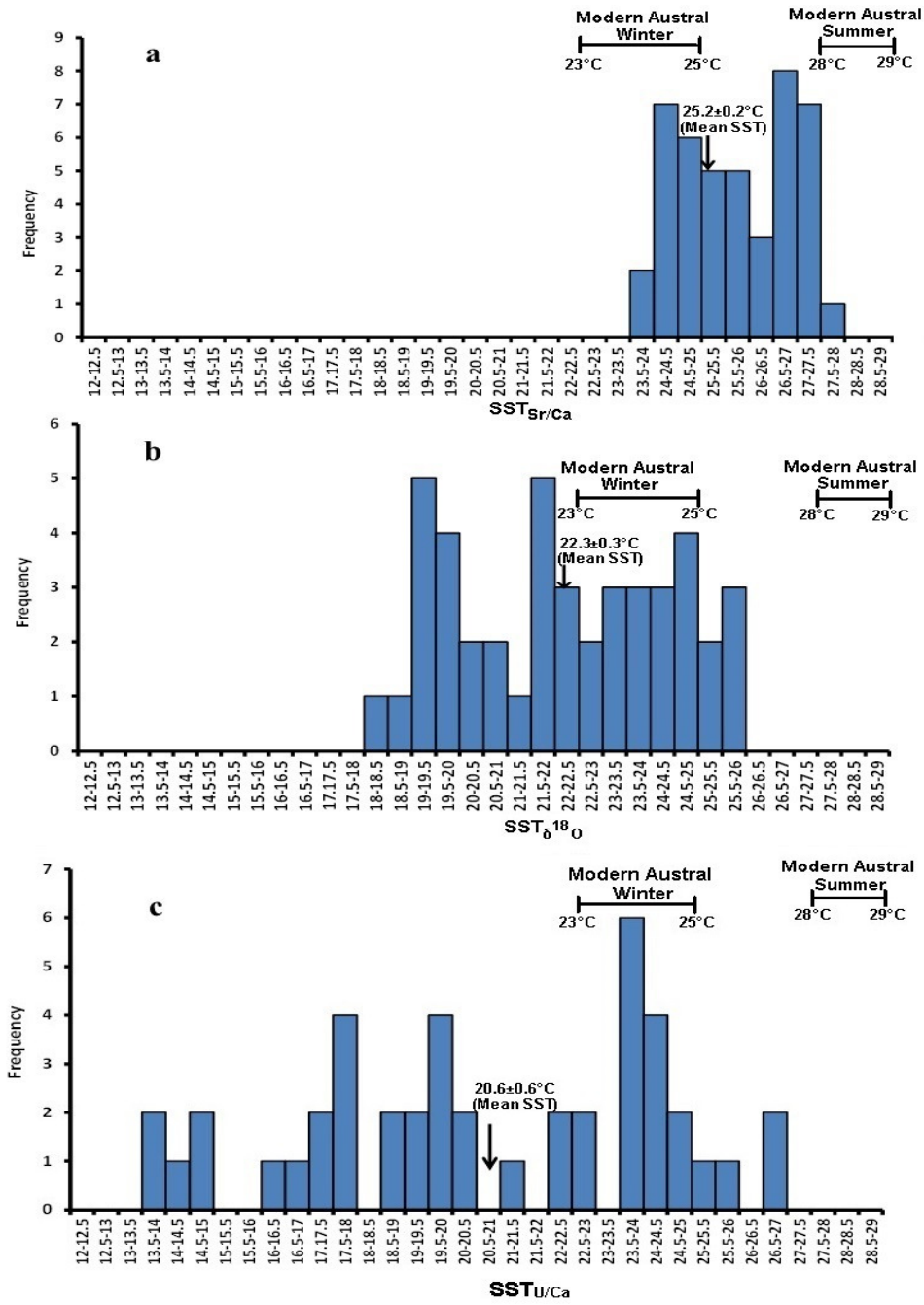

Fig. 7: This histogram plot shows the frequency of the proxy-SSTs in intervals of 0.5°C as a function of the corresponding absolute temperature. Fig. 7a: SST-Sr/Ca, Fig. 7b: SST-δ^{18}O and 7c: SST-U/Ca. It can be seen that there is a general trend towards a tailing of the values towards lower temperatures. In particualr, the recorded temperatures are lower than the present day austral summer values and even tend to be lower than the modern austral winter values. The temperature interval recorded is smallest for the SST-Sr/Ca-values (28 to 23.5 °C) and largest for SST-U/Ca (27 to 13.5 °C). This observation is interpreted as to reflect the addition of extra Sr and U to the coral skeleton and or ion exchange due to percolation of seawater through a system of connected micro-pores and the precipitation of secondary aragonite.

In order to account for the postmortem increase in the Sr/Ca we may interfere that beside the precipitation of secondary aragonite a simple ion exchange process may take place in the massive part in a way that presumably lattice bound Ca^{2+} ions are exchanged by Sr^{2+} ions originating from seawater. Following this approach we may assume that seawater is percolating and diffusing through the coral while exchanging ions between solid and liquid phases is happening. In particular, such or a similar process may then even occur in the massive parts of the coral.

Similar to that the SST-$\delta^{18}O$ values also show a bimodal distribution (Fig. 7b) like the SST-Sr/Ca values. However, values are shifted to even cooler temperatures than observed from the Sr/Ca record. In the $\delta^{18}O$ record even cooler temperatures are recorded than observed for the austral winter in this region. Whereas, the warmest SST-$\delta^{18}O$ values are about 3°C cooler than expected for the austral summer temperature. In order to account for this observation either the $\delta^{18}O$-temperature calibration is not correct resulting in an apparent offset toward cooler temperatures. Alternatively but similar to the inferences made for the SST-Sr/Ca values a postmortem ion exchange process may exchange the coral´s isotopically light oxygen with the relative isotopically heavy oxygen of the seawater percolating through the massive parts of the coral. As a consequence apparent SST-$\delta^{18}O$ values are shifted towards relatively low temperatures.

Similar to the Sr/Ca and $\delta^{18}O$ values the SST-U/Ca values also show temperatures (average SST-U/Ca values: 20.6±0.6°C) much below those expected from the modern temperature. Following the approach applied above it may also be assumed that either the U/Ca-temperature calibration shows a distinct offset shifting the SST-U/Ca values to lower temperatures. Similar to SST-$\delta^{18}O$ and SST-Sr/Ca we may also assume that postmortem U is taken up from the seawater percolating through the coral aragonite thereby shifting the SST-U/Ca to even much cooler values than expected from the modern seasonality. The shift of all proxies records towards lower SST values corresponds to the observation that the standard deviations of the SST-Sr/Ca, (25.2±0.2°C), SST-$\delta^{18}O$ (22.3±0.3°C) and SST-U/Ca (20.6±0.6°C) mean values increases as a function of the deviation from the modern mean value. This observation may indicate that the origin of the shift

toward cooler temperature is the ion exchange with seawater rather than a wrong proxy-temperature calibration.

In our samples we have detected secondary aragonite in the pores of diagenetic samples and no secondary aragonite in the massive part of the corals which have been assumed to follow closed system. However, Cuif and Dauphin [2005] have shown that there are microstructural patterns of organic layers in nanometer scale that are formed in the massive part of the skeleton that is related with the growth of the skeleton. After the death of a coral these organic layers might be exposed to microbial decomposition and therefore create some micro spaces and pathways in the massive part of the coral skeleton. Following this process we may assume that seawater is diffusing in the massive part of the coral while precipitating inorganic aragonite into these micro-spaces and probably also exchanging ions with the coral´s skeleton. The amount of extra strontium and uranium added to the coral appears to be constant rather than erratic in space and time. Otherwise the significant positive correlation between the three proxies cannot be explained. Latter approach offers the possibility to normalize the measured proxy values to their corresponding mean in order to further verify second order variations rather than absolute values.

4.7.7. Origin of the SST-variations and wider implications for the Late Holocene climate change

Following the above approach to circumvent the problem of comparing absolute values we subtracted the mean SST values from the single values (Table 2) to get ΔSST values in order to compare the individual deviations of the single SST reconstructions from their respective mean value (Fig. 8a). The three ΔSST records are in general agreement concerning the timing and phase whereas amplitudes are in part significantly different showing amplitudes of up to +6° and -7°C for ΔSST-U/Ca. The ΔSST-δ^{18}O data indicate smaller variations restricted to amplitudinal variations in between ±4°C. For latter application and comparison we calculated a weighted average mean from the three temperature records and performed a three-point running mean in order to eliminate single excursions of high and low deviations from the mean value (blue curve of Fig. 8a). The amplitudinal variation of the weighted mean curve (SST-all Proxies) shows a reduced temperature variation in the order of ±2.4°C. Excluding the U/Ca record showing the

larges amplitudinal variations, the weighted mean decreased the amplitudinal temperature variation down to the order of ~2°C (Fig. 8b).

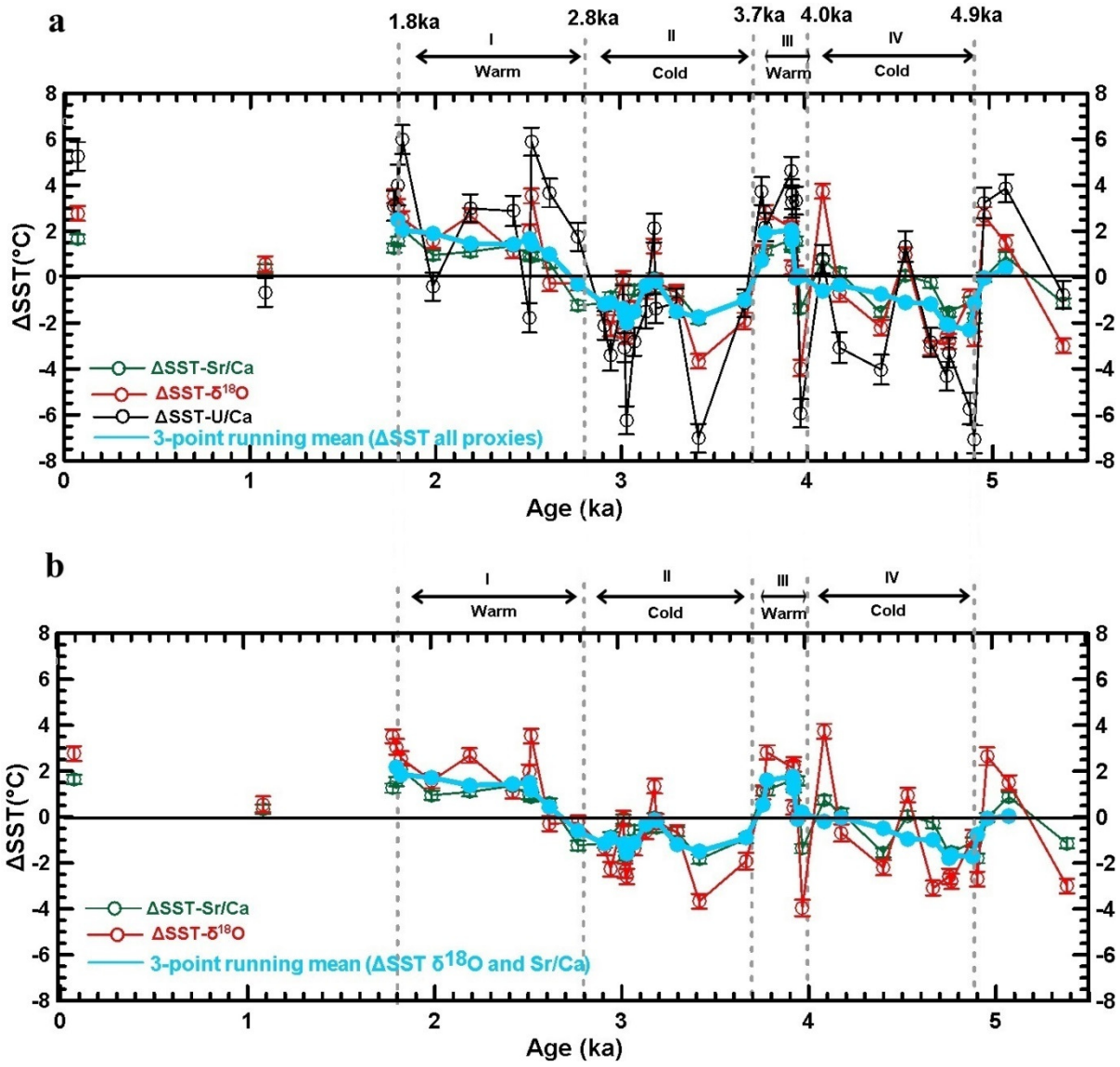

Fig. 8: (a) The ΔSST values (SST-Sr/Ca: green line, SST-$\delta^{18}O$: red line and SST-U/Ca: black line) are plotted as a function of their age together with the mean weighted average of all ΔSST proxies (blue curve). Four intervals of alternating SSTs can be identified. Two warm periods (where the SST is above the mean, interval I and III) and cold intervals where the SST is below than the mean (interval II and IV). Fig. 8 (b) shows the ΔSST variations with age that include only SST-Sr/Ca (green line) and SST-$\delta^{18}O$ (red line). The blue curve shows the mean weighted average of the ΔSST from these two proxies indicating a maximum amplitude of ~2°C.

The regional increase in temperature from Mid Holocene to the modern periods has been indicated in the order of ~1.5°C in the North Pacific [*Marchitto et al.*, 2010] and ~2°C for the Eastern Pacific [*Koutavas and Sachs*, 2008] which agree with our estimates. However, our data show four main time SST intervals, interval I (~1.8ka to ~2.8ka), interval II (~2.8 to ~3.7ka), interval III (~3.7 and 4.0ka) and interval IV (~4.0 to ~4.9ka). Interval II and IV show relatively low temperatures of up to ~-2.0°C below the average and interval I and interval III show higher temperatures of ~2°C higher than the long-term average (Fig. 8b).

Table 2: Sample name, Age (ka), the ΔSST (SST–Mean SST), weighted mean from each ΔSST proxy record and a three-point running mean.

Sample Name	Age (ky)	$SST_{Sr/Ca}$-MV (°C)	$SST\delta^{18}O$-MV (°C)	$SST_{U/Ca}$-MV (°C)	normal mean	Weighted Mean	3 Point Running mean
*RP4	0.072±0.003	1.65±0.20	2.77±0.32	5.25±0.62	3.22	2.60±0.64	---
*HM5	1.08±0.02	0.35±0.20	0.56±0.34	-0.67±0.63	0.08	0.25±0.22	---
H-V-1	1.78±0.01	1.26±0.20	3.52±0.30	3.10±0.65	2.63	2.31±0.40	
BB-MX 7/2	1.80±0.03	1.55±0.20	3.06±0.34	4.01±0.88	2.87	2.35±0.46	2.51
WL1	1.82±0.02	2.07±0.20	2.55±0.32	5.98±0.63	3.54	2.87±0.73	2.05
H-PT-1-A	1.98±0.02	0.96±0.20	1.58±0.32	-0.42±0.61	0.71	0.93±0.34	1.90
MCM10	2.19±0.02	1.10±0.20	2.68±0.32	2.99±0.61	2.26	1.92±0.35	1.45
BB-MM-13	2.42±0.02	1.36±0.20	1.11±0.30	2.88±0.66	1.78	1.51±0.32	1.43
MCM5	2.51±0.02	0.96±0.20	1.98±0.31	-1.78±0.64	0.39	0.86±0.65	1.65
BB-MP-3/2	2.52±0.03	0.88±0.20	3.53±0.32	5.89±0.61	3.43	2.57±0.87	1.42
MCM2	2.61±0.02	0.60±0.20	-0.28±0.33	3.66±0.62	1.33	0.84±0.69	1.00
BB-MX-3/2	2.77±0.02	-1.23±0.21	-0.26±0.33	1.75±0.61	0.08	-0.40±0.53	-0.31
BB-MP-4/2	2.91±0.02	-1.14±0.20	-1.33±0.33	-2.11±0.62	-1.53	-1.36±0.18	-1.17
LI-2	2.94±0.03	-0.87±0.21	-2.27±0.32	-3.42±0.66	-2.19	-1.75±0.45	-1.11
BB-MX-5/3	3.01±0.03	-0.10±0.20	-0.06±0.33	-1.01±0.65	-0.39	-0.23±0.18	-1.37
MCM1	3.02±0.04	-1.70±0.20	-2.34±0.32	-3.07±0.63	-2.37	-2.13±0.24	-1.67
BB-MX-1/2	3.03±0.02	-1.49±0.20	-2.59±0.33	-6.24±0.61	-3.44	-2.64±0.86	-1.99
LI-4	3.07±0.02	-0.57±0.21	-1.35±0.32	-2.82±0.61	-1.58	-1.22±0.40	-1.51
BB-MP-2/2	3.13±0.02	-0.49±0.20	-0.63±0.33	-1.51±0.72	-0.88	-0.69±0.19	-0.38
BB-MX-5/1	3.18±0.02	-0.03±0.20	1.35±0.32	2.13±0.63	1.15	0.77±0.38	-0.15
BB-MX-6/3	3.18±0.03	-0.45±0.21	-0.19±0.32	-1.37±0.64	-0.67	-0.52±0.21	-0.16
BB-MX-4/2	3.30±0.02	-0.64±0.20	-0.67±0.33	-1.13±0.62	-0.81	-0.73±0.10	-1.51
H-Tai-1	3.41±0.02	-1.84±0.20	-3.67±0.32	-7.02±0.62	-4.18	-3.28±0.91	-1.76
CM4	3.66±0.03	-0.94±0.20	-1.92±0.36	-1.15±0.61	-1.33	-1.26±0.17	-0.99
CM7	3.76±0.04	1.14±0.21	1.08±0.31	3.74±0.61	1.99	1.56±0.52	0.73
H-Tai-10	3.78±0.17	1.17±0.21	2.82±0.31	2.17±0.61	2.05	1.89±0.28	1.91
H-M-2	3.92±0.02	1.64±0.20	2.13±0.30	4.61±0.62	2.80	2.29±0.54	2.06

Sample Name	Age (ky)	$SST_{Sr/Ca}$-MV (°C)	$SST\delta^{18}O$-MV (°C)	$SST_{U/Ca}$-MV (°C)	normal mean	Weighted Mean	3 Point Running mean
H-M-1	3.92±0.04	1.29±0.20	2.29±0.32	3.61±0.64	2.39	1.98±0.41	1.88
H-Tai-13	3.92±0.05	1.41±0.20	0.42±0.31	3.24±0.66	1.69	1.37±0.48	1.59
H-Tai-8	3.94±0.05	1.57±0.20	0.17±0.32	3.32±0.61	1.69	1.42±0.52	-0.05
CM2	3.97±0.03	-1.37±0.20	-3.96±0.36	-5.94±0.62	-3.76	-2.92±0.82	0.07
H-Tai-9	4.08±0.14	0.74±0.20	3.74±0.32	0.78±0.62	1.75	1.71±0.55	-0.60
H-Tai-12	4.17±0.07	0.18±0.20	-0.69±0.38	-3.08±0.67	-1.19	-0.60±0.61	-0.35
CM1	4.40±0.04	-1.56±0.20	-2.20±0.33	-4.03±0.65	-2.60	-2.16±0.45	-0.74
BB-MP-5/3	4.53±0.02	0.06±0.20	0.96±0.32	1.33±0.67	0.78	0.55±0.23	-1.10
H-Tai-3	4.66±0.05	-0.25±0.23	-3.09±0.32	-2.85±0.63	-2.06	-1.68±0.55	-1.16
BB-MP-6/6	4.75±0.02	-1.58±0.20	-2.58±0.33	-4.32±0.63	-2.83	-2.35±0.49	-2.08
BB-MP-6/5	4.76±0.03	-1.53±0.20	-2.80±0.33	-3.30±0.64	-2.54	-2.22±0.32	-2.06
H-Tai-11	4.88±0.06	-1.09±0.20	-0.89±0.34	-5.73±0.68	-2.57	-1.75±0.95	-2.12
H-Tai-5	4.90±0.06	-1.80±0.21	-2.70±0.32	-7.07±0.61	-3.86	-3.00±0.97	-1.16
H-PT-1-2	4.95±0.04	-0.01±0.20	2.65±0.39	3.23±0.66	1.95	1.28±0.64	-0.05
H-MT-1	5.07±0.05	0.88±0.20	1.50±0.32	3.86±0.61	2.08	1.58±0.54	0.39
H-MT-2	5.38±0.03	-1.14±0.21	-3.00±0.32	-0.77±0.61	-1.64	-1.69±0.39	

Note: The data indicated by * are plotted as separate points because they is a gap of missing data in between these points. Note that, they are no three-point running mean from these points because they are only two points.

Variations of the solar activity have contributed to climate change especially on longer time scales [*Wanner et al.*, 2008] and together with the atmospheric CO_2 concentration it is probably the most important factor controlling Earth´s temperature on non-astronomical and millennial time scales [*Elsig et al.*, 2009; *Hansen et al.*, 2013]. Past solar variability can be reconstructed from cosmogenic ^{10}Be and ^{14}C records measured in the continental ice since they are produced in the upper part of the atmosphere as a direct function of solar activity (Fig. 9a). These isotopes can be considered as proxies for the intensity of solar radiation [*Bard and Frank*, 2006; *Wanner et al.*, 2008] and their variation are in good agreement with our mean SST record (Fig. 9a). In particular, we observe that the four intervals of lower and higher temperatures correspond to intervals of low and high solar activity and that general patterns of the solar activity are linked to our SST pattern concerning phase and amplitude. Solar activity variations are a global rather than a regional phenomenon hence solar activity also correlates with the ice dynamics of the important glaciated regions of the globe. For example, at ~2.8 to 3.7ka (interval II) and at ~4.4 to 4.9ka (interval IV) low temperature patterns correspond to times of glacial advances in several parts of the world, including the Alps, Scandinavia, Himalayas, Alaska, New Zealand and Patagonia [*Grove*, 2004; *Thompson et al.*, 2006]. In a more regional context this is also in accord

with SST records from the Eastern Pacific reporting colder temperatures between ~2.8 and 3.8ka and ~4.1 and 4.9ka [*Koutavas et al.*, 2002]. High SSTs were also reported ~4ka and 1.8 to 2.9ka [*Abram et al.*, 2009; *Koutavas et al.*, 2002] in the Southern Pacific which are also in accord with our data.

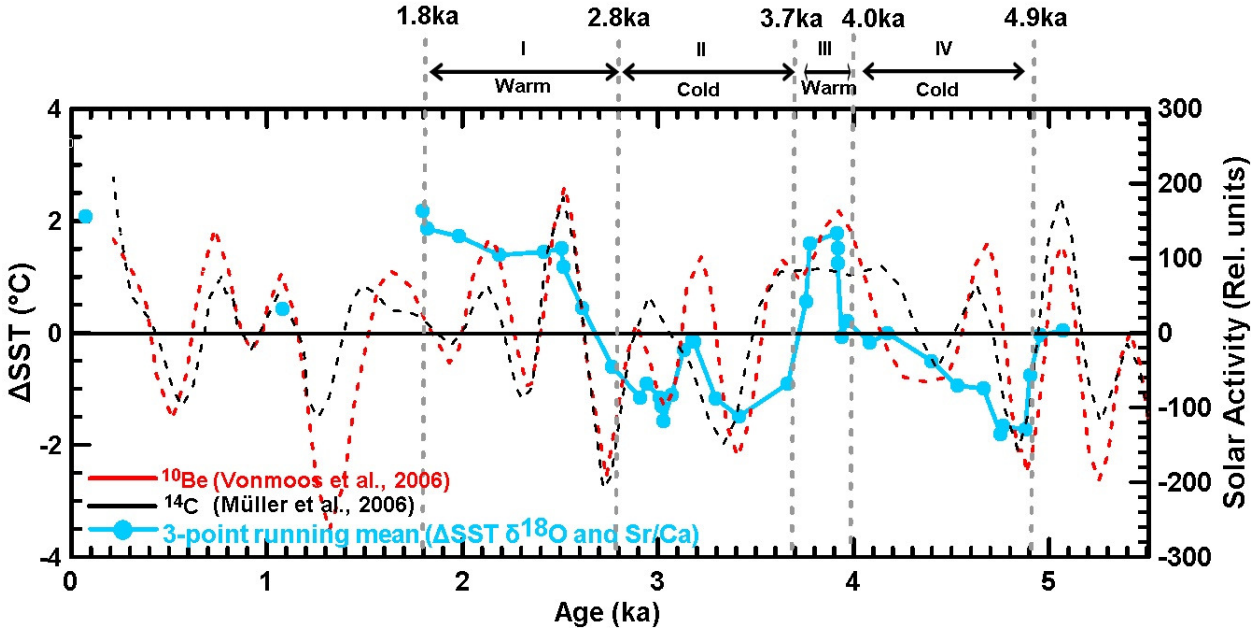

Fig. 9: (a) Comparison of mean weighted average of ΔSST estimates (blue line, 3-point running mean from $\delta^{18}O$ and Sr/Ca) with solar activity reconstructed using ^{10}Be from the Greenland (GRIP) ice core record ([*Vonmoos et al.,* 2006]; dashed red line) and ^{14}C ([*Müller et al.,* 2006]; dashed black line) from Wanner et al., [2008]. Our results are consistent with the reconstructed solar activity [*Wanner et al.,* 2008].

This indicates that (i) the reported SST variabilities in the order of up to ±2°C reflect global temperature oscillations throughout the Mid to Late Holocene, and (ii) that solar activity seems to be the major driver of centennial to millennial scale SST changes throughout the Mid to Late Holocene at least in the Southern Pacific.

The Holocene CO_2 concentration curve reconstructed from Antarctic ice cores [*Indermühle et al.*, 1999] also shows a distinct relationship with our proxy data (Fig. 9b). The CO_2 record of the last 6 ka indicates a distinct increase in CO_2 concentrations of about 16 ppm from about 264 ppm to about 280 ppm superimposed by 2nd order variation in the range of a few ppm. This increase in CO_2 may also be reflected in our SST. However, the increase of about 2°C related to an increase of 16 ppm CO_2 is too small compared to the amount of CO_2 (~100ppm) assumed to

change the temperature from pre-industrial to modern by 0.8°C *[IPCC, 2013]*. Probably, cyclic variations of the solar activity controlled the atmospheric temperature and SST variations in the Southern Pacific to a much larger extent.

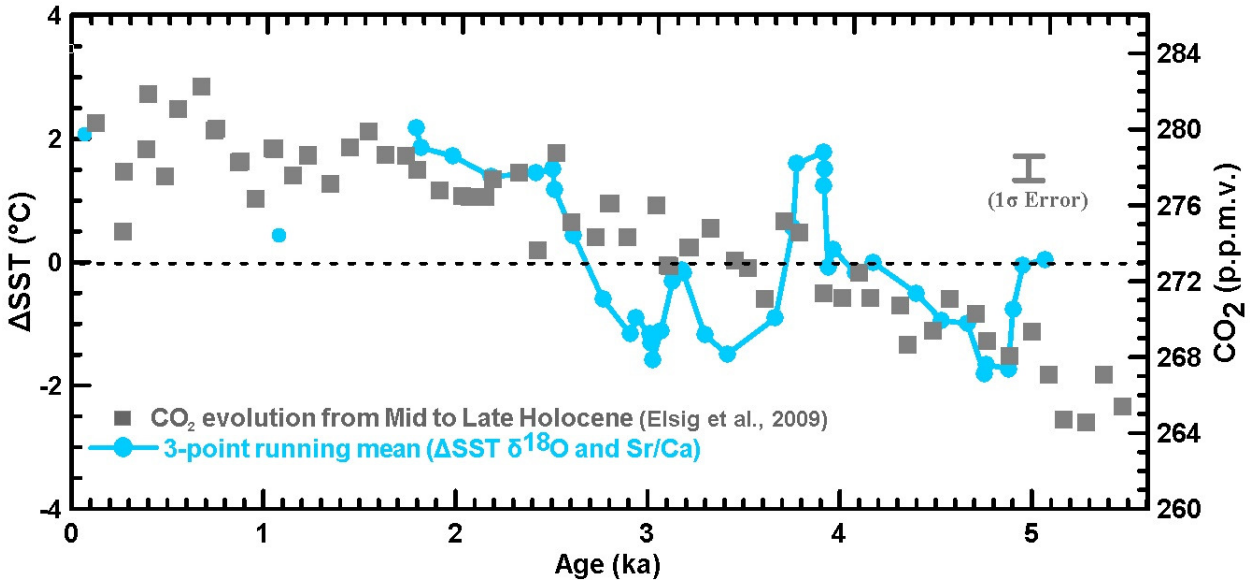

Fig. 9: (b) is the comparison of our mean weighted average of ΔSST estimates with the CO_2 concentration from Mid to Late Holocene collected from the Antarctic ice core record ([*Monnin et al.,* 2001], grey symbols) obtained from Elsig et al., (2009). The general trend in CO_2 evolution is additionally in agreement with our proxy data.

4.7.8. Implications for the sea level to temperature relationship in the Pacific

Our observation of periodic SST variations in the Pacific in the order of about 2°C may have direct consequences for the height of the sea level. This is because variation of temperature in this area is also reflected in the global scale (e.g. solar activity and glacial variations) that indicates that SST variations in the Pacific Ocean have significant impact on global SST. Alternating cool and warm SST cause water to expand or contract and relative sea level to rise and fall which has recently been quantified to be 0.2 to 0.7 m/°C [*Levermann et al.*, 2013]. In a recent study empirical sea level estimates are compared to Holocene sea level variations of numerical models taking only Glacial Isostatic Adjustments (GIA) related sea level variations into account. However, any SST related variations have been neglected [*Rashid et al.,* 2014]. Although there is general accord between GIA modeled sea level variations and the empirical data there are time intervals where empirical data indicate higher sea levels and intervals of lower sea level than predicted from GIA modelling. This probably indicates that GIA is not the

only factor controlling sea level rather cyclic SST variations may superimpose GIA controlled sea level height. In Fig. 10 the GIA related sea level fluctuations are combined with SST caused amplitudinal variations taking a SST-sea level relationship of about 0.2 m/°C into account. From Fig. 10 (blue curve) it can be seen that the sea level corresponding to interval I (1.8 – 2.8 ka) and III (3.7 to 4 ka) is in average about 0.4 m higher than the GIA controlled sea level alone. In contrast, for time intervals II (2.8 to 3.7 ka) and IV (4 to 4.9 ka) sea level reconstructed is lower than predicted from GIA modeling alone. For interval I the SST-GIA combined sea level curve fit the empirical data better than the theoretical GIA related curve alone. Apart from interval III the intervals II and IV the combined SST-GIA sea level curve is in general accord with each other and indistinguishable within statistical uncertainty. However, this should be considered as first order interpretation and it is open to future improvements.

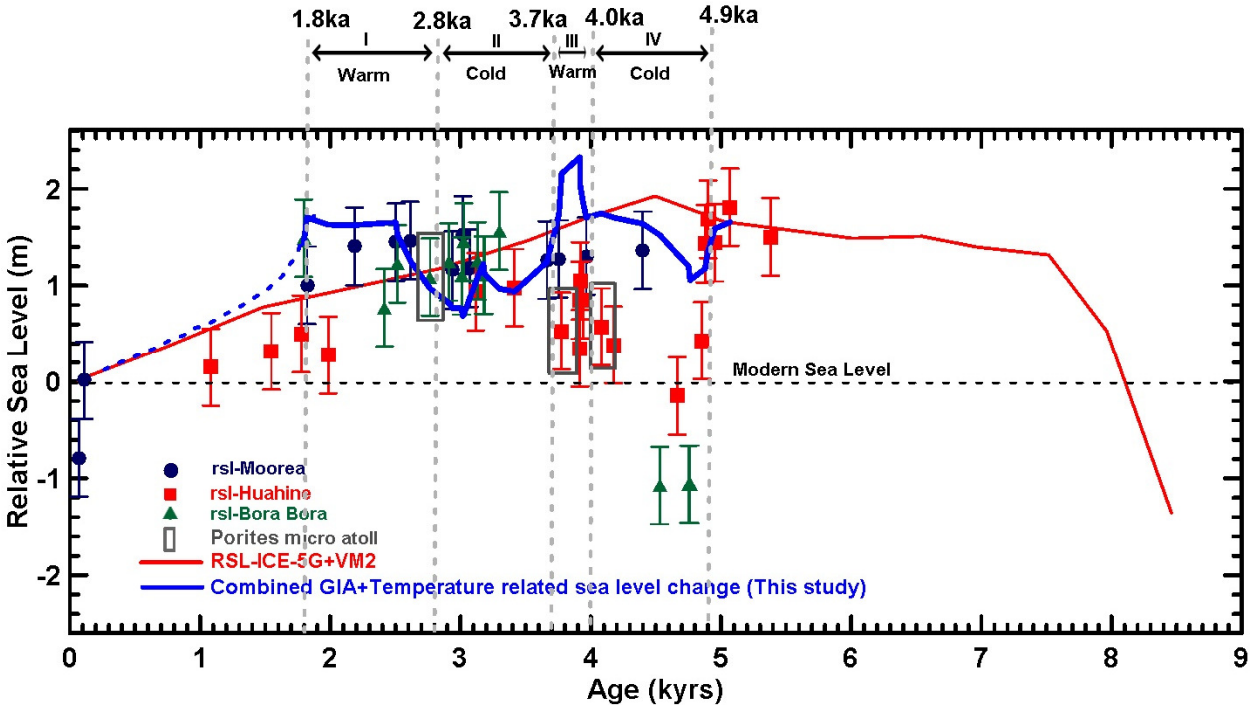

Fig. 10: Sea level-temperature relationship in the Pacific. The sea level estimations were previously published by Rashid et al., [2014] using empirical data and GIA model. The red curve represents the GIA model prediction of mean sea level curve for the Society Islands from Mid to Late Holocene. The data points are the sea level data obtained from coral samples from Moorea (blue), Huahine (red) and Bora Bora (green). In this study we combined the sea level estimation with the temperature in estimation obtained from this study (as blue curve). The combined GIA-temperature relationship reveals the amplitudinal sea level variations and reconciles the discrepancy between the GIA estimation and the empirical observations between 2 to 2.6ka

4.8. Conclusions

1. Secondary inorganic aragonite precipitation in a coral sample could results in a shift of Sr/Ca, U/Ca, $\delta^{18}O$ ratios towards higher values corresponding cooler SST temperatures. Even massive parts of corals are affected due the percolation of seawater along connected micro-pores.
2. Elemental contribution is not erratic rather seems to offset original values conserving original correlations among proxies. This may still allow gathering climatic information by normalizing the measured values relative to their mean values.
3. Although affected by early diagenesis and violation of the "closed system behavior" relative SST variations (ΔSST) indicate centennial to millennial SST variations (intervals I to IV) in the order of ±2°C.
4. Identified SST intervals I to IV are in phase with variations of the solar activity as indicated by ^{14}C and ^{10}Be variations measured in continental ice cores.
5. Variations of the solar activity in the Late Holocene are probably the major driver for climate oscillations and sea level change throughout the Holocene in the Southern Pacific.

Acknowledgements

This study was supported through funds from ESF/CHECKREEF project (EI272/22-1, DU129/141-1), DFG research group CHARON (D1655) and also by the GEOMAR, Helmholtz Zentrum für Ozeanforschung Kiel. The PhD program of Rashid R. J. was financially supported by the Tanzania Ministry of Education and Vocational Training (MoEVT) in collaboration with DAAD (Deutscher Akademischer Austauschdienst) fellowship. We gratefully acknowledge Ana Kolevica, Jutta Heinze, Brendan Ledwig and Patrick Reichert for their assistance in sample processing and data analysis.

Chapter Five

5. General conclusions

The general aim of this study is to reconstruct paleo-climate variability mainly focusing on the sea level variation (derived from age (U/Th) and elevation of sample collection) and sea surface temperature reconstruction (using Sr/Ca, $\delta^{18}O$ and U/Ca proxies) during Mid to Late Holocene in the Society Islands in French Polynesia. In addition, the impact of early marine diagenesis on SST estimates and intra-skeletal micro-scale Sr/Ca variation has been assessed. To achieve this study, the fossil corals from the reef platforms which are currently exposed above the modern sea level as a result of sea level fall were used for reconstruction. Massive *Porites* and *Porites* micro atoll corals *in situ* were considered for reconstructions of the climate history of the area. In this study the following conclusions have been achieved.

5.1. Sea level variation from Mid to Late Holocene

In terms of sea level, the empirical data from this study indicate that Mid to Late Holocene sea level in the Society Islands was not stable but rather oscillated in the order of 1 to 2 meters above the present sea level from 5.4 ka to 1.8 ka. After this period the sea level dropped to the modern level. The sea level amplitudes indicated here are in the same range as predicted for the near future as a consequence of global warming and may serve as a natural analogue. The Glacial Isostatic Adjustment (GIA) modelling predicted a sea level increase to 4.5 ka and a gentle (smooth) fall to the modern levels without oscillation, because GIA modelling predictions considers only the melting of ice sheets and isostatic adjustments (response of land masses that were depressed by the huge weight of ice sheets during the last glacial period), inclusion of temperature variability might improve the modelling results. Therefore, the GIA modelling is pending to future improvements.

The age range of our samples confirm that the emerged fossil platforms were formed after the sea level high stand (~6.5 ka) subsequent to complete disintegration of ice sheets in Northern Hemisphere that caused the reef to grow up to a water level above the elevation to which corals presently grow. According to the model of epicontinental reef growth (Davies and Marshal, 1980), the coral reefs accreted vertically following the sea level rise which was above the

modern sea level during sea level high stand. The continuous sea level fall during Late Holocene in the far-field regions restricted the vertical growth, subsequently exposed these platforms above modern sea level that caused a complete cessation of their growth. Theoretical explanation of Mitrovica and Milne, (2002) indicates that exposure of Late Holocene platforms above the sea level was due to migration of water from far-field to the near- field regions (Ocean Siphoning Effect). They assumed that post-glacial rebound (that causes collapsing of fore bulges) and extra gravitational force of the upwarping landmasses pressed into Earth's mantle during continental glaciation (gravitational pull) are the cause of migration of water from the far-field into the near-field regions. Since the age range of our data (~5.4 ka to ~0.07 ka) is around Mid Holocene to modern therefore, we conclude that our platforms reflect a consequence of migration of water away from these areas as a result of Ocean Siphoning Effect.

5.2. Temperature variability during Mid to late Holocene

Using a multi-proxy approach combining Sr/Ca, U/Ca and $\delta^{18}O$ we deduce that the sea surface temperature during Mid to Late Holocene was not stable but rather fluctuated on different time periods in the order of 1-2°C warmer than average from the modern mean temperature. The warm temperatures (~1-2°C) were observed between 1.8-2.8 ka, 3.7-4 ka as well as around 5 ka. The periods between ~2.8-3.7 ka and ~4.0 to ~4.9 ka are characterized by SSTs about 1-2°C lower than average. These temperature fluctuations are in good agreement with the solar activity variations reconstructed by Wanner et al., (2008). Carbon dioxide concentration (variability) from Mid to Late Holocene (Elsig et al., 2009), is in general agreement with our proxy data, but the variation is too little (16 ppmv) to increase the temperature from Mid to Late Holocene in the order of 2°C. Therefore, we conclude that solar activity was a major driver of the changes in the sea surface temperature during this time interval in our study area. The temperature variations during Mid to Late Holocene period partly influenced the sea level variation in this area.

5.3. Impact of diagenesis on the SST estimates

Inorganic $CaCO_3$ precipitated in the corals as marine secondary precipitates (early marine diagenesis) results in errors in the SST estimates. This is because inorganic precipitates incorporate elements in the proportions available from the ambient sea water without the influence of a living coral polyp (biogenic influence). Our study has found that the bulk samples

Sr/Ca ratios from our two diagenetic samples have higher Sr/Ca ratios (above 10mmol/mol) while the non diagenetic samples have ratios below 10mmol/mol. Our estimates indicate that about 2-3% secondary aragonite needles observed in the skeletons of these two diagenetic samples have led to a shift of SST estimates to colder temperatures in the order of 0.5-1.6°C.

5.4. Micro-scale intra-skeletal variability within the sample

Our results show that the Sr/Ca ratios precipitated within the coral skeleton are not homogeneous; there is a micro-scale variation with observed values between 5.4 mmol/mol and 9.9 mmol/mol for our samples. The reason of this variability is still unknown but part of it might presumably reflect diurnal fluctuations of calcifying fluid which is influenced by activation of Ca^{2+}ATPase pump by light during the day favoring active transport of Ca^{2+} (resulting into low Sr/Ca ratio) and low activity of Ca^{2+}ATPase during night time favors more Sr^{2+} over Ca^{2+} as explained by Al-Horani et al. (2003). However, this is not enough to explain our observed variation.

5.5. Recommendation and future perspectives

Several studies have focused on the sea level change of the exposed platforms in the far-field areas of the world oceans. However, using conglomerate platforms the sea level amplitude of the estimation could be exaggerated and resulting into higher or lower sea level estimates. This is because sea level estimates based on conglomerates are bound with a lot of uncertainties because some corals are reworked and not in their original growth positions (*in situ*). Therefore, to effectively reconstruct the sea level variation having massive corals taken from their original growth position is necessary. *Porites* micro atolls grow few centimeters on the lower intertidal areas. Their vertical growth is restricted by the exposure above the water surface. For this reason they are considered as good markers that allow paleo-sea level reconstruction into centimeter level. Therefore, to have precise estimates of paleo-sea level estimates the use of more micro atolls samples is essential.

Islands of volcanic origin tend to subside with age and a distance from the original hotspot. Without consideration of island's specific subsidence history, reconstructions of the sea level might be bound with a lot of uncertainties and hence the estimates might be incorrect. Currently

there are no studies about subsidence rates of some of the Society Islands such as Maupiti, Manuae, Tupai, Miao, Tahaa, Raiatea and the sea level estimations on these areas are still underway. For island's specific subsidence rates the researchers are obliged to use subsidence rates of nearby islands. Therefore, to correctly constrain paleo-elevation of the islands, having the correct island's specific subsidence rate is necessary.

Geoid distortion as a function of changes in gravitational field along the area of study must be considered. Ignoring it, might add an uncertainty to the sea level estimates especially when the sea level is reconstructed on a centimeter level. Therefore, having the Real Time Kinematic (RTK) GPS system that would be able to correct for the geoid distortion is recommended.

For paleo-climate studies using corals, the petrographic analysis involving pre-investigation of pore volume for secondary growth phase e.g. microscopic analysis (e.g. polarized microscope, scanning electron microscope) and thin sections, together with X-ray Diffraction (XRD) prior to geochemical analysis is necessary. This is because the inclusion of secondary aragonite cannot be detected using X-Ray Diffraction method. Relying onto XRD alone might lead into unreliable results. In addition micro analytical tools like micro-mills and/or Laser ablation technique based strategies that involves sampling on the massive part of a skeleton should be used for precise temperature estimation instead of bulk sampling strategy only.

6. References

Abram, N. J., McGregor, H. V., Gagan M. K., Hantoro, W. S. and Suwargadi, B. W. (2009). Oscillations in the southern extent of the Indo-Pacific Warm Pool during the mid-Holocene. Quaternary Science Reviews, 28, 2794-2803.

Adkins, J.F., Boyle, E.A., Curry, W.B., Lutringer, A. (2003). Stable isotopes in deep-sea corals and a new mechanism for vital effect. Geochimica et Cosmochimica Acta, 67, 1129-1143.

Al-Horani, F. (2003). Microsensor study of photosynthesis and calcification in the scleractinian coral, Galaxea fascicularis: Active internal carbon cycle. Journal of Experimental Marine Biology and Ecology, 288, 1-15.

Alibert, C. & McCulloch, M.T. (1997). Strontium/calcium ratios in modern Porites corals from the GreatBarrier Reef as a proxy for sea surface temperature: calibration of the thermometer and monitoring of ENSO. Paleoceanography, 12, 345–363.

Allemand, D., Ferrier-Pagès, C., Furla, P., Houlbrèque, F., Puverel, S., Reynaud, S., Tambutté, E., Tambutté, S., Zoccola, D. (2004). Biomineralization in reef-building corals: From molecular mechanisms to environmental control. Comptes Rendus Palevol, 3, 453-467.

Allemand, D., Tambutté, E., Zoccola, D., Tambutté, S. (2011). Coral calcification, cells to reefs. In: Dubinsky, Z., Stambler, N. (Eds.), Coral Reefs: An Ecosystem in Transition. Springer, pp. 119-150.

Alley, R., Berntsen, T., Bindoff, N., Chen, Z., Chidthaisong, A., Friedlingstein, P., Gregory, J., Hegerl, G., Heimann, M., Hewitson, B., Hoskins, B., Joos, F., Jouzel, J., Kattsov, V., Lohmann, U., Manning, M., Matsuno, T., Molina, M., Nicholls, N., Overpeck, J., Qin, D., Raga, G., Ramaswamy, V., Ren, J., Rusticucci, M., Solomon, S., Somerville, R., Stocker, T., Stott, P., Stouffer, R., Whetton, P., Wood, R., Wratt D. (2007). Intergovernmental Panel on Climate. Climate change 2007: the physical science basis. Agenda 6, 07.

Allison, N., Finch, A., Sutton, S., Newville, M. (2001). Strontium heterogeneity and speciation in coral aragonite: implications for the strontium paleothermometer. Geochimica et Cosmochimica Acta 65, 2669-2676.

Allison, N., Finch, A.,Webster, J. M., and Clague, D. A. (2007). Palaeoenvironmental records from fossil corals: the effects of submarine diagenesis on temperature and climate estimates. Geochimica et Cosmochimica Acta, 71, 4693-4703.

Andersen, M. B., Stirling, C. H., Potter, E.-K., Halliday, A. N., Blake, S. G., McCulloch, M. T., Ayling, B. F., and O'Leary, M. J. (2010). The timing of sea-level high-stands during Marine Isotope Stages 7.5 and 9: constraints from the uranium-series dating of fossil corals from Henderson Island. Geochimica et Cosmochimica Acta, 74, 3598-3620.

Banerjee, P. (2000). Holocene and Late Pleistocene relative sea level fluctuations along the east coast of India. Marine Geology 167, 243-260.

Bard, E., and Frank, M. (2006). Climate change and solar variability: What's new under the sun?. Earth and Planetary Science Letters, 248, 1-14.

Bard, E., Hamelin, B., Arnold, M., Montaggioni, L.F., Cabioch, G., Faure, G., and Rougerie, F. (1996a). Deglacial sea-level record from Tahiti corals and the timing of global meltwater discharge. Nature, 382, 241-244.

Bard, E., Hamelin, B., Delanghe-Sabatier, D. (2010). Deglacial meltwater pulse 1B and Younger Dryas sea levels revisited with boreholes at Tahiti. Science 327, 1235-1237.

Bard, E., Jouannic, C., Hamelin, B., Pirazzoli, P., Arnold, M., Faure, G., and Sumosusastro, P. (1996b). Pleistocene sea levels and tectonic uplift based on dating of corals from Sumba Island, Indonesia. Geophysical Research Letters, 23, 1473-1476.

Barnes, R. (1987). Invertebrate Zoology. Fort Worth, TX: Harcourt Brace Jovanovich College Publishers. Fifth Edition, 92-96, 127-134, 149-162.

Barnes, R., and Hughes, R. (1999). An Introduction to Marine Ecology; third edition. Oxford, UK: Blackwell Science Ltd. pp. 117-141.

Beck, J. W., Edwards, R. L., Ito, E., Taylor, F. W., Recy, J., Rougerie, F., Joannot, P., and Henin, C. (1992). Sea-surface temperature from coral skeletal strontium/calcium ratios. Science, 257, 644-647.

Beck, J., Edwards, R., Ito, E., Taylor, F., Recy, J., Rougerie, F., Joannot, P., Henin, C. (1992). Sea-surface temperature from coral skeletal strontium/calcium ratios. Science 257, 644–648.

Bernstein R., Betzer P., Feely R., Byrne R., Lamb M., and Michaels A. (1987). Acantharian fluxes and strontium to chlorinity ratios in the North Pacific Ocean. Science 237, 1490–1494.

Binard, N., Hekinian, R., Cheminée, J., Searle, R., Stoffers, P. (1991). Morphological and structural studies of the Society and Austral hotspot regions in the South Pacific. Tectonophysics 186, 293-312.

Binard, N., Maury, R., Guille, G., Talandier, J., Gillot, P., Cotten, J. (1993). Mehetia Island, South Pacific: geology and petrology of the emerged part of the Society hotspot. Journal of volcanology and geothermal research 55, 239-260.

Blais, S., G. Guille, H. Guillou, C. Chauvel, R. Maury, and Caroff, M. (2000). Geology, geochemistry and geochronology of Bora Bora island (Society islands, French Polynesia), Comptes Rendus de l'Academie des Sciences Series IIA, 331, 579-585.

Blais, S., Guille, G., and Maury, R. (1998). Geology and petrology of Raiatea Island (Society Islands, French Polynesia). Comptes Rendus de l'Academie des Sciences Series IIA, 324, 435–442.

Blais, S., Guille, G., Guillou, H., Chauvel, C., Maury, R.C., Pernet, G., Cotten, J. (2002). The island of Maupiti : the oldest emergent volcano in the Society hotspot chain (French Polynesia). Bulletin de la Société géologique de France 173, 45-55.

Blanchon, P., Eisenhauer, A., Fietzke, J., Liebetrau, V. (2009). Rapid sea-level rise and reef back-stepping at the close of the last interglacial highstand. Nature 458, 881-884.

Boiseau, M., Juillet-Leclerc, A., Yiou, P., Salvat, B., Isdale, P., and Guillaume, M. (1998). Atmospheric and oceanic evidences of El Niño-Southern Oscillation events in the south central Pacific Ocean from coral stable isotopic records over the last 137 years. Paleoceanography, 13, 671-685.

Bongers, T., and Wyrtki, K. (1987). Sea Level at Tahiti-A Minimum of Variability. Journal of Physical Oceanography, 17, 164–168.

Bourdon, B., Turner, S., Henderson, G., Lundstrom, C. (2003). Introduction to U-series geochemistry, in: Bourdon, B., Henderson, G. M., Lundstrom, C. C. and Turner, S. P. (Eds.), Uranium series Geochemistry, Mineralogical Society of America, Washington, DC.

Bradley, R. (1999). Paleoclimatology: Reconstructing climates of the Quaternary. Second edition. International Geophysics Series, volume 68. Academic Press, San Diego, CA, 613 pp.

Broecker, W., Peng, T-H. (1982). Tracers in the sea. Eldigio Press. Palisades, New York, pp. 690.

Cabioch, G., Camoin, G., and Montaggioni, L. (1999). Postglacial growth history of a French Polynesian barrier reef tract, Tahiti, central Pacific. Sedimentology, 46, 985-1000.

Camoin, G.F., Davies, P.J. (Eds.). (1998). Reefs and carbonate platforms in the Pacific and Indian oceans. Blackwell science.

Camoin, G.F., Seard, C., Deschamps, P., Webster, J.M., Abbey, E., Braga, J.C., Iryu, Y., Durand, N., Bard, E., Hamelin, B. (2012). Reef response to sea-level and environmental changes during the last deglaciation: Integrated Ocean Drilling Program Expedition 310, Tahiti Sea Level. Geology 40, 643-646.

Cardinal, D., Hamelin, B., Bard, E., Pätzold, J. (2001). Sr/Ca, U/Ca and 18O records in recent massive corals from Bermuda: Relationships with sea surface temperature. Chemical Geology, 176, 231-233.

Carlson, A. E. (2010). What caused the Younger Dryas cold event? Geology, 38, 383-384.

Carpenter, K.E., Abrar, M., Aeby, G., Aronson, R.B., Banks, S., Bruckner, A., Chiriboga, A., Cortés, J., Delbeek, J.C., DeVantier, L. (2008). One-third of reef-building corals face elevated extinction risk from climate change and local impacts. Science 321, 560-563.

Carriquiry, J., Risk, M., Schwarcz, H. (1994). Stable isotope geochemistry of corals from Costa Rica as a proxy indicator of the El Nino/Southern Oscillation (ENSO). Geochim. Cosmochim. Acta 58: 335-351.

Chappell, J. (1983). Evidence for smoothly falling sea level relative to north Queensland, Australia, during the past 6,000 yr. Nature 302, 406-408.

Chappell, J., Polach, H. (1991). Post-glacial sea-level rise from a coral record at Huon Peninsula, Papua New Guinea. Nature 349, 147-149.

Chen, J., Curran, H., White, B., Wasserburg, G. (1991). Precise chronology of the last interglacial period: 234U-230Th data from fossil coral reefs in the Bahamas. Geological Society of America Bulletin 103, 82-97.

Cheng, H., Adkins, J., Edwards, R.L., Boyle, E.A. (2000a). U-Th dating of deep-sea corals. Geochimica et Cosmochimica Acta 64, 2401-2416.

Cheng, H., Edwards, R., Hoff, J., Gallup, C., Richards, D., Asmerom, Y. (2000b). The half-lives of uranium-234 and thorium-230. Chemical Geology 169, 17-33.

Clode, P. L. and Marshall, A.T. (2002). Low temperature X-ray microanalysis of calcium in a scleractinian coral: Evidence of active transport mechanisms. Journal of Experimental Biology, 205, 3543-3552.

Cobb, K. M., Charles, C. D., Cheng, H., Kastner, M., and Edwards, R. L. (2003). U/Th-dating living and young fossil corals from the central tropical Pacific. Earth and Planetary Science Letters, 210, 91-103.

Cohen A.L. and Gaetani G.A. (2010). Ion Partitioning and the Geochemistry of Coral Skeletons: Solving the Mystery of the "Vital Effect". IN: "On partitioning in low temperature aqueous systems: from fundamentals to applications in climate proxies and environmental geochemistry" Editors: Manolo Prieto and Heather Stoll, European Mineralogical Union, Notes in Mineralogy, Volume 10 Chapter 11, pp. 377–397.

Cohen, A. L., and Hart, S. R. (2004). Deglacial sea surface temperatures of the western tropical Pacific: A new look at old coral. Paleoceanography, 19, PA4031.

Cohen, A., and McConnaughey, T. (2003). Geochemical perspectives on coral mineralization. In: Biomineralization (P.M. Dove, J.J. De Yoreo & S. Weiner, editors). Reviews in Mineralogy and Geochemistry, 54, 151–187. Mineralogical Society of America, Washington D.C. and the Geochemical Society, St. Louis,Missouri, USA.

Cohen, A., Hart, S. (2004). Deglacial sea surface temperatures of the western tropical Pacific: A new look at old coral. Paleoceanography 19, PA4031.

Corrège, T. (2006). Sea surface temperature and salinity reconstruction from coral geochemical tracers. Palaeogeography, Palaeoclimatology, Palaeoecology, 232, 408-428.

Corrège, T., Gagan, M.K., Beck, J.W., Burr, G.S., Cabioch, G., Le Cornec, F. (2004). Interdecadal variation in the extent of South Pacific tropical waters during the Younger Drys event, Nature, 428, 927-929.

Cuif, J., and Dauphin Y. (2005). The Environment Recording Unit in coral skeletons- a synthesis of structural and chemical evidences for a biochemically driven, stepping-growth process in fibres. Biogeosciences, 2, 61-73.

Davies, P.J., Marshall, J.F. (1980). A model of epicontinental reef growth. Nature 287, 37-38.

de Villiers, S. (1999). Seawater strontium and Sr/Ca variability in the Atlantic and Pacific oceans. Earth and Planetary Science Letters 171, 623-634.

de Villiers, S., Greaves, M., and Elderfield, H. (2002). An intensity ratio calibration method for the accurate determination of Mg/Ca and Sr/Ca of marine carbonates by ICP-AES. Geochemistry, Geophysics, Geosystems, 3, 1525-2027.

de Villiers, S., Nelson, B. K., and Chivas, A. R. (1995). Biological controls on coral Sr/Ca and δ18O reconstructions of sea surface temperatures. Science, 269, 1247-1249.

de Villiers, S., Shen, G.T. and Nelson, B. (1994). The Sr/Ca-temperature relationship in coralline aragonite: Influence of variability in (Sr/Ca) seawater and skeletal growth parameters. Geochimica et Cosmochimica Acta, 58, 197–208.

Delanghe, D., Bard, E., and Hamelin, B. (2002). New TIMS constraints on the uranium-238 and uranium-234 in seawaters from the main ocean basins and the Mediterranean Sea1. Marine Chemistry, 80, 79-93.

Delesalle, B., Galzin, R., Salvat, B. (1985). French Polynesian coral reefs. Proceedings of the 5th International Coral Reef Congress, Papeete, 1, pp. 1–554.

Denton, G., and Hughes, T. (1981). The last great ice sheets. John V1/Piley & Sons, New York, pp. 484.

Deschamps, P., Durand, N., Bard, E., Hamelin, B., Camoin, G., Thomas, A.L., Henderson, G.M., Okuno, J., Yokoyama, Y. (2012). Ice-sheet collapse and sea-level rise at the Bolling warming 14,600 years ago. Nature 483, 559-564.

Devey, C., Albarede, F., Cheminée, J., Michard, A., Mühe, R., Stoffers, P. (1990). Active submarine volcanism on the Society hotspot swell (West Pacific): a geochemical study. Journal of Geophysical Research 95, 5049-5066.

Dietzel, M., Gussone, N., and Eisenhauer, A. (2004). Precipitation of aragonite by membrane diffusion of gaseous CO2 and the coprecipitation of Sr2+ and Ba2+ (10° to 50°C). Chemical Geology, 203, 139-151.

Douville, E., Sallé, E., Frank, N., Eisele, M., Pons-Branchu, E., Ayrault, S. (2010). Rapid and accurate U-Th dating of ancient carbonates using inductively coupled plasma-quadrupole mass spectrometry. Chemical Geology 272, 1-11.

Dullo, W., Camoin, G., Blomeier, D., Colonna, M., Eisenhauer, A., Faure, G., Casanova, J., Thomassin, B. (1998). Morphology and sediments of the fore-slopes of Mayotte, Comoro Islands: direct observations from a submersible. Reefs and carbonate platforms in the Pacific and Indian Oceans, 217-236.

Dullo, W-C. (1986). Variation in diagenetic sequences: An example from Pleistocene coral reefs, Red Sea, Saudi Arabia. In: SCHROEDER, J.H. & PURSER, B. (eds.): Reefs Diagenesis. Heidelberg - Berlin - New York: Springer, pp. 77-90.

Duncan, R. A., and McDougall, I. (1976). Linear volcanism in French Polynesia. Journal of volcanology and geothermal research, 1, 197-227.

Duncan, R. A., Fisk, M. R., White, W. M., and Nielsen, R. L. (1994), Tahiti: Geochemical evolution of a French Polynesian volcano. Journal of Geophysical research, 99, 24341-24357.

Edmond, J. (1992). Himalayan tectonics, weathering processes, and the strontium isotope record in marine limestones. Science 258, 1594-1597.

Edwards, R., Gallup, C., Cheng, H. (2003). Uranium-series dating of marine and lacustrine carbonates. In: Bourdon, B., Henderson, G. M., Lundstrom, C. C. and Turner, S. P. (Eds.), Uranium-series Geochemistry, Mineralogical Society of America, Washington, DC.

Edwards, R.L., Taylor, F., Wasserburg, G. (1988). Dating Earthquakes with high-precision thorium-230 ages of very young corals. Earth and Planetary Science Letters 90, 371-381.

Eisenhauer, A., Heiss, G., Sheppard, C., Dullo, W. (1999). Reef and island formation and Late Holocene sea-level changes in the Chagos islands. Ecology of the Chagos Archipelago, 21-31.

Eisenhauer, A., Wasserburg, G.J., Chen, J.H., Bonani, G., Collins, L.B., Zhu, Z.R., Wyrwoll, K.H. (1993). Holocene sea-level determination relative to the Australian continent: U/Th (TIMS) and 14C (AMS) dating of coral cores from the Abrolhos Islands. Earth and Planetary Science Letters 114, 529-547.

Eisenhauer, A., Zhu, Z., Collins, L., Wyrwoll, K., Eichstätter, R. (1996). The Last Interglacial sea level change: new evidence from the Abrolhos islands, West Australia. Geologische Rundschau 85, 606-614.

Elsig, J., Schmitt, J., Leuenberger, D., Schneider, R., Eyer, M., Leuenberger, M., Joos, F., Fischer, H., and Stocker, T. F. (2009). Stable isotope constraints on Holocene carbon cycle changes from an Antarctic ice core. Nature, 461, 507-510.

Enmar, R., Stein, M., Bar-Matthews, M., Sass, E., Katz, A., and Lazar, B., (2000). Diagenesis in live corals from the Gulf of Aqaba. I. The effect on paleo-oceanography tracers. Geochimica et Cosmochimica Acta, 64, 3123-3132.

Fadil, A., Sichoix, L., Barriot, J.P., Ortéga, P., Willis, P. (2011). Evidence for a slow subsidence of the Tahiti Island from GPS, DORIS, and combined satellite. Comptes Rendus Geoscience 343, 331–341.

Fairbanks, R., Evans, M., Rubenstone, J., Mortlock, R., Broad, K., Moore, M., Charles, C. (1997). Evaluating climate indices and their geochemical proxies measured in corals. Coral Reefs 16, S93-S100.

Fairbanks, R.G. (1989). A 17,000-year glacio-eustatic sea level record: influence of glacial melting rates on the Younger Dryas event and deep-ocean circulation. Nature 342, 637-642.

Farrell, W., and Clark, J.A. (1976). On postglacial sea level. Geophysical Journal of the Royal Astronomical Society 46, 647-667.

Felis, T., Lohmann, G., Kuhnert, H., Lorenz, S.J., Scholz, D., Patzold, J., Al-Rousan, S.A. and Al-Moghrabi, S.M. (2004). Increased seasonality in Middle East temperatures during the last interglacial period. Nature 429, 164-168.

Felis, T., Pätzold, J. (2004). Climate reconstructions from annually banded corals. Global environmental change in the ocean and on land, 205-227.

Ferrier-Pagès, C., Boisson, F., Allemand, D., Tambutté, E. (2002). Kinetics of strontium uptake in the scleractinian coral Stylophora pistillata. Marine ecology. Progress series 245, 93-100.

Fietzke, J., Liebetrau, V., Eisenhauer, A., Dullo, C. (2005). Determination of uranium isotope ratios by multi-static MIC-ICP-MS: method and implementation for precise U-and Th-series isotope measurements. J. Anal. At. Spectrom. 20, 395-401.

Flood, P., Frankel, E. (1989). Late Holocene higher sea level indicators from eastern Australia. Marine Geology 90, 193-195.

Flora, C.J., and Ely, P.S. (2003). Surface growth rings of Porites lutea microatolls accurately track their annual growth. Northwest Science 77, 237–245.

Gaetani, G.A., Cohen, A.L., Wang, Z., Crusius, J. (2011). Rayleigh-Based, Multi-Element coral thermometry: A biomineralization approach to developing climate proxies. Geochimica et Cosmochimica Acta, 75(7), 1920-1932.

Gagan, M., Ayliffe, L., Beck, J., Cole, J., Druffel, E., Dunbar, R., and Schrag, D. (2000). New views of tropical paleo-climates from corals. Quaternary Science Reviews, 19, 45-64.

Gagan, M., Ayliffe, L., Hopley, D., Cali, J., Mortimer, G., Chappel, J., McCulloch, M.T., Head, M.J. (1998). Temperature and surface ocean water balance of mid- Holocene tropical western Pacific, Science, 279, 1014-1018.

Gass, S., Roberts, J. (2011). Growth and branching patterns of Lophelia pertusa (Scleractinia) from the North Sea. Journal of Marine Biological Association of the United Kingdom, 91, 831-835.

Goelzer, H., Huybrechts, P., Raper, S., Loutre, M., Goosse, H., Fichefet, T. (2012). Millennial total sea-level commitments projected with the Earth system model of intermediate complexity LOVECLIM. Environmental Research Letters 7, 045401.

Goldstein, S., Lea, D., Chakraborty S., Kashgarian M., Murrell M. (2001). Uranium series and radiocarbon geochronology of deep-sea corals: Implications for southern ocean ventilation rates and the oceanic carbon cycle. Earth and Planetary Science Letters, 193, 167–182.

Gripp, A., Gordon, R. (1990). Current plate velocities relative to the hotspots incorporating the NUVEL-1 global plate motion model. Geophysical Research Letters 17, 1109-1112.

Grossman, E.E., Fletcher III, C.H., Richmond, B.M. (1998). The Holocene sea-level highstand in the equatorial Pacific: analysis of the insular paleosea-level database. Coral Reefs 17, 309-327.

Grottoli, A. (2001). Past climate from corals. In: Encyclopedia of Ocean Sciences [Eds. J. Steele, S. Thorpe, K. Turekian]. Academic Press, London, pp. 2098-2107.

Grottoli, A., Eakin, C. (2007). A review of modern coral δ18O and Δ14C proxy records. Earth-Science Reviews 81, 67-91.

Grove, J. M. (2004). Little Ice Ages-Ancient and Modern. Second Edition London: Routledge, vol. I and II.

Guilderson, T., Fairbanks R., Rubenstone, J. (1994). Tropical temperature variations since 20,000 years ago: Modulating interhemispheric climate change. Science, 263, 663–665.

Guillou, H., Maury, R. C., Blais, S., Cotten, J., Legendre, C., Guille, G., and Caroff, M. (2005). Age progression along the Society hotspot chain (French Polynesia) based on new un spiked K-Ar ages. Bulletin de la Société géologique de France, 176, 135-150.

Hansen, J., Sato, M., Russell, G., and Kharecha, P. (2013). Climate sensitivity, sea level and atmospheric carbon dioxide. Philosophical Transactions of the Royal Society A: Mathematical, Physical and Engineering Sciences, 371, 20120294.

Hathorne, E. C., Felis, T., James, R. H., and Thomas, A. (2011). Laser ablation ICP-MS screening of corals for diagenetically affected areas applied to Tahiti corals from the last deglaciation. Geochimica et Cosmochimica Acta, 75, 1490-1506.

Hathorne, E., Gagnon, A., Felis, T., Adkins, J., Asami, R., Boer, W., Caillon, N., Case, D., Cobb, K.M., Douville, E., deMenocal, P., Eisenhauer, A., Garbe-Schönberg, C.-D., Geibert, W., Goldstein, S., Hughen, K., Inoue, M., Kawahata, H., Kölling, M., Le Cornec, F., Linsley, B.K., McGregor, H.V., Montagna, Paolo, Nurhati, I.S., Quinn, T.M., Raddatz, J., Rebaubier, H., Robinson, L., Sadekov, A., Sherrell, R., Sinclair, D., Tudhope, A.W., Wei, G., Wong, H., Wu, H.C., You, C.-F. (2013b). Inter-laboratory study for coral Sr/Ca and other element/Ca ratio measurements. Geochemistry, Geophysics, Geosystems 14, 3730-3750.

Hendy, E., Gagan, M., Lough, J., McCulloch, M., and Demenocal, P. (2007). Impact of skeletal dissolution and secondary aragonite on trace element and isotopic climate proxies in Porites corals, Paleoceanography, 22, PA4101.

Hernández-Mendiola, E., Bernal, J., Lounejeva, E., Mortimer, G., and McCulloch, M. (2011). U-series dating of carbonates using inductively coupled plasma-quadrupole mass spectrometry, Quaternary Geochronology, 6, 564-573.

Houghton, J.T. (1996). Climate change 1995: The science of climate change: contribution of working group I to the second assessment report of the Intergovernmental Panel on Climate Change. Cambridge University Press.

Indermühle, A., Stocker, T. F., Joos, F., Fischer, H., Smith, H. J., Wahlen, M., Deck, B., Mastroianni, D., Tschumi, J., and Blunier, T. (1999). Holocene carbon-cycle dynamics based on CO2 trapped in ice at Taylor Dome, Antarctica. Nature, 398, 121-126.

IPCC, (2013): Summary for Policymakers. In: Climate Change 2013: The Physical Science Basis. Contribution of Working Group I to the Fifth Assessment Report of the Intergovernmental Panel on Climate Change [Stocker, T.F., D. Qin, G.-K. Plattner, M. Tignor, S. K. Allen, J. Boschung, A. Nauels, Y. Xia, V. Bex and P.M. Midgley (eds.)]. Cambridge University Press, Cambridge, United Kingdom and New York, NY, USA.

Jaffey, A., Flynn, K., Glendenin, L., Bentley, W., Essling, A. (1971). Precision measurement of half-lives and specific activities of 235U and 238U. Phys. Rev. C4, 1889–1906.

Jones, P., and Mann, M. (2004). Climate over past millennia. Rev. Geophys., 42, RG2002.

Juillet-Leclerc, A., Reynaud, S., Rollion-Bard, C., Cuif, J.P., Dauphin, Y., Blamart, D., Ferrier-Pagès, C., Allemand, D. (2009). Oxygen isotopic signature of the skeletal microstructures in culturedcorals. Identification of vital effects. Geochimica et Cosmochimica Acta, 73, 5320-5332.

Kaufman, A., Broecker, W. (1965). Comparison of 230Th and 14C ages for carbonate materials from Lakes Lahontan and Bonneville. Journal of Geophys Research 70, 4039-4054.

Kench, P., Smithers, S., McLean, R., Nichol, S. (2009). Holocene reef growth in the Maldives: Evidence of a mid-Holocene sea-level highstand in the central Indian Ocean. Geology 37, 455-458.

Kennedy, D., and Woodroffe, C. (2002). Fringing reef growth and morphology: a review. Earth-Science Reviews 57, 255-277.

Kim, S.-T., O'Neil, J. (1997). Temperature dependence of δ18O. Geochim. Cosmochim. Acta 61, 3461–3475.

Kinsman, D. (1969). Interpretation of strontium concentration in carbonate minerals and rocks. J. Sediment. Petrol. 39, 486– 508.

Kotpal, P. (2004). Modern Text Book of Zoology: Invertebrates. Rastogi Publications. pp 313-314.

Koutavas, A., and Sachs, J. P. (2008). Northern timing of deglaciation in the eastern equatorial Pacific from alkenone paleothermometry. Paleoceanography, 23, PA4205.

Koutavas, A., Lynch-Stieglitz, J., Marchitto, T. M., and Sachs, J. (2002). El Nino-like pattern in ice age tropical Pacific sea surface temperature. Science, 297, 226-230.

Kuhnert, H., Pätzold, J., Hatcher, B., Wyrwoll, K.-H., Eisenhauer, A., Collins, L.B., Zhu, Z.R., Wefer, G. (1999). A 200-year coral stable oxygen isotope record from a high-latitude reef off Western Australia. Coral Reefs 18, 1–12.

Lalli, C. and Parsons, T. (1995). Biological Oceanography: An Introduction. Oxford, UK: Butterworth-Heinemann Ltd. pp. 220-233.

Lambeck, K., Antonioli, F., Purcell, A., Silenzi, S. (2004). Sea-level change along the Italian coast for the past 10,000 yr. Quaternary Science Reviews 23, 1567-1598.

Lambeck, K., Smither, C., Ekman, M. (1998). Tests of glacial rebound models for Fennoscandinavia based on instrumented sea-and lake-level records. Geophysical Journal International 135, 375-387.

Lambeck, K., Yokoyama, Y., Purcell, T. (2002). Into and out of the Last Glacial Maximum: sea-level change during Oxygen Isotope Stages 3 and 2. Quaternary Science Reviews 21, 343-360.

Land, L. S. (1973). Coral Reef Project-Papers in Memory of Dr. Thomas F. Goreau. 4. Contemporaneous Dolomitization of Middle Pleistocene Reefs by Meteoric Water, North Jamaica. Bulletin of Marine Science, 23, 64-92.

Larcombe, P., Carter, R., Dye, J., Gagan, M., Johnson, D. (1995). New evidence for episodic post-glacial sea-level rise, central Great Barrier Reef, Australia. Marine Geology 127, 1-44.

Lazar, B., Enmar, R., Schossberger, M., Bar-Matthews, M., Halicz, L., Stein, M. (2004). Diagenetic effects on the distribution of uranium in live and Holocene corals from the Gulf of Aqaba. Geochimica et Cosmochimica Acta 68, 4583-4593.

Lea D. W. (2006). Elemental and Isotopic Proxies of Past Ocean Temperatures. In: Elderfield H. (ed). Treatise on Geochemistry, Vol. 6: The Oceans and Marine Geochemistry, Oxford, UK, Elsevier , pp. 365-390.

Lepofsky, D., Kirch, P.V., Lertzman, K.P. (1996). Stratigraphic and paleobotanical evidence for prehistoric human-induced environmental disturbance on Mo'orea, French Polynesia. Pacific Science 50, 253-273.

Levermann, A., Clark, P. U., Marzeion, B., Milne, G. A., Pollard, D., Radic, V., and Robinson A. (2013). The multimillennial sea-level commitment of global warming. Proceedings of the National Academy of Sciences, 110, 13745-13750.

Levinton, J. (1995). Marine Biology: Function, Biodiversity, Ecology. New York: Oxford University Press, Inc. pp. 306-319.

Longman, M. W. (1980). Carbonate diagenetic textures from near surface diagenetic environments. AAPG Bulletin, 64, 461-487.

Loya, Y. (2004). The coral reefs of Eilat—past, present and future: three decades of coral community structure studies. Coral health and disease. Springer, pp. 1-34.

Maier, C., Felis, T., Pätzold, J., Bak, R.P.M. (2004). Effect of skeletal growth and lack of species effects in the skeletal oxygen isotope climate signal within the coral genus Porites. Marine Geology, 207, 193-208.

Marchitto, T. M., Muscheler, R., Ortiz, J. D., Carriquiry J. D.,, and van Geen, A. (2010). Dynamical response of the tropical Pacific Ocean to solar forcing during the early Holocene. Science, 330, 1378-1381.

Marshall, J.F., McCulloch, M.T. (2002). An assessment of the Sr/Ca ratio in shallow water hermatypic corals as a proxy for sea surface temperature. Geochimica et Cosmochimica Acta 66, 3263-3280.

McConnaughey, T.A. (1989). 13C and 18O isotopic disequilibrium in biological carbonates: II. In vitro simulations of kinetic isotope effects. Geochim. Cosmochim. Acta, 53, 163–171.

McCulloch, M., Gagan, M., Mortimer, G., Chivas, A., Isdale, P. (1994). A high resolution Sr/Ca and 18O coral record from the Great Barrier Reef, Australia and the 1982-1983 El Niño. Geochimica et Cosmochimica Acta, 58, 2747-2754.

McCulloch, M., Mortimer, G., Esat, T., Xianhua, L., Pillans, B., Chappell, J. (1996). High resolution windows into early Holocene climate: SrCa coral records from the Huon Peninsula. Earth and Planetary Science Letters 138, 169-178.

McGranahan, G., Balk, D., Anderson, B. (2007). The rising tide: assessing the risks of climate change and human settlements in low elevation coastal zones. Environment and Urbanization 19, 17-37.

McGregor, H. V., and Abram, N. (2008). Images of diagenetic textures in Porites corals from Papua New Guinea and Indonesia. Geochem. Geophys. Geosyst. 9, Q10013.

McGregor, H. V., and Gagan, M. K. (2003). Diagenesis and geochemistry of Porites corals from Papua New Guinea: Implications for paleo-climate reconstruction. Geochimica et Cosmochimica Acta, 67, 2147-2156.

McNutt, M., Menard, H. (1978). Lithospheric flexure and uplifted atolls. Journal of Geophysical Research: Solid Earth 83, 1206-1212.

Meibom, A., Yurimoto, H., Cuif, J.-P., Domart-Coulon, I., Houlbrèque, F., Constantz, B., Dauphin, Y., Tambutté, E., Tambutté, S., Allemand, D., Wooden, J., Dunbar, R. (2006). Vital effects in coral skeletal composition display strict three-dimensional control. Geophysical Research Letters, 33, L11608.

Milne, G.A., Gehrels, W.R., Hughes, C.W., Tamisiea, M.E. (2009). Identifying the causes of sea-level change. Nature Geoscience 2, 471-478.

Milne, G.A., Mitrovica, J.X. (1996). Postglacial sea-level change on a rotating Earth: first results from a gravitationally self-consistent sea-level equation. Geophysical Journal International 126, F13-F20.

Milne, G.A., Mitrovica, J.X. (1998). Postglacial sea-level change on a rotating Earth. Geophysical Journal International 133, 1-19.

Min, G., Edwards, R. L., Taylor, F. W., Recy, J., Gallup, C. D., and Beck, J. (1995). Annual cycles of UCa in coral skeletons and UCa thermometry. Geochimica et Cosmochimica Acta, 59, 2025-2042.

Mitrovica, J., Davis, J., Shapiro, I. (1994). A spectral formalism for computing three-dimensional deformations due to surface loads: 2. Present-day glacial isostatic adjustment. Journal of Geophysical Research: Solid Earth 99, 7075-7101.

Mitrovica, J.X., and Milne, G.A. (2002). On the origin of late Holocene sea-level highstands within equatorial ocean basins. Quaternary Science Reviews 21, 2179-2190.

Mitrovica, J.X., and Peltier, W. (1991). On postglacial geoid subsidence over the equatorial oceans. Journal of Geophysical Research 96, 20053-20071.

Mitsuguchi, T., Matsumoto, E., Abe, O., Uchida, T., and Isdale, P. (1996). Mg/Ca thermometry in coral skeletons. Science, 274, 961-963.

Monnin, E., Indermühle, A., Dällenbach, A., Flückiger, J. Stauffer, B., Stocker, T., Raynaud, D., and Barnola J. M. (2001). Atmospheric CO2 concentrations over the last glacial termination. Science, 291, 112-114.

Montaggioni, L. (2011). Tahiti/Society Islands, in: Hopley, D. (Ed.), Encyclopedia of Modern Coral Reefs. Springer Netherlands, pp. 1073-1075.

Montaggioni, L., Cabioch, G., Faure, G., Rougerie, F. (1996). Deglacial sea-level record from Tahiti corals and the timing of global meltwater discharge. Nature 382, 18.

Montaggioni, L.F. (2005). History of Indo-Pacific coral reef systems since the last glaciation: development patterns and controlling factors. Earth-Science Reviews 71, 1-75.

Montaggioni, L.F., and Pirazzoli, P.A. (1984). The significance of exposed coral conglomerates from French Polynesia (Pacific Ocean) as indicators of recent relative sea-level changes. Coral Reefs 3, 29-42.

Müller, A., Gagan, M. K., and McCulloch, M. T. (2001). Early marine diagenesis in corals and geochemical consequences for paleoceanographic reconstructions. Geophysical Research Letters, 28, 4471-4474.

Müller, S., Joos, F., Edwards, N., Stocker, T. (2006). Water Mass Distribution and Ventilation Time Scales in a Cost-Efficient, Three-Dimensional Ocean Model. Journal of Climate, 19, 5479-5499.

Neall, V.E., Trewick, S.A. (2008). The age and origin of the Pacific islands: a geological overview. Philosophical Transactions of the Royal Society B: Biological Sciences 363, 3293-3308.

NOAA, (2013). Tide tables (2013). High and low water predictions Central and Western Pacific Ocean and Indian Ocean. North Wind Publishing, Brewer, ME 04915, USA.

Nolasco, R., Tarits, P., Filloux, J.H., Chave, A.D. (1998). Magnetotelluric imaging of the Society Islands hotspot. Journal of Geophysical Research: Solid Earth 103, 30287-30309.

Nothdurft, L., Webb, G. (2009). Earliest diagenesis in scleractinian coral skeletons: implications for palaeoclimate-sensitive geochemical archives. Facies 55, 161-201.

Nurhati, I. S., Cobb, K., Charles, C. D., Dunbar, R. (2009). Late 20th century warming and freshening in the central tropical Pacific. Geophysical Research Letters, 36, 21.

Okai, T., Suzuki, A., Kawahata, H., Terashima, S., Imai, N. (2002). Preparation of a New Geological Survey of Japan Geochemical Reference Material: Coral JCp-1. Geostandards Newsletter 26, 95–99.

Oomori, T., Kaneshima, K., Nakamura, Y., Kitano, Y. (1982). Seasonal variation of minor elements in coral skeletons. Galaxea 1, 77– 86.

Peltier, W. (1974). The impulse response of a Maxwell Earth. Reviews of Geophysics 12, 649-669.

Peltier, W. (2004). Global glacial isostasy and the surface of the ice-age Earth: The ICE-5G (VM2) model and GRACE. Annu. Rev. Earth Planet. Sci. 32, 111-149.

Peltier, W.R. (2002). On eustatic sea level history: Last Glacial Maximum to Holocene. Quaternary Science Reviews 21, 377-396

Pernice, M., Meibom, A., Van Den Heuvel, A., Kopp,C., Domart-Coulon, I., Hoegh-Guldberg, O., and Dove S. (2012). A single-cell view of ammonium assimilation in coral–dinoflagellate symbiosis. The ISME journal, 6, 1314-1324.

Pingitore Jr., Iglesias, A., Lytle, F., Wellington, G. (2002). Xray absorption spectroscopy of uranium at low ppm levels in coral skeletal aragonite. Microchem. J. 71, 261– 266.

Pirazzoli, P. A. (1996). Sea-Level Changes The last 20000 years. Wiley Chichester, pp. 211.

Pirazzoli, P., and Montaggioni, L. (1985). Lithospheric deformation in French Polynesia (Pacific Ocean) as deduced from Quaternary shorelines. Proceedings of the 5th Int. Coral Reef Congress, Tahiti, pp. 195-200.

Pirazzoli, P., Montaggioni, L., Delibrias, G., Faure, G., Salvat, B. (1985). Late Holocene sea-level changes in the Society Islands and in the northwest Tuamotu atolls, Delesalle B., Galzin R. & Salvat B.(éds) 5th Int. Coral Reef Congress, Tahiti, pp. 131-136.

Pirazzoli, P., Montaggioni, L.F., Salvat, B., Faure, G. (1988). Late Holocene sea level indicators from twelve atolls in the central and eastern Tuamotus (Pacific Ocean). Coral Reefs 7, 57-68.

Pirazzoli, P.A., and Montaggioni, L.F. (1988). Holocene sea-level changes in French Polynesia. Palaeogeography, Palaeoclimatology, Palaeoecology 68, 153-175.

Pirazzoli, P.A., and Montaggioni, L.F. (1986). Late Holocene sea-level changes in the northwest Tuamotu islands, French Polynesia. Quaternary Research 25, 350-368.

Pirazzoli, P.A., Pluet, J. (1991). Holocene changes in sea level as climate proxy data in Europe. Evaluation of Climate Proxy Data in Relation to the European Holocen. Paleoklimaforschung 6, 205-225.

Pratchett, M.S., McCowan, D., Maynard, J.A., Heron, S.F. (2013). Changes in bleaching susceptibility among corals subject to ocean warming and recurrent bleaching in Moorea, French Polynesia. PloS one 8, e70443.

Quinn, T.M., Sampson, D.E. (2002). A multiproxy approach to reconstructing sea surface conditions using coral skeleton geochemistry. Paleoceanography 17, 14-11-14-11.

Rashid, R., Eisenhauer A., Stocchi P., Liebetrau V., Fietzke J., Rüggeberg A., and Dullo, C. (2014). Constraining Mid to Late Holocene relative sea level change in the southern equatorial Pacific Ocean relative to the Society Islands, French Polynesia. Geochemistry, Geophysics, Geosystems, 15, 2601–2615.

Reeder, R., Nugent, M., Lamble, G., Tait, C., and Morris, D. (2000). Uranyl incorporation into calcite and aragonite: XAFS and luminescence studies. Environmental Science and Technology, 34, 638-644.

Reynaud, S., Ferrier-Pagès, C., Boisson, F., Allemand, D., Fairbanks, R.G. (2004). Effect of light and temperature on calcification and strontium uptake in the scleractinian coral Acropora verweyi. Marine Ecology Progress Series, 279, 105-112.

Rogers, A.D. (2004). The Biology, ecology and vulnerability of seamount communities. Report for the World Conservation Union for the 7th Convention of Parties, Convention for Biodiversity, Kuala Lumpur, 8–19 February, 8pp.

Sayani, H. R., Cobb, K. M., Cohen, A. L., Elliott, W. C., Nurhati, I. S., Dunbar, R. B., Rose, K. A., and Zaunbrecher L. (2011). Effects of diagenesis on paleo-climate reconstructions from modern and young fossil corals. Geochimica et Cosmochimica Acta, 75, 6361-6373.

Scholz, D., and Mangini, A. (2007). How precise are U-series coral ages? Geochimica et Cosmochimica Acta 71, 1935-1948.

Schrag, D. (1999). Rapid analysis of high-precision Sr/Ca ratios in corals and other marine carbonates. Paleoceanography 14, 97-102.

Scoffin, T., Le Tissier, M. (1998). Late Holocene sea level and reef-flat progradation, Phuket, South Thailand. Coral Reefs 17, 273-276.

Scoffin, T.P., Stoddart, D., Rosen, B.R. (1978). The nature and significance of microatolls. Philosophical Transactions of the Royal Society of London. B, Biological Sciences 284, 99-122.

Scott, G.A., Rotondo, G.M. (1983a). A model for the development of types of atolls and volcanic islands on the Pacific lithospheric plate. Atoll Research Bulletin 260, 33.

Scott, G.A.J., Rotondo, G.M. (1983b). A model to explain the differences between Pacific plate island-atoll types. Coral Reefs 1, 139-150.

Seard, C., Camoin, G., Yokoyama, Y., Matsuzaki, H., Durand, N., Bard, E., Sepulcre, S., Deschamps, P. (2011). Microbialite development patterns in the last deglacial reefs from Tahiti (French Polynesia; IODP Expedition# 310): Implications on reef framework architecture. Marine Geology 279, 63-86.

Shen, C. C., Lee, T., Chen, C. Y., Wang, C. H., Dai, C. F., and Li, L. A. (1996). The calibration of D[Sr/Ca] versus sea surface temperature relationship for Porites corals. Geochimica et Cosmochimica Acta, 60, 3849-3858.

Shen, G. T., and Dunbar, R. (1995). Environmental controls on uranium in reef corals. Geochimica et Cosmochimica Acta, 59, 2009-2024.

Sinclair, D., Risk, M. (2006). A numerical model of trace-element coprecipitation in a physicochemical calcification system: application to coral biomineralization and trace-element ‘vital effects’. Geochimica et cosmochimica acta 70, 3855-3868.

Smithers, S. G., and Woodroffe, C. D. (2001). Coral microatolls and 20th century sea level in the eastern Indian Ocean. Earth and Planetary Science Letters, 191, 173-184.

Smithers, S. G., and Woodroffe, C. D. (2000). Microatolls as sea-level indicators on a mid-ocean atoll. Marine Geology, 168, 61-78.

Spada, G., and Stocchi, P. (2007). SELEN: A Fortran 90 program for solving the "sea-level equation". Computers & Geosciences, 33, 538-562.

Spada, G., Antonioli, A., Cianetti, S., and Giunchi, C. (2006). Glacial isostatic adjustment and relative sea-level changes: the role of lithospheric and upper mantle heterogeneities in a 3-D spherical Earth. Geophysical Journal International, 165, 692-702.

Spada, G., Melini, D., Galassi, G., and Colleoni, F. (2012). Modeling sea level changes and geodetic variations by glacial isostasy: the improved SELEN code. arXiv preprint arXiv:1212.5061.

Stephans, C.L., Quinn, T.M., Taylor, F.W., Corrège, T. (2004). Assessing the reproducibility of coral-based climate records. Geophysical research letters 31, L18210.

Stirling, C. H., and Andersen, M. B. (2009). Uranium-series dating of fossil coral reefs: extending the sea-level record beyond the last glacial cycle. Earth and Planetary Science Letters, 284, 269-283.

Stirling, C., Esat, T., Lambeck, K., McCulloch, M., Blake, S., Lee, D.C., Halliday, A. (2001). Orbital forcing of the marine isotope stage 9 interglacial. Science 291, 290-293.

Stuiver, M., and Reimer, P. (1993). Extended (super 14) C data base and revised CALIB 3.0 (super 14) C age calibration program. Radiocarbon, 35, 215-230.

Suess, E., and Waagen, L. (1888). Das antlitz der erde. Vol.2. F. Tempsky.

Sumich, J. (1996). An Introduction to the Biology of Marine Life, sixth edition. Dubuque, IA: Wm. C. Brown. pp. 255-269.

Tambutté, E., Allemand, D., Mueller, E., Jaubert, J. (1996). A compartmental approach to the mechanism of calcification in hermatypic corals. The journal of experimental biology, 199, 1029-1041.

Tambutté, S., Holcomb, M., Ferrier-Pagès, C., Reynaud, S., Tambutté, E., Zoccola, D., Allemand, D. (2011). Coral biomineralization: From the gene to the environment. Journal of Experimental Marine Biology and Ecology, 408, 58-78.

Taylor, F. J. (1979). Rhizophora in the Society Islands. Pac. Sc. 33, 173-176.

Thomas, A. L., Fujita, K., Iryu, Y., Bard, E., Cabioch, G., Camoin, G., Cole, J. E., Deschamps, P., Durand, N., and Hamelin B. (2012). Assessing subsidence rates and paleo water-depths for Tahiti reefs using U–Th chronology of altered corals. Marine Geology, 295, 86-94.

Thompson, L. G., Mosley-Thompson, E., Brecher, H., Davis, M., León, B., Les, D., Lin, P. Mashiotta, T., and Mountain, K. (2006). Abrupt tropical climate change: Past and present. Proceedings of the National Academy of Sciences, 103, 10536-10543.

Tribble, G. W., Sansone, F. J., and Smith, S. (1990). Stoichiometric modeling of carbon diagenesis within a coral reef framework. Geochimica et Cosmochimica Acta, 54, 2439-2449.

Tucker, M. E., and Wright, V. P. (2009). Carbonate sedimentology. John Wiley & Sons. Blackwell, Oxford, pp. 314-362.

Tushingham, A. M., and Peltier, W. (1992). Validation of the ICE-3G Model of Würm-Wisconsin Deglaciation using a global data base of relative sea level histories. Journal of Geophysical Research: Solid Earth, 97(B3), 3285-3304.

Uto, K., Yamamoto, Y., Sudo, M., Uchiumi, S., Ishizuka, O., Kogiso, T., Tsunakawa, H. (2007). New K-Ar ages of the Society Islands, French Polynesia, and implications for the Society hotspot feature. Earth, Planets, and Space 59, 879-885.

Veron, J. (2000). Corals of the World. Vol 3. Australia: Australian Institute of Marine Sciences and CRR Qld Pty Ltd. Australian Institute of Marine Sciences and CRR Qld Pty Ltd., 3, 206-209 pp.

Vonmoos, M., Beer, J., Muscheler, R. (2006). Large variations in Holocene solar activity constraints from 10Be in the GRIP ice core. Journal of Geophysical Research 111, A10105.

Wanner, H., Beer, J., Bütikofer, J., Crowley, T. J., Cubasch, U., Flückiger, J., Goosse, H., Grosjean, M., Joos F., and Kaplan, J. (2008). Mid-to Late Holocene climate change: An overview. Quaternary Science Reviews, 27, 1791-1828.

Watanabe, T., Winter, A., Oba, T. (2001) Seasonal changes in sea surface temperature and salinity during the Little Ice Age in the Caribbean Sea deduced from Mg/Ca and 18O/16O ratios in corals. Marine Geology, 173, 21–35.

Weber J., Woodhead, P. (1972). Temperature dependence of oxygen-18 concentration in reef coral carbonates. J. Geophys. Res. 77: 463-473.

Weber, J. (1973). Incorporation of strontium into reef coral skeletal carbonate. Geochimica et Cosmochimica Acta 37, 2173-2190.

Wei, G., Sun, M., Li, X., Nie, B. (2000). Mg/Ca, Sr/Ca and U/Ca raios of a Porites coral from Sanya Bay, Hainan Island, South China Sea and their relationships to sea surface temperature. Paleogeography Paleoclimatology Paleoecology, 162, 59-74.

Weil, S., Buddemeier, R., Smith, S., Kroopnick, P. (1981). The stable isotopic composition of coral skeletons: controlled by environmental variables. Geochim. Cosmochim. Acta 45: 1174-1153.

Weiner, S. and Dove, P.M. (2003). An overview of biomineralization processes and the problem of the vital effect. Reviews in mineralogy and geochemistry, 54, 1-29.

Wellington G., Dunbar, R., Merlen, G. (1996). Calibration of stable isotope signature in Galapagos corals. Paleoceanography 11: 467-480.

White, W. M., and Duncan, R. A. (1996). Geochemistry and geochronology of the Society Islands: new evidence for deep mantle recycling. Geophysical Monograph-American Geophysical Union, 95, 183-206.

Woodroffe, C. D. (2005). Late Quaternary sea-level highstands in the central and eastern Indian Ocean: a review. Global and Planetary Change, 49, 121-138.

Woodroffe, C., and McLean, R. (1990). Microatolls and recent sea level change on coral atolls. Nature, 344, 531-534.

Woodroffe, C., McGregor, H., Lambeck, K., Smithers, S., Fink, D. (2012). Mid-Pacific microatolls record sea-level stability over the past 5000 yr. Geology 40, 951-954.

Woodroffe, C., McLean, R., Polach, H., Wallensky, E. (1990). Sea level and coral atolls: Late Holocene emergence in the Indian Ocean. Geology 18, 62-66.

Woodroffe, S., and Horton B. P. (2005). Holocene sea-level changes in the Indo-Pacific. Journal of Asian Earth Sciences, 25, 29-43.

Woodward, R. S. (1888). On the form and position of the sea level. United States Geol. Survey Bull. 48, 87-170.

Wu, P., and Peltier, W. (1983). Glacial isostatic adjustment and the free air gravity anomaly as a constraint on deep mantle viscosity. Geophysical Journal of the Royal Astronomical Society, 74, 377-449.

Yates, M., Le Cozannet, G., Garcin, M., Salaï, E., Walker, P. (2013). Multidecadal Atoll Shoreline Change on Manihi and Manuae, French Polynesia. Journal of Coastal Research, 29, 870-882.

Yokoyama, Y., and Esat, T. (2004). Long term variations of uranium isotopes and radiocarbon in the surface seawater recorded in corals. Global Environmental Change in the Ocean and on Land, 1, 279-309.

Young, R., Bryant, E., Price, D., Wirth, L., and Pease, M. (1993). Theoretical constraints and chronological evidence of Holocene coastal development in central and southern New South Wales, Australia. Geomorphology, 7, 317-329.

Yu, K. F., Zhao, J. X. Liu, T. S. Wei, G. J. Wang, P. X. and Collerson, K. D. (2004). High-frequency winter cooling and reef coral mortality during the Holocene climatic optimum. Earth and Planetary Science Letters, 224, 143-155.

Yu, K. F., Zhao, J. X., Lawrence, M. G., and Feng, Y. (2010). Timing and duration of growth hiatuses in mid Holocene massive Porites corals from the northern South China Sea. Journal of Quaternary Science, 25, 1284-1292.

Zinke, J., Dullo, W. C., Heiss, G. A., and Eisenhauer, A. (2004). ENSO and Indian Ocean subtropical dipole variability is recorded in a coral record off southwest Madagascar for the period 1659 to 1995. Earth and Planetary Science Letters, 228, 177–194.

Curriculum Vitae

Personal information:
Name: Rashid Juma
Surname: Rashid
Date of birth: 11.04.1977
Place of birth: Pemba, Zanzibar-Tanzania
Nationality: Tanzanian
Marital status: Married, 2 children

Academic qualifications:
October 2011 to date: PhD student at Helmholtz Centre for Ocean Research Kiel, University of Kiel Germany. Thesis title: Sea Level Change and Sea Surface Temperature Reconstruction in the Southern Equatorial Pacific Ocean Relative to the Society Islands, French Polynesia.

2004-2006: Master of Science in Ecological Marine Management (Marine Pollution and Risk Management). Vrije Universiteit Brussel and Universiteit Antwerpen (Interuniversity programme) in Belgium. Thesis title: Heavy metal accumulation of *Littoraria scabra* in coastal areas of Tanzania.

2002-2004: Assisting dolphin conservation researches, Institute of Marine Sciences, Tanzania.

1999-2002: Bachelor of Science in Marine biology and Botany, University of Dar es Salaam, Tanzania.

Work experience:
2010-2011: Assistant lecturer-The State University of Zanzibar (SUZA), Department of Natural Sciences, Zanzibar, Tanzania.

Publications:
Rashid, R., Eisenhauer A., Stocchi P., Liebetrau V., Fietzke J., Rüggeberg A., and Dullo, C. (2014). Constraining Mid to Late Holocene relative sea level change in the southern equatorial Pacific Ocean relative to the Society Islands, French Polynesia. Geochemistry, Geophysics, Geosystems, 15, 2601–2615.

De Wolf, H., Rashid, R. (2008). Heavy metal accumulation in *Littoraria scabra* along polluted and pristine mangrove areas of Tanzania. Environmental Pollution 152, 636-643.

Scientific Conferences:
07–12, April, 2013: European Geosciences Union (EGU). Poster presentation with a title: Constraining Mid to Late Holocene Sea Level change of Society Islands, French Polynesia. Vienna, Austria.

15–19, December, 2014: American Geophysical Union (AGU). Poster presentation with a title: Early Diagenetic Imprint on Temperature Proxies in Holocene Corals: A Case Study from French Polynesia. San Francisco, United States.